## Title

NO{sub 3}, the Study of Molecular Properties and Photodissociation by AB Initio Method, Spectroscopy, and Translational Spectroscopy



## Author

Kim, B.

## Publication Date

1990-10-01

LBL-29688

Lawrence Berkeley Laboratory
UNIVERSITY OF CALIFORNIA

Materials & Chemical Sciences Division

# $NO_3$, the Study of Molecular Properties and Photodissociation by Ab Initio Method, Spectroscopy, and Translational Spectroscopy

B. Kim
(Ph.D. Thesis)

October 1990



Prepared for the U.S. Department of Energy under Contract Number DE-AC03-76SF00098.

## DISCLAIMER

LBL-29688

# $NO_3$, the Study of Molecular Properties and Photodissociation by Ab Initio Method, Spectroscopy, and Translational Spectroscopy

Bongsoo Kim
Ph.D. Thesis

Materials and Chemical Sciences Division
Lawrence Berkeley Laboratory
University of California
Berkeley, CA 94720

October 1990

This work was supported by the U.S. Department of Energy under
Contract No. DE-AC03-76SF00098.

*Acknowledgements*

I would like to thank the support from the great teacher Buddha.

This study was carried out under the guidance and direction of Professor Harold S. Johnston, to whom I am deeply indebted. Especially I appreciate his patience and the enthusiasm in pursuing the research. I learned a lot from him about the science and how to be a good scientist. He was very gentle and fair and tried to make his students happy in every possible way. I would remember for a long time the beautiful bay bridge seen from the living room of his house on the hill and the taste of steamed salmon. I also wish to acknowledge the supports and encouragements by Professor Y. T. Lee in pursuing photodissociation study of $NO_3$ in his laboratory. It was a great privilege to be able to collaborate with him and his students. I deeply appreciate the support from Professor H. F. Schaefer and Professor W. Lester in the ab initio calculation of $NO_3$.

I wish to thank my coworkers for making this thesis possible. Phillip Hunter was a coworker in the LIF experiment of $NO_3$ in the flow cell (Chapter 1). He helped a lot in the beginning stage of my research. Floyd Davis was a graduate student in Y. T. Lee group and was a coworker in the molecular beam LIF and time-of-flight experiments (Chapter 2). I learned a lot from him about the translational spectroscopy. I admire his enthusiasm for science. The nights of 1989 winter when those experiments were done were very intensive and productive. I wish I could

have another winter like that again. Allen Clabo and Brian Hammond were then graduate students in Schaefer group and W. Lester group, respectively. I appreciate their help in pursuing the ab initio calculation. I would also like to thank other members of my group who helped me in various forms: Dr. Anthony Young, Dr. Daniel Oh, Dr. Doug Kinnison, Wade Sisk, Ken Patten, Jr., Charles Miller, and Joel Burly. I appreciate the kindness of Ken who never forgot to say "Hello" to me. I wish good luck to all of them.

I want to thank for the continuous encouragement from my former graduate advisor in the master study, Professor Kookjo Shin at Seoul National University, although he might be a little disappointed that I pursued experimental study rather than theoretical works.

All this work would not have been possible without the help of my small family, my daughters, Solbori and Solne, and my wife, Sunim. Once Prof. Shin said, " You cannot do science unless you are happy." . I appreciate especially for Solbori, who was born right when I was struggling and provided all the smiles, hugs and kisses I needed. I would like to thank my parents and parents-in-laws for helping me out to finish this work. My brothers, sister, sisters-in law, brother-in law all helped me whenever I needed their supports.

This work was supported by the Director, Office of Energy Research, Office of Basic energy Sciences, Chemical Sciences Division of the U.S. Department of Energy under Contract No. DE-AC03-76SF00098.

## Table of contents

## Introduction

The subject of this thesis is the $NO_3$ radical. The study of nitrogen oxides has been one of the main research subjects of our group. When I first started experimental study in Johnston group, I was quite surprised to find out that there were still a lot more to study about the small molecules such as the nitrogen dioxide and the nitrate radical. For $NO_3$, even the fluorescence has not been detected until 1983.[1] When I started the research about $NO_3$, Ishiwata et al.[2] just published a very interesting paper about the geometry of $NO_3$ radical by the analysis of IR spectrum.

It has been known that $NO_3$ absorbs strongly around 580 – 680 nm. According to theoretical calculations,[3] this state of strong absorption corresponds to the 2nd excited electronic state of $NO_3$ which belongs to $^2E'$ symmetry. My first project was to detect experimentally the first excited electronic state of $NO_3$, which belongs to $^2E''$, and investigate the properties of that state.

Before starting the experiment, we thought that it would be helpful to find out the approximate location of the first electronic state by the *ab initio* calculation. By working with H. F. Shaefer group, we were able to obtain the vertical excitation energy at Ishiwata et al.'s geometry using very high level calculations. (Configuration Interaction and Multi-reference CISD) The result of this calculation is presented in Chapter 3, which was also published in J. Chem. Phys. **88**, 3204, (1988); B. Kim, H. S. Johnston, D. A. Clabo, Jr., and H. F. Schaefer III. The best guess about the location of the $^2E''$ state was 3600 $cm^{-1}$ above the ground state.

We intended to detect that state by the laser induced fluorescence (LIF). If 662 nm (15111 $cm^{-1}$) laser light is used as an excitation source, we could detect photons up to 900 nm (11115 $cm^{-1}$) in wavelength with red sensitive RCA 31034A photomultiplier. That means if the $^2E''$ state lies lower than 4000 $cm^{-1}$ from the ground electronic state, it can be detected by LIF. When excited by 605 nm (16533 $cm^{-1}$) laser, we can search for up to 5400 $cm^{-1}$. Unfortunately, we could not find any new electronic states in that LIF experiment. In 1989, Weaver et al.[4] discovered that $^2E''$ state was located at 7000 $cm^{-1}$ above the ground state from the photoelectron spectrum of $NO_3^-$.

However, since we improved the signal to noise of the LIF of $NO_3$ by more than an order of magnitude compared to previous researchers, interesting features in the shape of the fluorescence bands were observed. Also more new bands were detected. The analysis of this LIF data is presented in Chapter 1. The result of this study will be submitted to a journal soon.

Since our experimental data provided very accurate position for the fluorescence bands, we tried to fit most of the bands assuming $D_{3h}$ or $C_{2v}$ geometry of ground state structure. However, to our surprise, no theoretical calculation was done about the vibrational frequencies of $NO_3$. Therefore, we decided to do the calculation ourselves in order to aid the assignment of the fluorescence bands. This study was done in collaboration with W. Lester group. Chapter 4 shows the result of the vibrational frequency analysis of ground state $NO_3$. It was published in Chem.

Phys. Lett., **168**, 131 (1990); B. Kim, B. L. Hammond, W. A. Lester Jr., and H. S. Johnston.

One of the reasons why $NO_3$ caused so many difficulties both in experimental studies and theoretical calculations was the strong vibronic coupling between the nearby electronic states and the complexity of the spectrum due to that perturbation. By cooling the $NO_3$ radicals in the molecular beam, dramatic simplification of the complex spectrum was expected.

Also due to its importance in atmospheric chemistry, the photodissociation of $NO_3$ had been studied extensively in our lab. Magnotta and Johnston[5] studied the photodissociation of $NO_3$ by the laser flash photolysis in a flow cell. Although they detected the dissociation products of $NO_3$ into $NO + O_2$ and $NO_2 + O$ at wavelengths longer than the then known thermodynamic threshold (580 nm for $NO_2 + O$ channel, the existence of $NO + O_2$ channel was not clearly confirmed), it was thought that the dissociation was induced by collisional activation.[6] By making a molecular beam of $NO_3$, the photodissociation of $NO_3$ can be studied in collision free conditions.

By pyrolyzing $N_2O_5$ for a very short time, we succeeded in generating a continuous molecular beam of $NO_3$ radicals for the first time. The LIF excitation spectra was taken in the beam and the time-of-flight/mass spectrometer study of the $NO_3$ photodissociation confirmed the findings of Magnotta and Johnston. Chapter 2 shows the experimental results of this study in detail. This study was done in collaboration with Y. T. Lee group. The findings of this study are planned to be

published in 3 separate papers. ("LIF excitation spectrum of $NO_3$", "The dissociation energy for $NO_3 \rightarrow NO_2 + O$", and "Photodissociation dynamics of the $NO_3$ radical")

**References**


1. (A) T. Ishiwata, I. Fugiwara, Y. Naruge, K. Obi, and I. Tanaka, J. Phys. Chem. **87**, 1349 (1983).

   (B) H. H. Nelson, L. Pasternack, and J. R. McDonald, J. Phys. Chem. **87**, 1286 (1983).

2. T. Ishiwata, I. Tanaka, K. Kawaguchi, and E. Hirota, J. Chem. Phys. **82**, 2196 (1985).

3. T. E. H. Walker and J. A. Horsely, Mol. Phys. **21**, 939 (1971).

4. A. Weaver, D. W. Arnold, S. E. Bradforth, and D. M. Neumark, submitted to J. Chem. Phys..

5. a) F. Magnotta and H. S. Johnston, Geophys. Res. Lett. **7**, 769 (1980).

   b) F. Magnotta, Ph. D. Thesis, University of California, Berkeley and Lawrence Berkeley Laboratory report LBL-9981 (1979).

6. H. H. Nelson, L. Pasternack, and J. R. McDonald, J. Chem. Phys. **79**, 4279 (1983).

# Chapter 1. Molecular Structure of $NO_3$ radical studied by laser induced fluorescence


## Abstract

The fluorescence emission spectra of $NO_3$ excited at 15109, 15882, 16053, and 16555 $cm^{-1}$ are reported. More than 20 vibrational bands are observed. The fluorescence bands exhibit two different shapes, one shows a sharp spike overlapped with broad band, the other shows a broad band only. The band at 2010 $cm^{-1}$ from the excitation frequency could not be assigned to any combination or overtone band when $D_{3h}$ symmetry is assumed. An effort is made to assign most of the observed vibrational bands with the help of recent theoretical studies.


## I. Introduction

In atmospheric chemistry $NO_3$ affects the ozone balance in the upper atmosphere and night-time chemistry in the troposphere. Although many studies have been reported on $NO_3$, some questions remain to be answered. Especially there has been uncertainty over the ground state structure of $NO_3$.

At high resolution the absorption spectrum of $NO_3$ was observed by Ramsay[1] and Marinelli et al.[2], but both of them reported that all the $NO_3$ bands were diffuse.

The diffuseness was ascribed to extensive vibronic perturbation (Douglas coupling).[3] In 1982 Ishiwata et al.[4] reported dispersed laser induced fluorescence of $NO_3$, which showed bands at 380, 1060, 1490, and 760 $cm^{-1}$ when excited by a 661.8 nm laser. Their spectral resolution was about 40 $cm^{-1}$ at 700 nm. They suggested $D_{3h}$ symmetry for the ground state structure of $NO_3$ with the fundamental frequencies assigned to 380(e′), 1060($a_1'$), and 1480 $cm^{-1}$(e′). Nelson et al.[5] favored $C_{2v}$ geometry, reporting similar laser induced fluorescence spectrum with slightly better resolution (35 $cm^{-1}$ at 700 nm). Their assigned fundamental frequencies are 1050($a_1$), 754($a_1$), 1489($b_2$), and 360($b_2$) $cm^{-1}$. They observed but did not assign frequencies at 1910, 2000, and 2334 $cm^{-1}$.

In 1985 Ishiwata et al.[6] reported the observation of the infrared spectrum of $NO_3$ in the 1492 $cm^{-1}$ region using a Zeeman modulation diode laser spectrometer. The analysis of the IR spectrum yields $D_{3h}$ geometry, since only K″ = 3n (n = integer) transitions were observed, although several anomalous features were noticed. Also Friedl and Sander[7] observed 3 vibrational bands of $NO_3$ in 759.6, 762, and 1492 $cm^{-1}$ using Fourier Transform IR spectroscopy with 0.005 $cm^{-1}$ resolution. The IR spectrum at 762 and 1492 $cm^{-1}$ showed $D_{3h}$ symmetry. The band centered at 759.6 $cm^{-1}$ showed features characteristic of a parallel band but resisted any simple assignment. A possible existence of a low-lying electronic state approximately 100 $cm^{-1}$ above the ground state was suggested to explain that band.

Very recently Kawaguchi et al.[8] reported the reinvestigation of the $NO_3$ 1492 $cm^{-1}$ band, where they were able to remove all of the anomalies for the ground state

in the previous assignment.[6] However, the spin-orbit interaction constant for the upper state at 1490 $cm^{-1}$ above the ground state was unusually small compared with other cases, and they wrote, "It is still quite difficult to conceive and prove a particular model for the $NO_3$ radical that is compatible with all the experimental evidences.". Their suggestion for one of most plausible models is the one in which one of the N – O bonds is longer than the other two bonds of equal length, with a low barrier between the three equivalent $C_{2v}$ minima.

Weaver et al.[9] observed ultraviolet photoelectron spectra of the nitrate anion, which showed the transition to $^2A_2'$ and $^2E''$ electronic states of $NO_3$. In the transition to $^2A_2'$ they observed about 12 vibrational peaks, among which the most intense 5 peaks were assigned as the vibrational progressions of 1080 $cm^{-1}(v_1)$ and 363 $cm^{-1}(v_4)$. The instrumental resolution for their experiment was 64 $cm^{-1}$. Anomalies in the intensities and the peak positions of the vibrational progressions were seen and explained by using pseudo-Jahn-Teller coupling between the $^2A_2'$ and $^2E'$ states of $NO_3$. They reported that the coupling strength necessary to reproduce their results did not break the $D_{3h}$ symmetry of the $^2A_2'$ state.

In parallel with the experimental study, many theoretical calculations[10,11,12,13,14,15] have been performed to determine the ground state structure of $NO_3$. Using Unrestricted-Hartree-Fock (UHF) wavefunctions, Lund and Thuomas[10] found the ground state of $NO_3$ possessed $D_{3h}$ symmetry with an N – O bondlength of 1.24 Å. Siegbahn[11] tried geometry optimization on $NO_3$ using CASSCF and CI wave functions. Optimization was restricted to planar geometries,

while the three N−O bondlengths were kept the same to explore around $D_{3h}$ geometry. In his calculation the restricted optimization did not converge to $D_{3h}$ geometry.

Boehm and Lohr[12] reported theoretical results for several electronic states of $NO_3$. They used UHF wave functions, to which Møller-Plesset perturbation theory was applied. Their optimized geometry of $NO_3$ ground state depended on the level of perturbation theory. It was suggested that the UHF wave functions may not be a good starting point to solve the delicate problem of the $D_{3h}-C_{2v}$ energy difference.[13] The very high level Complete-active-space SCF (CASSCF) calculation by Davy and Schaefer,[13] where more than 100,000 configuration state functions were used, resulted in $C_{2v}$ geometry. The energy of this $C_{2v}$ minimum geometry is 1.4 kcal/mol (490 $cm^{-1}$) below that of the $D_{3h}$ minimum geometry. The vibrational frequencies obtained at the $D_{3h}$ minimum geometry showed large deviation from the experimental frequencies.

Kaldor's calculation[14] in which the CCSD method was used resulted in $D_{3h}$ geometry. The frequency analysis is done at the optimized $D_{3h}$ geometry. Using Multi-configuration SCF (MCSCF) wavefunctions, Kim et al.[15] predicted $C_{2v}$ geometry; also the vibrational frequencies were calculated at that geometry. Similar results were obtained in the vibrational frequency analyses by Davy[16] and Morris et al.[17]

The excitation spectrum of $NO_3$ taken by Nelson et al.[5] has strong absorption peaks around 15110, 15880, 16050, and 16560 $cm^{-1}$. According to recent ab initio calculation, the state at 15110 $cm^{-1}$ belongs to $^2E'$ symmetry.[18]

In this chapter laser induced fluorescence (LIF) spectra of $NO_3$ are obtained for several excitation frequencies and the analysis of the spectra are presented. The highest resolution of the spectrum reported here has about 14 times higher resolution (2.5 $cm^{-1}$) than the previous fluorescence studies,[4,5] and additional vibrational bands are detected in a region that was not covered before.

The LIF spectrum with higher resolution shows an interesting feature in the bandshape. Two different kinds of bandshapes are observed. One has a sharp spike overlapped with a broad continuous band, while the other shows the broad band only. The analysis of these bandshapes provides additional information for the molecular properties of $NO_3$. Also an effort is made to assign the observed vibrational bands with the help of theoretical studies.

## II. Experimental

The experimental set up is illustrated in Figure 1. The nitrate radical is generated in a discharge flow system where fluorine atoms are produced by passing 5% $F_2$/He mixtures through a microwave driven plasma (2450 MHz) and

subsequently react with $HNO_3$ to produce $NO_3$. The discharge cell was made of quartz or pyrex tubes. $NO_3$ radicals are produced by the reaction

$$F + HNO_3 \rightarrow HF + NO_3$$

The pressure in the cell was adjusted by adding He buffer gas to the system and was varied from 120 mTorr to 600 mTorr. A portion of the He carrier gas flowed through the saturator containing $HNO_3$ into the cell. The flow of the $F_2$/He and $HNO_3$/He were monitored by the Hastings mass flowmeter. Typically the pressure of $F_2$/He mixture was adjusted to 100 ~ 200 mTorr and that of $HNO_3$/He mixture to 50 ~ 200 mTorr, to give optimum $NO_3$ fluorescence signal. Total pressure was measured by an MKS Baratron capacitance manometer.

The Spectra Physics 165-09 $Ar^+$ laser was used to pump the Spectra Physics 375 standing wave dye laser. The laser bandwidth was nominally 1 $cm^{-1}$ at 15109 $cm^{-1}$ when operating in multimode. The laser beam (TEM (0,0)) was focused down onto the detection region of the cell, giving 2 mm in diameter of beam size. With 4.2 W pumping power, the dye laser, using DCM, delivered 500 to 700 mW in the 620 ~ 680 nm range. Rh6G dye gave 300 ~ 700 mW of power covering the 580 ~ 630 nm range. Dye laser power was stabilized through an internal light stabilization circuit, which adjusted the $Ar^+$ laser power and maintained the power stability within ± 1 % during 10 hrs.

The dispersed fluorescence spectrum was collected by 14 cm focal length, 12 cm diameter plano-convex lens placed 19 cm away from the detection cell and focused onto the entrance slit, which is placed 75 cm away from the fluorescence collection lens, of a 1 m Czerny-Turner monochromator (Interactive Technology CT-103). It was equipped with slit lenses with focal length of 33 cm, which then utilized the full height of the slits (5 cm). A grating with 1200 grooves per mm blazed at 500 nm is used. The dispersed fluorescence was focused again onto the cooled photocathode of RCA 31034A PMT. The system response, which was measured using a tungsten lamp, is shown in Figure 2.

Wavelength calibration of the 1 m monochromator was achieved using known emission lines from a low pressure mercury lamp and a neon pilot lamp. The wavelength of the dye laser radiation was determined by the monochromator through scattered laser light. The monochromator slits were typically set at 250 $\mu$m resulting in a bandpass of 0.2 nm (FWHM) which gives 4 $cm^{-1}$ resolution at 700 nm. Some of the spectra are taken with the slit width of 150 $\mu$m giving the resolution of 2.5 $cm^{-1}$ at 700 nm.

Initially a lock-in amplifier operated at 1.8 kHz was used to detect the signal, but much better signal-to-noise was obtained by replacing the detection system with a gated photon counter. All of the spectra reported here were obtained by the photon counting method. For photon counting detection, the output from the fluorescence collection PMT was sent to a PAR 1121 high gain amplifier/discriminator. The amplifier/discriminator was interfaced to a home

made pulse counter card which was installed in a microcomputer (IBM AT). The photomultiplier was maintained at −45°C with dry ice and the dark count was less than 2 counts per second when the PMT bias voltage was −1650 V.

To obtain the excitation spectrum, the laser wavelength was scanned using a stepping motor to drive the birefringent filter. The stepping motor was driven by the IBM AT computer. The excitation specrum was recorded by collecting the fluorescence dispersed at 662 nm or at 711 nm depending on the excitation wavelength with the slits of the monochromator wide open to 3 mm.

Anhydrous $HNO_3$ was prepared by distilling a mixture of $NaNO_3$ and concentrated $H_2SO_4$ at 310 K and collecting $HNO_3$ at 233 K. During the experiment, $HNO_3$ was kept at 287 K. The gases used in the experiment were obtained from Lawrence Berkeley Laboratory (He) and Matheson (5 % $F_2$ in He) and used as received.

## III. Results

### A. 0-0 excitation at 15109 $cm^{-1}$

The LIF spectrum of $NO_3$ with the excitation frequency of 15109 $cm^{-1}$, which corresponds to the 0−0 excitation from the ground state to $^2E'$ state, corrected for monochromator and PMT response, is presented in Figure 3. By scale expansion,

the shape and peak location of the weak peaks are well defined. The positions of the vibrational peaks in the spectrum are listed in Table I.

Most of the peaks in the spectrum show a sharp spike on top of the broad band, while some peaks including the one at 368 $cm^{-1}$ from the excitation frequency show a broad band only. The bands of two different bandshapes around 1800 $cm^{-1}$ are magnified in Figure 4 for comparison. Although the vibrational bands at 1799 $cm^{-1}$ and 1923 $cm^{-1}$ are among the weakest peaks in intensity, Figure 4 clearly shows that the band at 1799 $cm^{-1}$ has a spike and the one at 1923 $cm^{-1}$ does not. The shape of the band at 368 $cm^{-1}$, which is the strongest band among those without the spike, is shown in Figure 6. The magnified bandshapes for several other bands are also shown in other figures (Fig. 4 & 5).

The fluorescence spectrum obtained with the slit width of 150 $\mu$m is shown in Figure 7. Since it does not show much difference from the spectra taken with 250 $\mu$m slit width (Figure 6-2), all the other spectra are acquired with 250 $\mu$m slit (4 $cm^{-1}$ resolution at 700 nm).

The frequencies of the sharp spikes move along with the change of the excitation frequency, with the positions of the spikes with respect to the excitation frequency remaining constant. This is illustrated in Figure 5 and the spike locations are presented in Table II. This observation confirms that the excited electronic state of $NO_3$ shows a continuous spectrum as seen in absorption.[2] In Figure 5 it is shown that the frequencies of the broad bands do not change when the excitation frequency

is changed. This behavior is observed for all the bands which have the sharp spike without exception.

The ratios of the height of the sharp spike to the broad band which is under the spike for several bands are listed in Table IV. The spectrum was obtained at 120 mTorr of total pressure. Since the overlapping of the bands makes the broadband height look higher, only those bands which are not significantly overlapped with others are shown. The height of the spike is measured from the top of the spike to the top of the broad band contour. Table IV shows that the intensity of the spike is proportional to that of the broad band.

The pressure dependence of the fluorescence bandwidth was investigated and is presented in Figure 6 and Table III. When the total pressure is increased from 120 mTorr to about 600 mTorr, of which He consists more than 95 %, FWHM for the broad band is increased. The ratio of the area of sharp spike to the broadband area decreases as the total pressure is increased. The pressure dependences and the observation that the location of the broad band does not move with the change of excitation frequency indicate that the broad band fluorescence is due to emission from nearby vibronic states which are populated by collisional relaxation.

**B. The assignments of the vibrational peaks**

In Figure 8, Figure 9, and Figure 10 the dispersed spectra excited at 16053, 16555, and 15882 $cm^{-1}$ are shown. The excitation frequencies are chosen at the absorption peaks which are seen in the excitation spectrum by Nelson et al.[5] Nelson

assigned 418 and 820 $cm^{-1}$ as upper state vibrational frequencies. Ramsay[1] assigned 944 $cm^{-1}$ as another upper state frequency, and we observed total fluorescence peaks at 1166 and 1446 $cm^{-1}$ above the 0–0 transition. The positions of the absorption peaks observed in this experiment are slightly different from others. The excitations in Figures 7, 8, and 9 correspond respectively to T + 944, T + 1446, and T + 773 $cm^{-1}$, where T is 15109 $cm^{-1}$.

At 16555 $cm^{-1}$ (T + 1446 $cm^{-1}$) it is known that photo-dissociation to $NO_2$ + O occurs and competes with fluorescence. (See Chapter 2.) 15882 $cm^{-1}$ (T + 773 $cm^{-1}$) corresponds to one of the several peaks which are seen overlapped between 16000 and 15800 $cm^{-1}$. It is the peak with lowest excitation energy among nearby peaks and chosen in order to minimize the occurrence of fluorescence bands induced by collisional relaxation.

The band positions for each spectrum are presented in Table V and Figure 8, Table VI and Figure 9, and Table VII and Figure 10. The first column in each table (I, V, VI, and VII) gives the frequency $\nu$ ($cm^{-1}$) of the observed fluorescence peak. The second column gives the difference between the excitation frequency and the observed peak. The third column in Table I shows the relative intensity of the peaks compared to 1053 $cm^{-1}$ peak (=100). The fourth column of Table I and the fourth column of Tables V, VI, VII are the assignments of the transitions. These $D_{3h}$ assignments are supplemented with two frequencies: A = 2010 and B = 775 $cm^{-1}$. Some assignments are a question mark, indicating that no combination of the six frequencies (including A and B) gives reasonably close agreement with the given

observed frequency. The fifth column is the difference, harmonic frequency of assignment minus frequency observed. The last column of these tables gives Y (yes) if the observed peak has a sharp spike, N (no) if it has no sharp spike, and left blank if the signal is not strong enough to produce a clear Y or N statement.

The assignments in Tables I, V-VII show several patterns:

(i) When $NO_3$ is excited to states well above T, strong fluorescence is observed which originates from the state at 15109 $cm^{-1}$, suggesting that the rates of vibrational deactivation and fluorescence are comparable in this system. (ii) For $\nu_1$ (1053 $cm^{-1}$), the first overtone is strongly observed (2115, 2114, 2116, 2119 $cm^{-1}$) with values close to twice the fundamental (2106), the second overtone is observed (3156, 3154, 3160) at values close to three times the fundamental (3159), and the third overtone observed at 4201 $cm^{-1}$ is close to the harmonic value of 4212. The mode $\nu_1$ is very nearly harmonic up to the third overtone. For $\nu_2$ (1500 $cm^{-1}$), the first overtone is observed (2998, 2998) at values close to the harmonic value of 3000. Higher overtones would be out of the detectible wavelength region of PMT. For $\nu_3$ (753 $cm^{-1}$), the first harmonic overtone is 1506, which would be masked by the fundamental at $\nu_2$ (1500), there is no peak at the position of its second overtone at 2259, and no peaks were assigned at any higher overtone. For $\nu_4$ (368 $cm^{-1}$), there is no fluorescence peak at either its first overtone (736) or at its second overtone (1104).

(iii-a) In Table I, there are 23 fluorescence peaks. Using the four $D_{3h}$ frequencies to construct overtone and combination bands, we assign all peaks except those at 1174, 1923, 2010, 2358, 2808, 3063, and 3345 $cm^{-1}$. There is a peak (**A**) at 2010 $cm^{-1}$ with high intensity (14% of $\nu_1$), and it appears in 3 combination bands in the 0-0 excitation spectrum. In Tables V and VI, a peak (**B**) is observed at about 775 $cm^{-1}$, and it appears in several combination bands.

A possible assignment for the peak at 1174 is $\nu_4$ + B, and for the peak at 1923 is $\nu_4$ + 2B. The peaks not assigned using the four $D_{3h}$ frequencies are examined with the 6 frequencies including A and B. All 23 peaks of Table I are then assigned, except for the one at 3343. Large deviations ( > 25 $cm^{-1}$) remain for the peaks at 1174, 2511, and 2808.

(iii-b) For the excited state of $NO_3$, the vibrationally excited state at 16555, 16275, 16053, and several states at around 15882 $cm^{-1}$ are seen in absorption spectrum.[5] However, the absorption band at 15698 $cm^{-1}$ (637 nm) and 15514 $cm^{-1}$ (644 nm) coincide with the positions of the hot bands from 368 $cm^{-1}$ state to 16053 $cm^{-1}$ and 15882 $cm^{-1}$, respectively. It is not very clear whether the peak at 15514 $cm^{-1}$ (644 nm) represents a real state or a hot band. When $NO_3$ is excited above the 0−0 transition, the number of accessible states by collisional deactivation and the fluorescence peaks emitted from those states increases, which makes assignments more difficult. Therefore, in Table V, VI, and VII assignments are given only to those peaks which show substantial intensity. For collisionally induced peaks only

the fluorescence bands from the 15109 and 16053 $cm^{-1}$ states, which are strong in intensity, are assigned.

The transition from the hot band at 368 $cm^{-1}$ to the upper state at T = 15109 $cm^{-1}$ is at 14742 $cm^{-1}$, and excitation at this frequency is shown in Figure 11. The shape of the observed peaks is quite similar to the dispersed spectrum with 15109 $cm^{-1}$ excitation. In Figure 12 several bands at the 14742 $cm^{-1}$ excitation are magnified. The peaks that showed sharp spikes when excited by 15109 $cm^{-1}$ do not show spikes with 14742 $cm^{-1}$ excitation. This feature will be explained in the Discussion section. Since the transition is weak, the slit width of the monochromator was set at 500 $\mu$m, which gives about 8 $cm^{-1}$ resolution. The resolution and signal-to-noise ratio are considered to be good enough to show the spikes if there are any.

It is noted that the FWHM's of the fluorescence bands are changed when $NO_3$ is excited to different vibronic states. The FWHM of the 368 $cm^{-1}$ band is 32, 49, and 67 $cm^{-1}$ when excited by 16555, 16053, and 15109 $cm^{-1}$, respectively. Those spectra are shown in Figure 13. It may be related with the possible depletion of electronically excited $NO_3$ by the photodissociation into $NO_2$ + O.

**C. Source of noise**

We explored the possibility that the LIF from $NO_2$ which is generated in reaction mixture might be a source of noise. The absorption cross section of $NO_2$ is 2 orders of magnitude smaller than $NO_3$ in the range observed.

Figure 14 presents the $NO_2$ spectra obtained at several excitation frequencies at which $NO_3$ LIF spectra are taken. The main peaks are at about 749, 1328, and 1498 $cm^{-1}$ from the excitation frequencies. At 15109 $cm^{-1}$ excitation the location of 2 $NO_2$ peaks at 749 $cm^{-1}$ and 1498 $cm^{-1}$ are the same as those of $NO_3$ peaks, but the $NO_3$ spectrum does not show any other peaks which are close to the positions of $NO_2$ fluorescence peaks. By comparing the locations and intensities of the peaks in these spectra with $NO_3$ LIF spectra, it appears that all the peaks presented here as $NO_3$ spectra are not due to $NO_2$. Also the chemiluminescence peaks induced by the microwave discharge are carefully investigated and eliminated when they show up in the $NO_3$ spectra.

The fluorescence excitation spectrum obtained here closely matched the absorption spectra obtained by others.[2,5] Comparing the ratio of the intensity of the 662 nm peak to that of 678 nm peak to other room temperature spectra, the vibrational temperature of $NO_3$ in this reaction system seems to be close to room temperature. The main collisional partner for excited $NO_3$ molecule is He, which consists of more than 90 % of total pressure.

## IV. Discussion

### A. $D_{3h}$ and $C_{2v}$ symmetry in $NO_3$

Morse et al.[22] carried out a complete analysis of the spectrum of the trimer of copper, fitting a potential surface to the data, and solving Schröedinger's equation for the overall $D_{3h}$ potential energy surface with three shallow $C_{2v}$ minima. A portion of the potential energy surface is given as Figure 15. In view of their analysis we can outline three possible cases for $NO_3$:

(i) If the $C_{2v}$ minima are deep compared to several vibrational energy levels, the geometrical structure of the molecule is $C_{2v}$, with one bond longer than the other two. It is then appropriate to use the curvatures at the $C_{2v}$ minimum for a normal-coordinate analysis, although unusual anharmonicity might be encountered at high vibrational energy levels.

(ii) If the $C_{2v}$ minima are absent, the structure is $D_{3h}$, and the curvatures at the potential energy minimum are suitable for a normal-mode analysis.

(iii-a) If the three minima exist and are very shallow compared to all zero-point energies of the molecule, their presence might distort the curvatures at the $D_{3h}$ center, giving force constants that are not representative of the main potential energy well. In this case a very high quality molecular structure calculation could give poor vibrational frequencies.

(iii-b) If the $C_{2v}$ minima and the barriers between them are shallow compared to zero-point vibrational energies, the quadratic parameters (force constants) derived

from the curvatures at the potential minimum might give a poor set of normal coordinates.

The vibrational coordinates and frequencies as derived by Morse et al.[22] for such a case with $Cu_3$ show rather normal symmetric stretching motion, but the anti-symmetric motions are strongly perturbed and unusual. The anti-symmetric stretching mode shows "pseudo-rotation", that is, the stretched corner of the triangle permutes as if a rotation around the three positions. The $D_{3h}$ degeneracy is split. On a time scale long compared to molecular vibrations, the molecule has $D_{3h}$ structural symmetry, which would be registered as such in the vibration-rotational spectrum.

As noted in the Introduction, about half the quantum mechanical structure studies have found the lowest point on the potential energy surface to have $D_{3h}$ symmetry and the other half have found $C_{2v}$ symmetry.

The infrared studies of Ishiwata et al.[6], Kawaguchi et al[8], and Friedel and Sander[7] require $D_{3h}$ symmetry for absorption bands centered at 762 and 1492 $cm^{-1}$. In previous fluorescence studies, Ishiwata et al.[4] favored $D_{3h}$ symmetry, and Nelson et al.[5] favored $C_{2v}$ symmetry, but these studies did not have data that required either symmetry. In this Discussion, we review our present experimental data to see what evidence it gives for each of the three cases:

(i) $D_{3h}$, (ii) $C_{2v}$, and (iii) the intermediate case of pseudo-rotation about shallow $C_{2v}$ minima in a global $D_{3h}$ potential energy structure.

**B. Analysis of these fluorescence data in terms of harmonic overtones and combinations**

As pointed out in Results section, we interpreted as many of our peaks as possible using the four frequencies (368, 753, 1053, and 1500 $cm^{-1}$) associated with $D_{3h}$ symmetry. The peak at 1053 ($\nu_1$) shows a strong, almost harmonic progression up to 4 $\nu_1$. The first overtone of $\nu_2$ at 1500 was observed at 2998 $cm^{-1}$, very close to twice the fundamental. The other vibrations did not reveal overtones.

Although most fluorescence peaks could be accounted for in this manner, 32 percent of the peaks, including a strong one at 2010 $cm^{-1}$ and a weaker one at 775 $cm^{-1}$, could not be assigned. The frequencies at 2010 and 775 $cm^{-1}$ appeared in 8 bands assigned as combinations. For 2010 $cm^{-1}$ band the closest harmonic vibrational band made of $D_{3h}$ fundamentals is at least 150 $cm^{-1}$ away, other than the assigned $2\nu_1$. (See Appendix A.) On this basis, our data indicate that $NO_3$ does not have a set of fundamental frequencies associated with a molecule of $D_{3h}$ symmetry.

At the time of this experiment there was no theoretical study reported on the vibrational frequencies of $NO_3$. A vibrational frequency analysis for ground state $NO_3$ using ab initio methods was performed by the author[15] (also see chapter 4) as an aid in interpreting the experimental data. The geometry optimization resulted in $C_{2v}$ minimum, and the vibrational frequencies at that geometry are presented in Table IX and the normal coordinates are given by Figure 16. In particular, this calculation predicted the asymmetric stretch vibration ($b_2$) to be 1890 $cm^{-1}$.

From the ab initio study by Kim[19], it was noted that the calculated properties of the $NO_3$ ground electronic state are similar to those of the ground electronic state of $FNO_2$, including nuclear structure, vibrational frequencies, and the IR intensities of the vibrational modes. The observed vibrational frequencies of $FNO_2$ and $ClNO_2$ are included in Table VIII.

Meanwhile, other vibrational frequencies have been calculated and reported. With minimum potential energy having $C_{2v}$ symmetry, Davy[16] performed a vibrational frequency analysis using configurational interaction wave functions. A vibrational frequency analysis using Unrestricted-Hartree-Fock (UHF) wavefunctions was done by Morris et al.[17] at optimized $C_{2v}$ geometry. At optimized $D_{3h}$ geometry, Davy et al.[13] and Kaldor[14] calculated the $NO_3$ frequencies. All of these results are included in Table VIII.

The frequencies found in this study, including A and B, are entered in Table VIII as the "observed $C_{2v}$ values". The observed frequencies of Ishiwata et al.[6] and Friedl and Sander[7] are entered in Table IX as "observed $D_{3h}$ values". All the calculations performed at $C_{2v}$ symmetry give vibrational frequencies that are similar to each other, to those observed for $FNO_2$, and to those found here for $NO_3$, asde from the 32 % of unassigned peaks. The calculations made for $D_{3h}$ symmetry give much lower frequencies than those observed for $NO_3$.

**C. The nature of the sharp spike**

In Results section it was suggested that the broad band is the fluorescence emitted from the states populated by collisional relaxation. Also, the intensity of the sharp spike is proportional to the intensity of the broad band fluorescence. (See Table IV.)

This proportionality indicates that the sharp spikes correspond to the same fluorescence radiation as the broad band. The frequency of the spikes changes by the same amount as the excitation frequency changes, which is possible since $NO_3$ shows broad, continuous absorption for the bands centered at 15109, 16053, and at other excitation frequencies employed here. This observation suggests that the sharp spikes are the fluorescence emitted by initially excited states before collisional relaxation occurs.

However, why are there bands which do not show sharp spikes? The absence of the spike indicates that the fluorescence from the initially excited state to a certain ground vibrational state is practically forbidden and allowed only after relaxation.

Let's investigate the electronic structure of the excited state of $NO_3$. The calculation by Kim et al.[18] shows that the excited state at 15109 $cm^{-1}$ above the ground state is $^2E'$. As a result of Jahn-Teller effect, the geometry of the $^2E'$ state, which is in $D_{3h}$ symmetry, will be distorted and have $C_{2v}$ symmetry. The two components of the Jahn-Teller split state $^2E'$ would be $^2B_2$ and $^2A_1$.

Marinelli, et al.[2] reported a distorted Lorentzian absorption line shape for $NO_3$ absorption at 15108 $cm^{-1}$ and they fitted the absorption line with two separate

Lorentzian lines that are separated by about 60 $cm^{-1}$. A similar asymmetric bandshape is obtained in this experiment for the excitation spectra around 15109 $cm^{-1}$, as in Figure 17 A. The excitation spectra around 14742 $cm^{-1}$, which is a hot band excitation from 368 $cm^{-1}$ to 15109 $cm^{-1}$, is presented for comparison, as in Figure 17 B. These findings suggest that the absorption spectrum could be the overlapped spectrum of a Jahn-Teller split pair.

Since the excited states belong to $C_{2v}$, it will be proper to treat the symmetry selection rule in $C_{2v}$ regardless of the ground state belonging to $C_{2v}$ or $D_{3h}$. In $C_{2v}$ symmetry the ground state has $B_2$ symmetry. Among the 4 vibrational bands which correspond to the 4 fundamental frequencies, 368, 753, 1053, and 1500 $cm^{-1}$, only the band at 368 $cm^{-1}$ does not show a sharp spike.

Two possible cases are illustrated in Figure 18 (a) and (b). In case (a) the total symmetry of the vibronic wavefunction for the ground $^2B_2$ state with one quantum of vibration of 368 $cm^{-1}$ (Let's denote it as $\alpha$ state.) is $A_2$ when the vibration belongs to $b_1$ symmetry ($a_2'$ in $D_{3h}$ point group). If the upper $B_2$ state has negligible absorption cross section compared to the upper $A_1$ state at the excitation frequency, most of the fluorescence will come from the $A_1$ state. But the upper $A_1$ state cannot fluoresce to $\alpha$ state because of symmetry selection rules. Then most of the fluorescence falling on $\alpha$ state is emitted from upper $B_2$ state, which was populated by collisional relaxation from upper $A_1$ state. The fluorescence bandshape at 368 $cm^{-1}$ would therefore not show a sharp spike.

A second possible case is that the vibration at 368 $cm^{-1}$ belongs to $b_2$ symmetry (e′ in $D_{3h}$ point group), the upper $A_1$ state has negligible absorption cross section compared to the upper $B_2$ state at the excitation frequency, and the fluorescence from the upper $B_2$ state to the $\alpha$ state is forbidden by poor Franck–Condon overlap, as shown in Figure 18 (b). Other cases are not possible when the symmetry selection rule is considered.

Friedl and Sander analyzed 762 $cm^{-1}$ band as a parallel band, which should be out of plane mode, assigning 368 $cm^{-1}$ band as e′ symmetry.[7] In view of their observation and the vibrational frequency analysis results (See Table IX), we choose $b_2$ symmetry (e′ in $D_{3h}$ point group) for 368 $cm^{-1}$ mode (case (b)) as our assignment.

It is shown in Figure 12 that the peaks which show sharp spikes with 15109 $cm^{-1}$ excitation do not show them with 14742 $cm^{-1}$ excitation. This observation is completely compatible with the case described above in Figure 18. With 14742 $cm^{-1}$ excitation the initial state is the $\alpha$ state and the transitions take place in the opposite direction. The absence of spike in the fluorescence bands suggests that the transitions between the upper $A_1$ state and corresponding vibrational states are not allowed. In Figure 12 (c) the band at 15109 $cm^{-1}$ does not show a spike, which confirms the previous assumption that the radiative transition between the lower $B_2$ state and the upper $A_1$ state is very weak.

**D. Qualitative resolution of the $C_{2v}$ and $D_{3h}$ aspects**

The infrared spectra of $NO_3$[6,7,8] prove that there is $D_{3h}$ symmetry with respect to the rotational structure of two vibrational bands. However, analysis of our observed laser induced fluorescence frequencies suggests that $NO_3$ has $C_{2v}$ structure.

One possible explanation to resolve this apparent conflict is that $NO_3$ may be an intermediate case analogous to $Cu_3$ as interpreted by Morse et al.[22] As suggested by Kawaguchi et al.[8], there are shallow potential wells that tend to make one NO bond in $NO_3$ slightly longer than the other two bonds with low barriers between the three equivalent $C_{2v}$ minima. Davy and Schaefer[13] found the energy difference between the $D_{3h}$ minimum and $C_{2v}$ minima to be 490 $cm^{-1}$. The barriers between the three $C_{2v}$ minima would be lower than that. For all vibrational frequencies except that at 368 $cm^{-1}$ and 753 $cm^{-1}$, these considerations indicate that the zero-point energies are greater than the barrier height between the three equivalent mini-wells. The zero-point energy of stretching modes (1500 and 2010 $cm^{-1}$) should be above the barrier and may be perturbed strongly. At a time scale slow compared to molecular vibrations, in particular during a molecular rotation, the structure is $D_{3h}$, but at the time scale of molecular vibrations there are interactions that split the degeneracy of the modes normally associated with a $D_{3h}$ molecule.

*Acknowledgement*

The support from Dr. R. Davy and Dr. K. Kawaguchi by sharing important information about their research results is greatly appreciated. I want to thank Prof. H. F. Schaefer and A. Weaver for communicating their results prior to publication, and also Prof. E. Hirota for very helpful discussion. This work was supported by the Director, Office of Energy Research, Office of Basic energy Sciences, Chemical Sciences Division of the U.S. Department of Energy under Contract No. DE-AC03-76SF00098.

**References**

1. D. A. Ramsay, Proc. Colloq. Spectrosc. Int. **10**, 583 (1962).

2. W. J. Marinelli, D. M. Swanson, and H. S. Johnston, J. Chem. Phys. **76**, 2864 (1982).

3. A. E. Douglas, J. Chem. Phys. **45**, 1007 (1966).

4. T. Ishiwata, I. Fugiwara, Y. Naruge, K. Obi, and I. Tanaka, J. Phys. Chem. **87**, 1349 (1983).

5. H. H. Nelson, L. Pasternack, and J. R. McDonald, J. Phys. Chem. **87**, 1286 (1983).

6. T. Ishiwata, I. Tanaka, K. Kawaguchi, and E. Hirota, J. Chem. Phys. **82**, 2196 (1985).

7. R. R. Friedl and S. P. Sander, J. Phys. Chem. **91**, 2721 (1987).

8. K. Kawaguchi, E. Hirota, T. Ishiwata, and I. Tanaka, J. Chem. Phys. **93**, 951 (1990).

9. A. Weaver, D. W. Arnold, S. E. Bradforth, and D. M. Neumark, submitted to J. Chem. Phys.

10. A. Lund and K. Thuomas, Chem. Phys. Lett. **44**, 569 (1976).

11. P. E. M. Siegbahn, J. Comput. Chem. **6**, 182 (1985).

12. R. C. Boehm and L. L. Lohr, J. Phys. Chem. **93**, 3430 (1989).

13. R. D. Davy and H. F. Schaefer III, J. Chem. Phys. **91**, 4410 (1989).

14. U. Kaldor, Chem. Phys. Lett. **166**, 599 (1990).

15. B. Kim, B. L. Hammond, W. A. Lester, Jr., and H. S. Johnston, Chem. Phys. Lett. **168**,131 (1990).

16. R. D. Davy (private communication).

17. V. R. Morris, S. C. Bhatia, and J. H. Hall, J. Phys. Chem. to be published.

18. B. Kim, H. S. Johnston, D. A. Clabo, Jr., and H. F. Schaefer III, J. Chem. Phys. **88**, 3204 (1988).

19. B. Kim ; HONDO 7.0 and Restricted HF wave functions with DZP basis set were used in calculation.

20. J. P. Devlin and I. C. Hisatsune, Spectrochim. Acta **17**, 206 (1961).

21. ACUCHEM, Computer program to solve chemical kinetics problem, written by Walter Braun and John T. Herron, Chemical Kinetics Division and David Kahaner, Scientific Computing Division, National Bureau of Standards, Gaithersburg, Md 20899

22. M. D. Morse, J. B. Hopkins, P. R. R. Langridge-Smith, and R. E. Smalley, J. Chem. Phys. **79**, 5316 (1983).

Table I. Dispersed fluorescence with 15109 $cm^{-1}$ excitation (Figure 3)

| $\bar{\nu}$,$cm^{-1}$ | $\Delta\bar{\nu}$,$cm^{-1}$ | intensity | assignment | $\Delta_b$,$cm^{-1}$ | sharp?[c] |
|---|---|---|---|---|---|
| 15109 | 0 | 166 | 0−0 transition | | |
| 14742 | 368 | 17 | $\nu_4$[a] | 0 | N |
| 14425 | 684 | 3 | $\nu_1 - \nu_4$ | 1 | ? |
| 14356 | 753 | 11 | $\nu_3$ | 0 | Y |
| 14056 | 1053 | 100 | $\nu_1$ | 0 | Y |
| 13935 | 1174 | shoulder | ($\nu_4$ + B[d]) | −31 | ? |
| 13689 | 1420 | 6 | $\nu_1 + \nu_4$ | 1 | N |
| 13609 | 1500 | 51 | $\nu_2$ | 0 | Y |
| 13310 | 1799 | 6 | $\nu_1 + \nu_3$ | 7 | Y |
| 13186 | 1923 | 4 | ($\nu_4$ + 2 X B[d]) | −5 | N |
| 13099 | 2010 | 14 | A[e] | 0 | Y |
| 12994 | 2115 | 24 | $2\nu_1$ | −9 | Y |
| 12959 | 2150 | 15 | $\nu_1 + 3\nu_4$ | 7 | N |
| 12751 | 2358 | 7 | $\nu_4$ + A | 18 | Y |
| 12624 | 2481 | shoulder | $2\nu_1 + \nu_4$ | 2 | ? |
| 12598 | 2511 | 27 | $\nu_1 + \nu_3 + 2\nu_4$ | 31 | Y |
| 12572 | 2537 | shoulder | $\nu_1 + \nu_2$ | 16 | ? |
| 12301 | 2808 | 6 | $2\nu_1 + \nu_3$ | 51 | Y |
| 12111 | 2998 | 9 | $2\nu_2$ | 2 | Y |
| 12046 | 3063 | 10 | $\nu_1$ + A | 0 | Y |
| 11953 | 3156 | 10 | $3\nu_1$ | 3 | Y |
| 11766 | 3343 | 5 | | | ? |
| 11597 | 3512 | 4 | $\nu_2$ + A | −2 | ? |
| 11217[f] | 3892 | | $3\nu_1 + \nu_3$ | 20 | ? |

[a] The numbering of the vibrational mode is based on $C_{2v}$ structure. See Figure 17 for the description of $NO_3$ normal vibrations

[b] The deviation between the expected harmonic position and the observed position in $cm^{-1}$.

[c] The shape of the band. Y indicates that the band shows a spike, N indicates no spike, and ? means "not clear".

[d] B = 775 $cm^{-1}$. This is just a trial to match the number. 775 $cm^{-1}$ is another observed band position with 16053 and 16555 $cm^{-1}$ excitation.

[e] This is a band which could not be assigned with the combination of 4 fundamental frequencies. See text.

[f] This is a band observed with S1 Photomultiplier which has better red sensitivity.

Table II. The location of the sharp spike

| $\lambda_{ex}$ ($cm^{-1}$) | peak position | $\Delta$($cm^{-1}$) | data file | Figure |
|---|---|---|---|---|
| (A) 711.3 nm peak | | | | |
| 15018 | 13967 | 1051 | 2246i | 5-1A |
| 15069 | 14017 | 1052 | 2246j | 5-1B |
| 15107 | 14057 | 1050 | 2266ade | |
| 15109 | 14056 | 1053 | k6d | 5-1C |
| 15110 | 14057 | 1053 | 2267d | |
| 15111 | 14059 | 1052 | 2278eg | |
| 15111 | 14059 | 1052 | 2281cde | |
| 15114 | 14063 | 1051 | 2282abc | |
| 15127 | 14075 | 1052 | 2243g | |
| (B) 734.9 nm peak | | | | |
| 15018 | 13518 | 1500 | 2246i | 5-1A |
| 15069 | 13569 | 1500 | 2246j | 5-1B |
| 15069 | 13569 | 1500 | 2246m | |
| 15109 | 13609 | 1500 | k6d | 5-1C |
| 15110 | 13609 | 1501 | 2265a | |
| 15111 | 13613 | 1498 | 2281cde | |
| 15113 | 13611 | 1502 | 2245hi | |
| 15127 | 13626 | 1501 | 2243h | |
| (C) 696.9 nm peak | | | | |
| 15107 | 14355 | 752 | 2266d | |
| 15109 | 14356 | 753 | k7a | 5-2A |
| 15111 | 14359 | 752 | 2281cde | |
| 15113 | 14357 | 756 | 2245p | |
| 15127 | 14372 | 755 | 2243fgh | 5-2B |
| 15127 | 14372 | 755 | 2244m | |
| (D) 763.4 nm peak | | | | |
| 15069 | 13059 | 2010 | 2246k | 5-3A |
| 15107 | 13100 | 2007 | 2266ade | |
| 15109 | 13099 | 2010 | k6f | |
| 15111 | 13103 | 2008 | 2281fgh | 5-3B |
| 15127 | 13116 | 2011 | 2244k | |
| 15129 | 13119 | 2010 | 2265fg | 5-3C |
| (E) 769.7 nm peak | | | | |
| 15069 | 12954 | 2115 | 2246k | 5-3A |
| 15107 | 12991 | 2116 | 2266ade | |
| 15111 | 12996 | 2115 | 2281fgh | 5-3B |
| 15127 | 13009 | 2118 | 2244k | |
| 15129 | 13011 | 2118 | 2265f | 5-3C |

Table III. The pressure dependence of the fluorescence bandwidth

| frequency ($cm^{-1}$) | pressure (mTorr) | peak ratio[a] | FWHM ($cm^{-1}$) | pressure (mTorr) | peak ratio | FWHM ($cm^{-1}$) |
|---|---|---|---|---|---|---|
| 368 | 590 | no spike | 67 | 140 | no spike | 63 |
| 1053 | 590 | 0.045 | 67 | 140 | 0.171 | 57 |
| 1500 | 620 | 0.032 | 72 | 140 | 0.051 | 65 |
| 2511 | 580 | 0.009 | 115 | 200 | 0.023 | 101 |

[a] This is the ratio of the area of the sharp spike to that of the area under the broad band. The area of the broad band is integrated over 200 $cm^{-1}$ centered around the sharp spike. For the area of the spike the area under the broad band is excluded.

Table IV. The ratios of the height of the sharp spike to the broad band for several vibrational bands at the frequency of spike. $\lambda_{ex}$ = 15109 $cm^{-1}$. Total pressure was 120 mTorr. The height of the spike is measured from the top of the spike to the top of broad band contour.

| frequency( $cm^{-1}$) | ratio |
|---|---|
| 753 | 0.85 |
| 1053 | 0.93 |
| 1500 | 0.80 |
| 1798 | 0.80 |

Table V. Dispersed fluorescence with 16053[a] $cm^{-1}$ excitation (Figure 8)

| $\bar{\nu}$, $cm^{-1}$ | $\Delta\bar{\nu}$, $cm^{-1}$ | assignment | $\Delta$, $cm^{-1}$ | sharp? |
|---|---|---|---|---|
| 15693 | 360 | $\nu_4$ | 8 | N |
| 15534 | | *[b] | | N |
| 15281 | 772 | B[c] | | N |
| 15110 | | * (15109 $cm^{-1}$ → ground state) | −1 | N |
| 15003 | 1050 | $\nu_1$ | 3 | Y |
| 14876 | 1177 | B + $\nu_4$ | −34 | N |
| 14719 | 1334 | * (15109 $cm^{-1}$ → 368 $cm^{-1}$) | −22 | |
| 14556 | 1497 | $\nu_2$ | 3 | Y |
| 14434 | | * | −14 | N |
| 14233 | 1820 | $\nu_1 + \nu_3$ | 5 | |
| 14128 | 1925 | $\nu_4$ + 2 X B[d] | 5 | |
| 14061 | | * (15109 $cm^{-1}$ → 1053 $cm^{-1}$) | | N |
| 14033 | 2020 | | | |
| 13939 | 2114 | $2\nu_1$ | 1 | Y |
| 13643 | 2410 | * (15109 $cm^{-1}$ → 1500 $cm^{-1}$) | 44 | N |
| 13427 | 2626 | | | |
| 13156 | 2897 | | | |
| 13055 | 2998 | $2\nu_2$ | 2 | |
| 12899 | 3154 | $3\nu_1$ | 5 | Y |
| 12712 | 3341 | | | |
| 12664 | 3389 | | | |
| 12619 | 3434 | | | |
| 12518 | 3535 | | | |
| 12446 | 3607 | | | |

| | | | | |
|---|---|---|---|---|
| 12427 | 3627 | $2\nu_1 + \nu_2$ | −21 | Y |
| 12255 | 3798 | | | |
| 12023 | 4030 | | | |
| 11852 | 4201 | $4\nu_1$ | 11 | Y |

[a] T + 944 $cm^{-1}$.

[b] a fluorescence band which is collisionally induced.

[c] a band which is not observed with 15109 $cm^{-1}$ excitation. See text.

[d] This band is seen with 15109 $cm^{-1}$ excitation. The assignment is tentative.

Table VI. Dispersed fluorescence with 16555 $cm^{-1}$ [a] excitation. (Figure 9, k11f.dat)

| $\bar{\nu}$, $cm^{-1}$ | $\Delta\bar{\nu}$, $cm^{-1}$ | assignment | $\Delta$, $cm^{-1}$ | sharp? |
|---|---|---|---|---|
| 16185 | 370 | $\nu_4$ | −2 | |
| 16053 | | * (16053 $cm^{-1}$ → ground state) | | |
| 15777 | 778 | B | −3 | |
| 15715 | | * (16053 $cm^{-1}$ → 368 $cm^{-1}$) | 30 | N |
| 15501 | 1054 | $\nu_1$ | −1 | |
| 15372 | 1182 | B + $\nu_4$ | −39 | |
| 15130 | | * (15109 $cm^{-1}$ → ground state) | −21 | N |
| 14907 | 1647 | | | |
| 14760 | 1795 | * (15109 $cm^{-1}$ → 368 $cm^{-1}$) | −14 | N |
| 14438 | 2116 | $2\nu_1$ | −10 | Y |
| 14345 | | | | |
| 14300 | 2254 | $3\nu_3$ | 5 | |
| 14063 | | * (15109 $cm^{-1}$ → 1053 $cm^{-1}$) | 7 | N |
| 13748 | 2806 | $2\nu_1 + \nu_3$ | 53 | |
| 13628 | | * (15109 $cm^{-1}$ → 1500 $cm^{-1}$) | 19 | N |
| 13235 | 3319 | | | |
| 12996 | 3558 | | | |

[a] T + 1446 $cm^{-1}$.

Table VII. Dispersed fluorescence with 15882[c] $cm^{-1}$ excitation. (Figure 10)

| $\bar{\nu}$, $cm^{-1}$ | $\Delta\bar{\nu}$, $cm^{-1}$ | assignment | $\Delta$, $cm^{-1}$ | sharp? |
|---|---|---|---|---|
| 16053 | | * (16053 $cm^{-1}$ → ground state) | | N |
| 15687 | | * (16053 $cm^{-1}$ → 368 $cm^{-1}$) | 2 | N |
| 15123 | | *[b] (15109 $cm^{-1}$ → ground state) | 14 | N |
| 14828 | 1054 | $\nu_1$ | −1 | Y |
| 14758 | | * (15109 $cm^{-1}$ → 368 $cm^{-1}$) | 17 | N |
| 14666 | 1216 | | | |
| 14461 | 1421 | | | |
| 14380 | 1502 | $\nu_2$ | −2 | |
| 14275 | 1607 | | | |
| 14073 | | * (15109 $cm^{-1}$ → 1053 $cm^{-1}$) | 17 | N |
| 13953 | 1929 | | | |
| 13763 | 2119 | $2\nu_1$ | −4 | ? |
| 13628 | | * (15109 $cm^{-1}$ → 1500 $cm^{-1}$) | 19 | N |
| 13367 | 2515 | $\nu_1 + \nu_2$ | −4 | ? |
| 13244 | 2638 | | | |
| 13040 | 2842 | | | |
| 13004 | 2878 | | | |
| 12722 | 3160 | $3\nu_3$ | −4 | |
| 12414 | 3468 | | | |
| 12371 | 3511 | | | |
| 12130 | 3752 | | | |

| | | | | |
|---|---|---|---|---|
| 11975 | 3907 | | | |

[a] This is the fluorescence emitted from the vibrational state at 16053 $cm^{-1}$.

[b] This is the fluorescence from the vibrationless state at 15109 $cm^{-1}$.

[c] T + 773 $cm^{-1}$.

Table VIII. Fundamental Frequencies for similar molecules and those obtained by ab initio calculation with comparison to $NO_3$

| normal mode[a] | $FNO_2$ | | $NO_2Cl$ | $NO_3$ | | | | | | |
|---|---|---|---|---|---|---|---|---|---|---|
| | | | | $C_{2v}$ | | | | $D_{3h}$ | | |
| | ab initio[b] | Exp.[c] | Exp.[d] | ab initio[e] | ab initio[f] | ab initio[g] | Exp.[h] | ab initio[i] | ab initio[j] | Exp.[k] |
| $\nu_1(a_1)$ | 1122 | 822 | 794 | 1112 | 1122 | 1024 | 1053 | 1068 | 1133 | 1060 |
| $\nu_2(a_1)$ | 1559 | 1310 | 1294 | 1562 | 1590 | 1483 | 1500 | 963 | 1163 | 1492 |
| $\nu_3(a_1)$ | 774 | 568 | 367 | 738 | 741 | 682 | 753 | . | . | . |
| $\nu_4(b_1)$ | 886 | 742 | 651 | 884 | 877 | 801 | 775 | . | 776 | 762 |
| $\nu_5(b_2)$ | 1972 | 1792 | 1685 | 1864 | 2005 | 1843 | 2010 | . | . | . |
| $\nu_6(b_2)$ | 687 | 560 | 411 | 595 | 686 | 506 | 368 | 596i | 277 | 380 |

[a] See Figure 16.

[b] Reference 19.

[c] Reference 20.

[d] Reference 20.

[e] Reference 15. TZP basis set Restricted HF calculation.

[f] Reference 17. DZP basis set Unrestricted HF calculation.

[g] Reference 16. DZP basis set CISD calculation.

[h] This experiment. Tentative assignment when $C_{2v}$ symmetry is assumed, the 775 $cm^{-1}$ band and the 2010 $cm^{-1}$ band are regarded as additional fundamental frequencies. It is possible that 775 $cm^{-1}$ band and 368 $cm^{-1}$ band might have to be interchanged.

[i] Reference 13. $D_{3h}$ geometry was assumed.

[j] Reference 14. $D_{3h}$ frequency was calculated.

[k] Reference 6, 7. $D_{3h}$ assignment.

**Figure caption**

In all figures the Y-axis is in arbitrary unit and represents the intensity of the fluorescence signal.

Figure 1. The experimental set up of the laser induced fluorescence experiment. An IBM At computer controls dye laser stepping motor, photon counter, and the momochromator. MW discharge represents a microwave discharge.

Figure 2. System response data (wsc154c.spr). The fluorescence data were corrected to account for the nonuniform response of the system (the quantum yield of photocathode and the grating). This was accomplished by a tungsten lamp at a temperature T scanned by a monochromator and collected by the same PMT.

Figure 3. Dispersed fluorescence with 15109 $cm^{-1}$ excitation. The x axis is the frequency of the fluorescence subtracted by the excitation frequency ($\Delta\nu$). The sharp spike at the excitation frequency is about 50 % scattered

laser light. The spectrum on the right side of the dotted line is magnified by 5 times to show details. The fluorescence was detected to 900 nm (4000 $cm^{-1}$).

Figure 4. The two different bandshapes. $\lambda_{ex}$ = 15109 $cm^{-1}$. Presents the bands at 1799 and 1923 $cm^{-1}$. 1799 $cm^{-1}$ band corresponds to $\nu_1 + \nu_3$.

Figure 5. The frequencies of the excitation laser and the vibrational bands are listed below. The frequency of the sharp spikes moves along with the change of $\lambda_{ex}$ (excitation frequency), while that of broad bands does not move.

$\Delta = \lambda_{ex}$ - peak position.

| $\lambda_{ex}$ ($cm^{-1}$) | peak position | $\Delta$ ($cm^{-1}$) | data file | Figure |
|---|---|---|---|---|
| (A) 711.3 nm peak | | | | |
| 15018 | 13967 | 1051 | 2246i | 5-1A |
| 15069 | 14017 | 1052 | 2246j | 5-1B |
| 15109 | 14056 | 1053 | k6d | 5-1C |
| (B) 734.9 nm peak | | | | |
| 15018 | 13518 | 1500 | 2246i | 5-1A |
| 15069 | 13569 | 1500 | 2246j | 5-1B |
| 15109 | 13609 | 1500 | k6d | 5-1C |

(C) 696.9 nm peak

| | | | | |
|---|---|---|---|---|
| 15109 | 14356 | 753 | k7a | 5-2A |
| 15127 | 14372 | 755 | 2243fgh | 5-2B |

(D) 763.4 nm peak

| | | | | |
|---|---|---|---|---|
| 15069 | 13059 | 2010 | 2246k | 5-3A |
| 15111 | 13103 | 2008 | 2281fgh | 5-3B |
| 15129 | 13119 | 2010 | 2265fg | 5-3C |

(E) 769.7 nm peak

| | | | | |
|---|---|---|---|---|
| 15069 | 12954 | 2115 | 2246k | 5-3A |
| 15111 | 12996 | 2115 | 2281fgh | 5-3B |
| 15129 | 13011 | 2118 | 2265f | 5-3C |

Figure 6. Pressure dependence of the fluorescence bandwidth.

Fig. 6-1 : 368 $cm^{-1}$ band

6-2 : 1053

6-3 : 1500

6-4 : 2511

Spectrum A is obtained at higher pressure and B is at lower pressure. (See Table III.)

Figure 7. The fluorescence spectrum obtained with 150 $\mu$m slit (2.5 $cm^{-1}$ resolution). $\lambda_{ex}$ = 15110 $cm^{-1}$. The width of the spike is reduced.

Figure 8. Dispersed fluorescence with 16053 $cm^{-1}$ excitation. This corresponds to 944 $cm^{-1}$ above 0-0 transition.

Figure 9. Dispersed fluorescence with 16555 $cm^{-1}$ excitation. This corresponds to 1446 $cm^{-1}$ above 0-0 transition.

Figure 10. Dispersed fluorescence with 15882 $cm^{-1}$ excitation. This corresponds to 773 $cm^{-1}$ above 0-0 transtion.

Figure 11. Dispersed fluorescence with 14742 $cm^{-1}$ excitation. The monochromator slits are set at 500 $\mu$. The hot band population at 368 $cm^{-1}$ is excited to $^2E'$ state. The huge spike at the excitation frequency is scattered laser light.

Figure 12. The magnified bandshape of the dispersed fluorescence when excited by 14742 $cm^{-1}$. (a) is the band which corresponds to 1500 $cm^{-1}$ vibrational state, (b) to 1053 $cm^{-1}$, and (c) to ground state. No spike is observed.

Figure 13. The change of the bandwidth of 368 $cm^{-1}$ band with the change of the excitation frequency.

| $\lambda_{ex}$ | FWHM ($cm^{-1}$) |
|---|---|
| A. 15109 $cm^{-1}$ | 67 $cm^{-1}$ |
| B. 16053 $cm^{-1}$ | 49 $cm^{-1}$ |
| C. 16555 $cm^{-1}$ | 32 $cm^{-1}$ |

Figure 14. Dispersed fluorescence spectrum of $NO_2$ at $NO_3$ excitation frequencies. The pressure of $NO_2$ was a few hundred mTorr.

A. $\lambda_{ex}$ = 15109 $cm^{-1}$

B. $\lambda_{ex}$ = 16050 $cm^{-1}$

C. $\lambda_{ex}$ = 16538 $cm^{-1}$

Figure 15. Contour diagram of the lower component of the $^2E''$ potential energy surface deduced by fitting the observed energy levels. $Q_1$ is held at its equilibrium value, and the values of $Q_x$ and $Q_y$ are in angstroms. Potential energy contours are plotted for -7.5, -5.0, 0, 50, 100 $cm^{-1}$, ..., where 0 $cm^{-1}$ corresponds to the central cusp. Adapted from Ref. 22.

Figure 16. Normal vibrations of $NO_3$. Calculated by RHF wave functions with TZP basis set at optimized $C_{2v}$ geometry[15]. For $D_{3h}$ geometry the vibrations $\nu_2$ and $\nu_5$, $\nu_3$ and $\nu_6$ are degenerate.

Figure 17. Magnified $NO_3$ excitation spectrum around 15109 $cm^{-1}$ (A) and 14742 $cm^{-1}$ (B).

Figure 18. The explanation of the bandshape without sharp spike. For case (a), $\alpha$ state, which is the ground state with one quantum of 368 $cm^{-1}$ vibrational mode, has $B_2$ electronic symmetry and $b_1$ vibrational symmetry, with the total symmetry of $A_2$. For case (b), $\alpha$ state has $B_2$ electronic symmetry and $b_2$ vibrational symmetry, with the total symmetry of $A_1$.

## Appendix

### A. Assignment of vibrational bands

Expected harmonic overtone and combination band positions of $NO_3$ when the ground state geometry is $D_{3h}$. First digit for the number in the first column indicates the number of vibrational quanta in $\nu_1$, second digit in $\nu_2$, and so on. The number in second column shows the harmonic position in $cm^{-1}$.

$\nu_1$ = 1053 $cm^{-1}$ $\quad$ $\nu_3$ = 753 $cm^{-1}$
$\nu_2$ = 1500 $cm^{-1}$ $\quad$ $\nu_4$ = 368 $cm^{-1}$

| vibrational quanta | harmonic position | vibrational quanta | harmonic position |
|---|---|---|---|
| 0000 | 0 | 0007 | 2576 |
| 0001 | 368 | 0103 | 2604 |
| 0002 | 736 | 0111 | 2621 |
| 0010 | 753 | 0031 | 2627 |
| 1000 | 1053 | 2002 | 2842 |
| 0003 | 1104 | 2010 | 2859 |
| 0011 | 1121 | 1101 | 2921 |
| 1001 | 1421 | 1021 | 2927 |
| 0004 | 1472 | 0112 | 2989 |
| 0012 | 1489 | 0200 | 3000 |
| 0100 | 1500 | 0120 | 3006 |
| 0020 | 1506 | 0040 | 3012 |
| 1002 | 1789 | 3000 | 3159 |
| 1010 | 1806 | 2011 | 3227 |
| 0013 | 1857 | 1102 | 3289 |
| 0005 | 1840 | 1110 | 3306 |
| 0101 | 1868 | 1030 | 3312 |
| 0021 | 1874 | 0201 | 3368 |
| 2000 | 2106 | 0121 | 3374 |
| 1003 | 2157 | 3001 | 3527 |
| 1011 | 2174 | 2100 | 3606 |
| 0006 | 2208 | 2020 | 3612 |
| 0102 | 2236 | 1111 | 3674 |
| 0022 | 2242 | 0202 | 3736 |
| 0110 | 2253 | 0210 | 3753 |
| 0030 | 2259 | 0130 | 3759 |
| 2001 | 2474 | 3010 | 3912 |
| 1012 | 2542 | 2101 | 3974 |
| 1100 | 2553 | 1200 | 4053 |
| 1020 | 2559 | 1120 | 4059 |

## B.The circuit diagram of the photon counting board

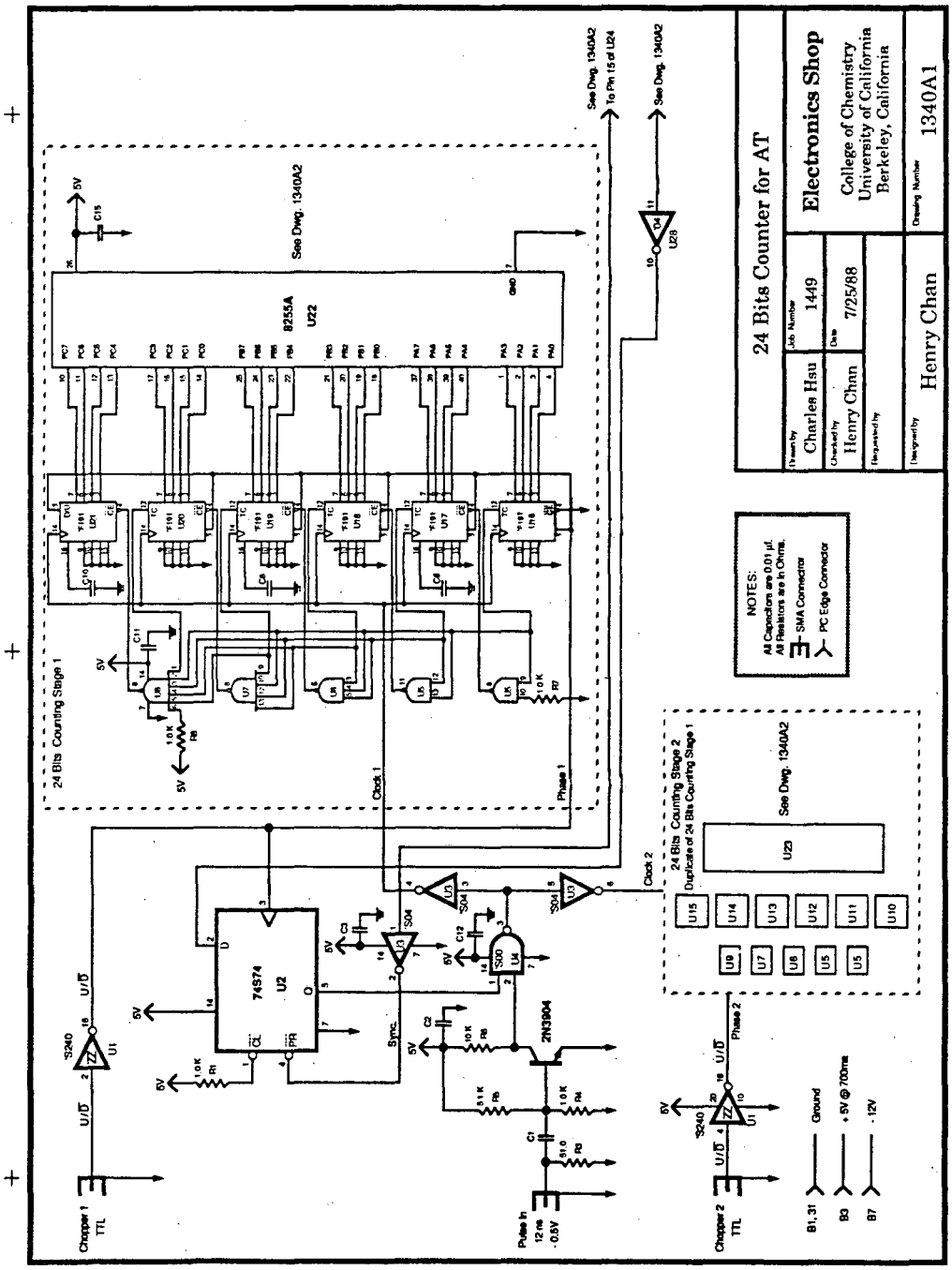

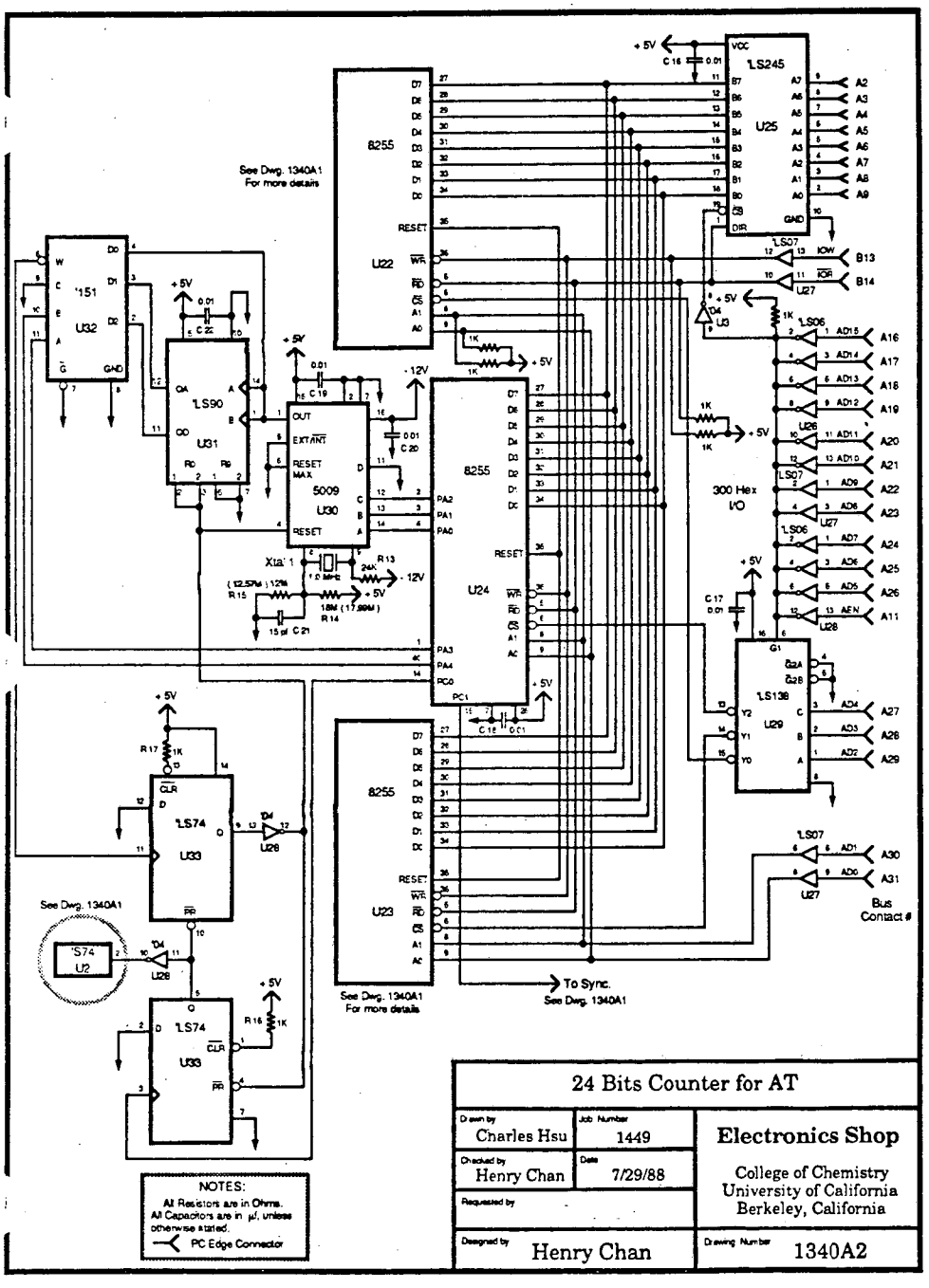
24 Bits Counter for AT
Drawn by
Charles Hsu
Job Number
1449
Checked by
Henry Chan
Date
7/29/88
Requested by
Designed by
Henry Chan
Electronics Shop
College of Chemistry
University of California
Berkeley, California
Drawing Number
1340A2
NOTES:
All Resistors are in Ohms.
All Capacitors are in µf, unless otherwise stated.
PC Edge Connector
See Dwg. 1340A1
For more details
To Sync.
See Dwg. 1340A1
300 Hex
I/O
Bus
Contact #

Figure 1

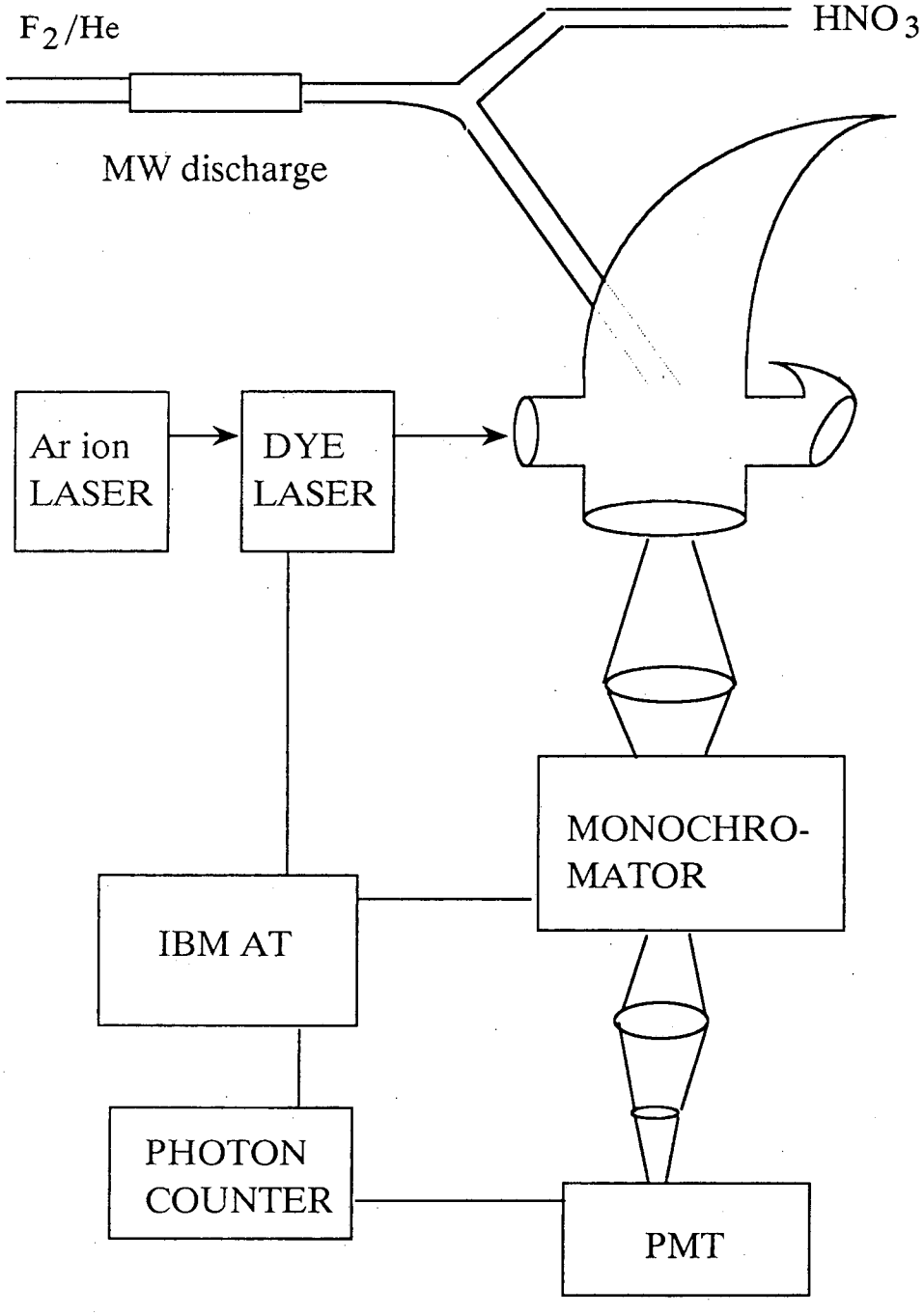
F2/He
HNO3
MW discharge
Ar ion LASER
DYE LASER
MONOCHRO-MATOR
IBM AT
PHOTON COUNTER
PMT

Figure 2

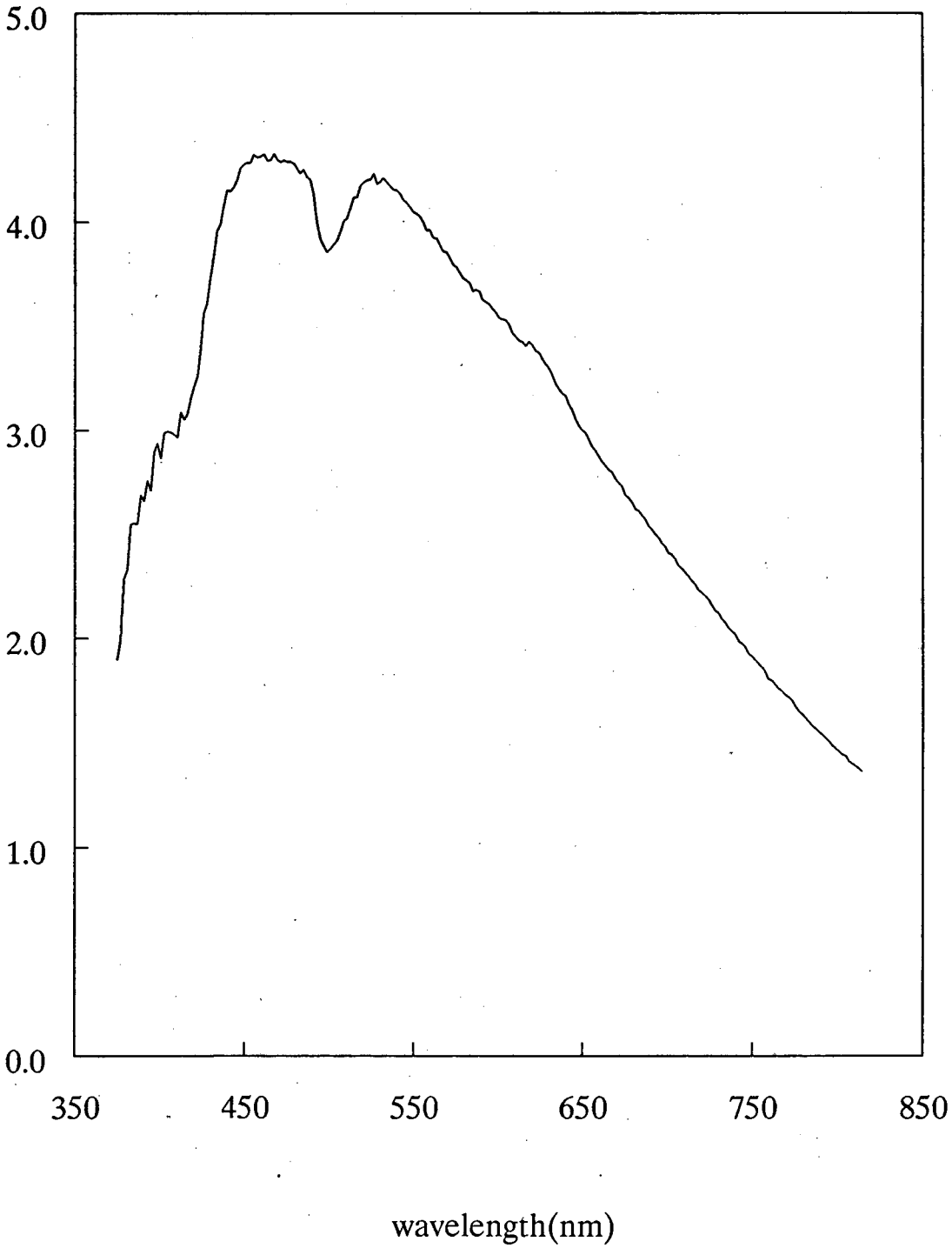

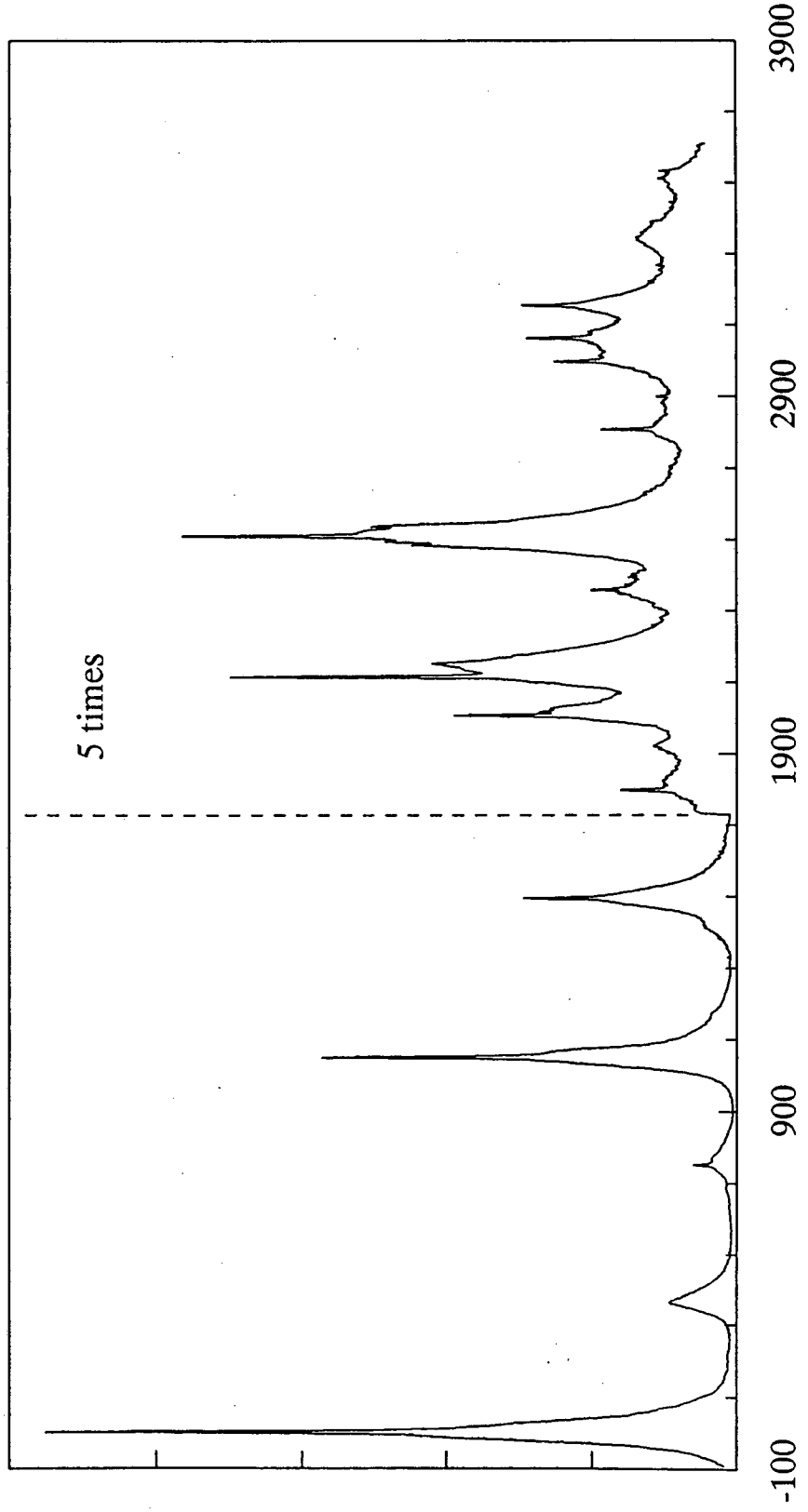


Figure 3

Figure 4

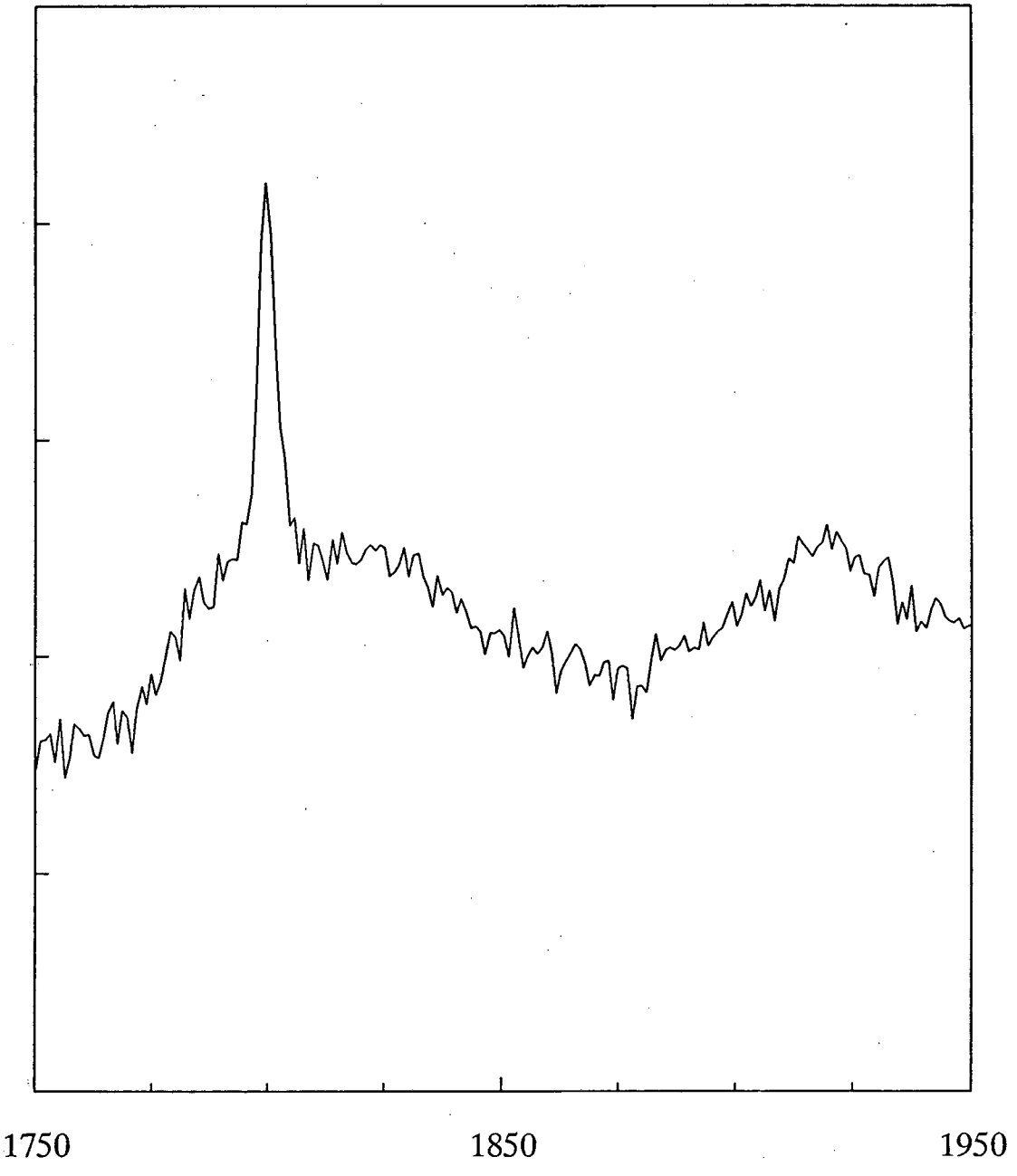

Figure 5-1

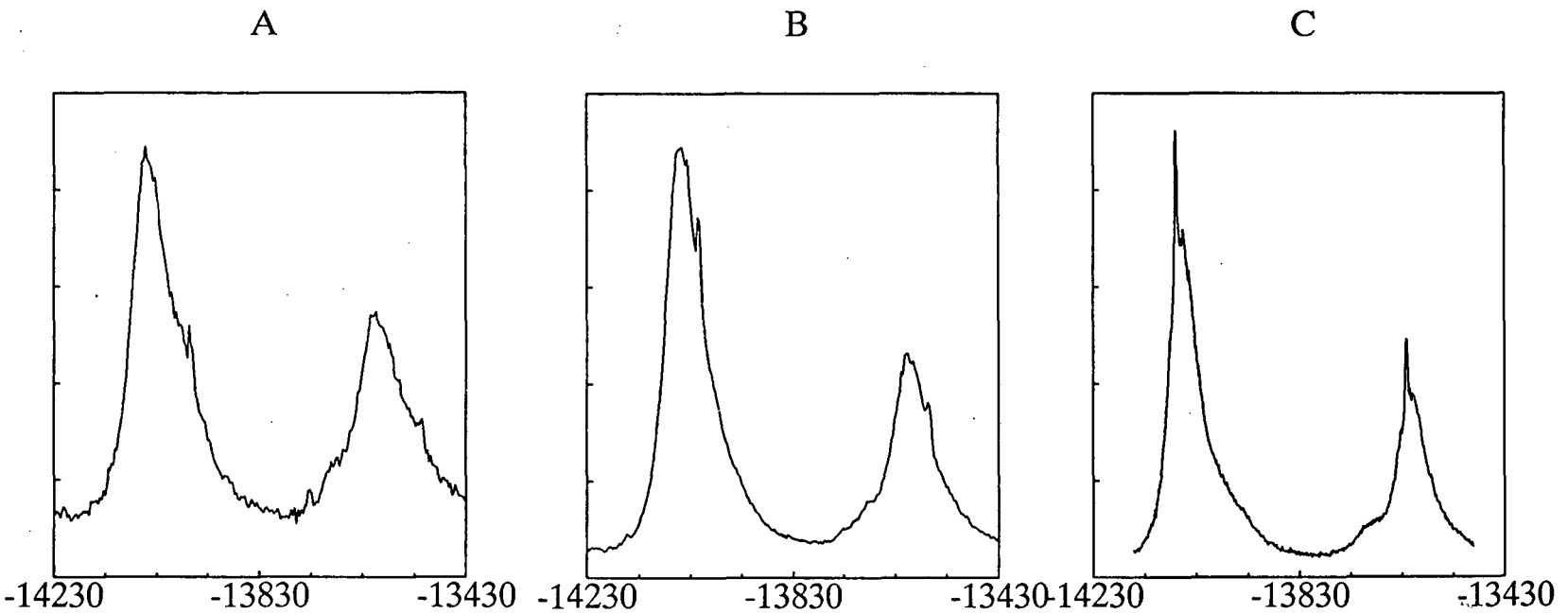
A
B
C
-14230
-13830
-13430
-14230
-13830
-13430
-14230
-13830
-13430
frequency(cm-1)
15018 cm-1 excitation
15069 cm-1 excitation
15107 cm-1 excitation

Figure 5-2

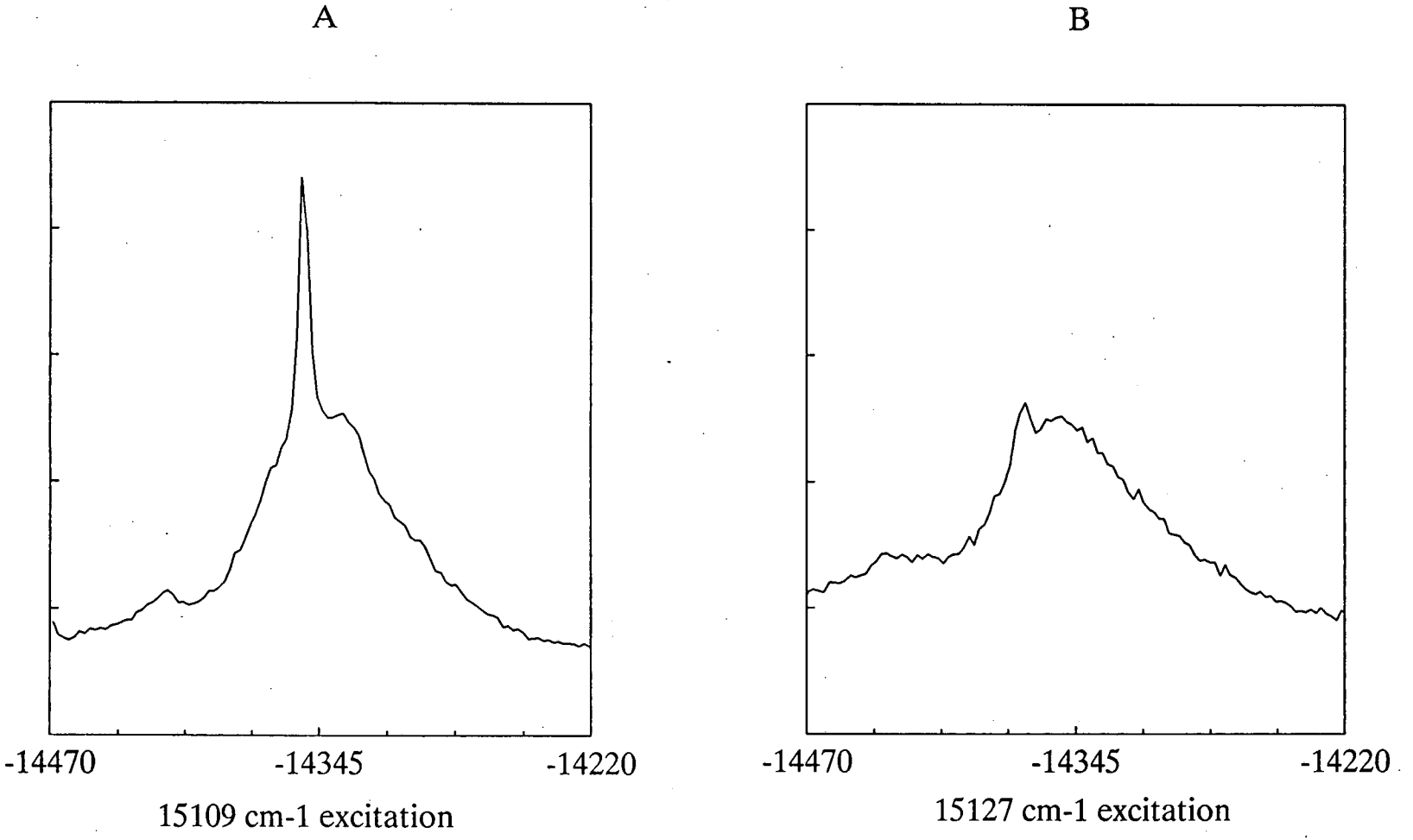
A
B
-14470
-14345
-14220
-14470
-14345
-14220
15109 cm-1 excitation
15127 cm-1 excitation
frequency(cm-1)

Figure 5-3

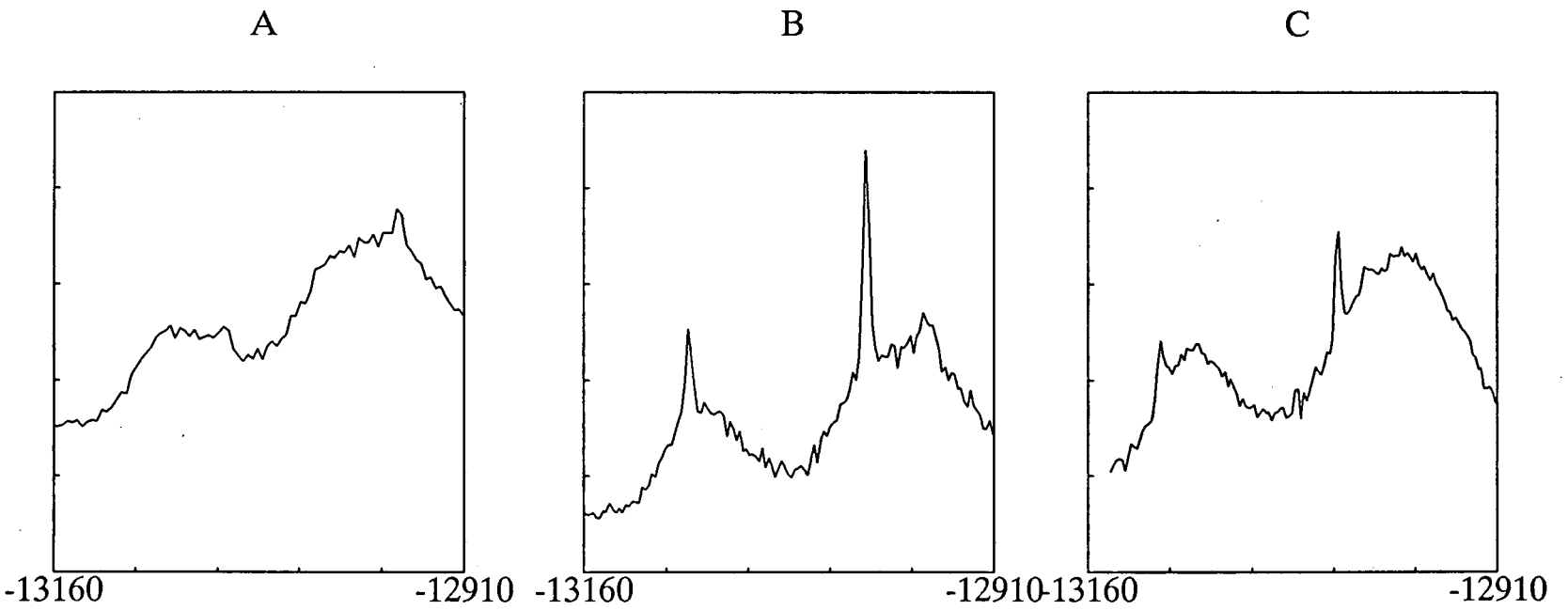
A
B
C
-13160
-12910
-13160
-12910
-13160
-12910
frequency(cm-1)
15069 cm-1 excitation
15111 cm-1 excitation
15129 cm-1 excitation

Figure 6-1

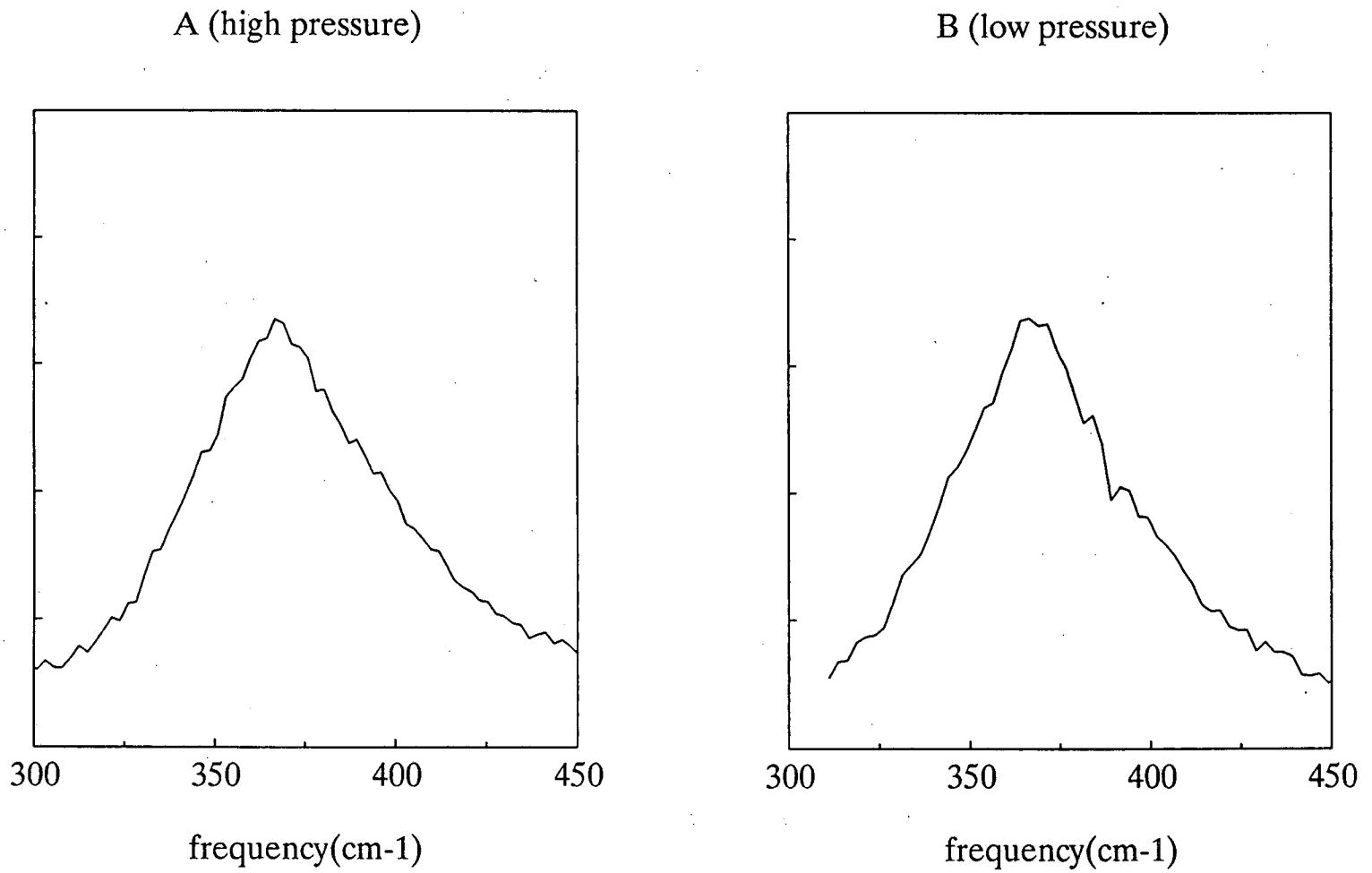
A (high pressure)
B (low pressure)
300
350
400
450
frequency(cm-1)
300
350
400
450
frequency(cm-1)

Figure 6-2

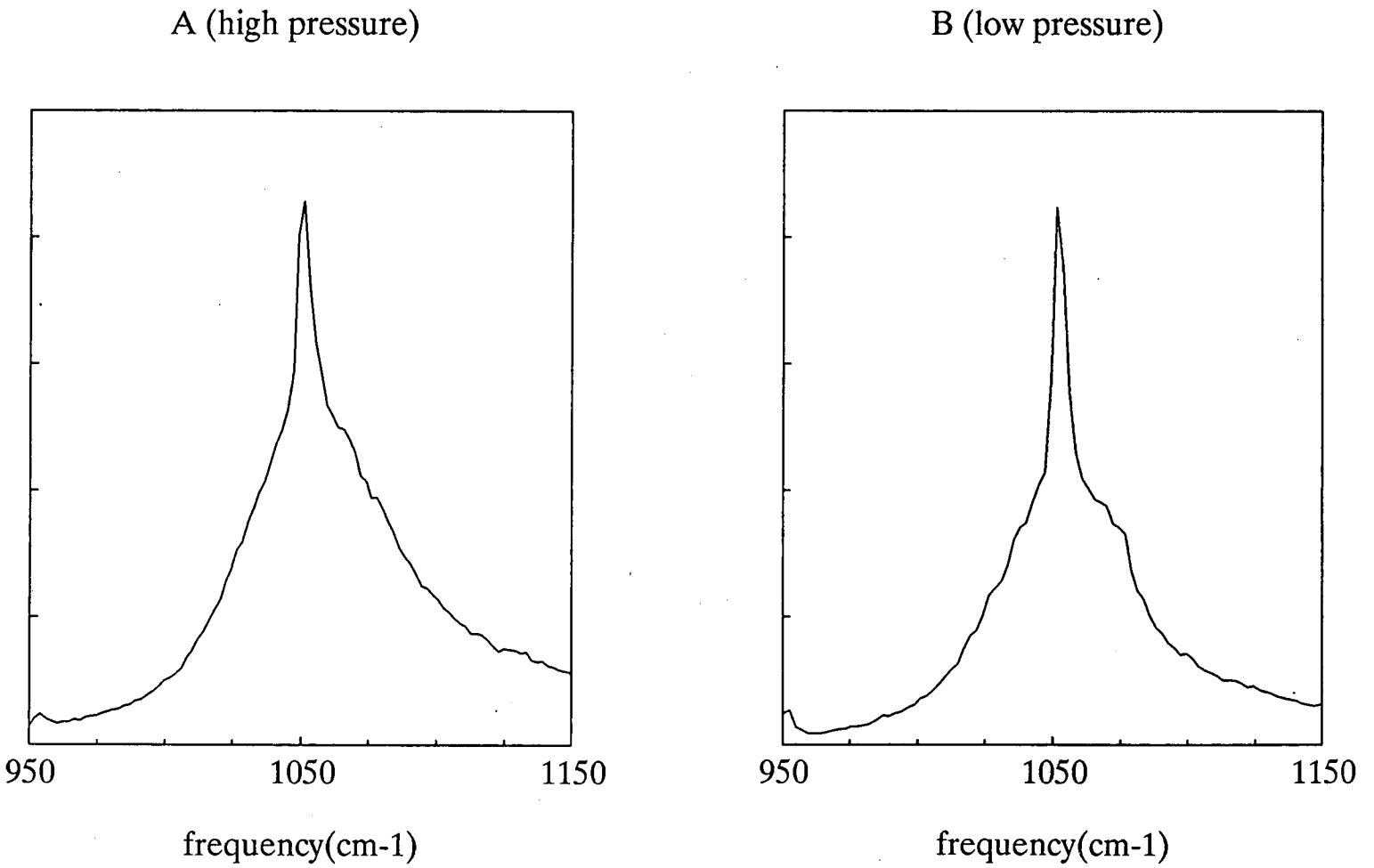
A (high pressure)
B (low pressure)
950
1050
1150
frequency(cm-1)
950
1050
1150
frequency(cm-1)

Figure 6-3

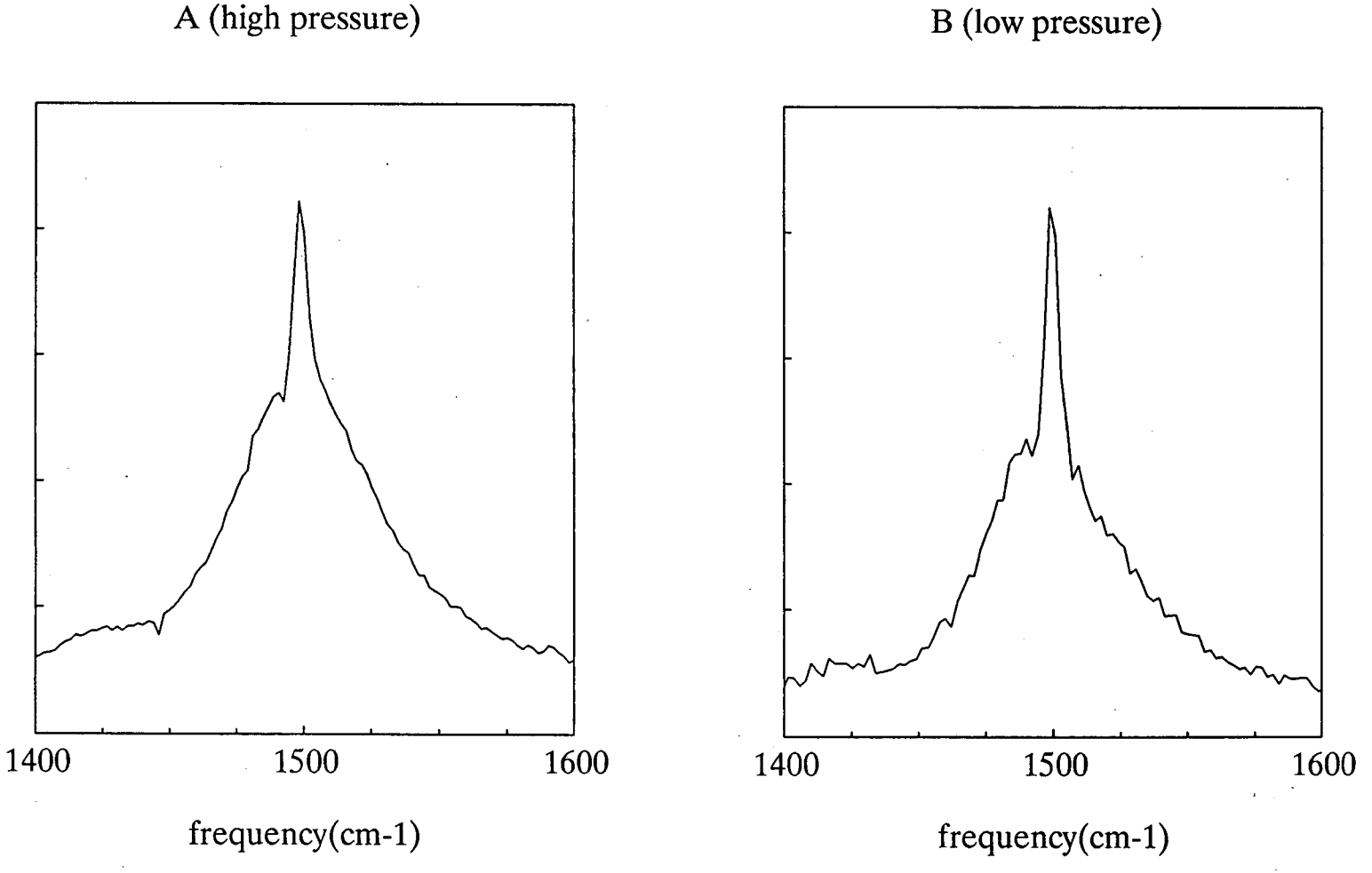
A (high pressure)
B (low pressure)
1400
1500
1600
frequency(cm-1)
1400
1500
1600
frequency(cm-1)

Figure 6-4

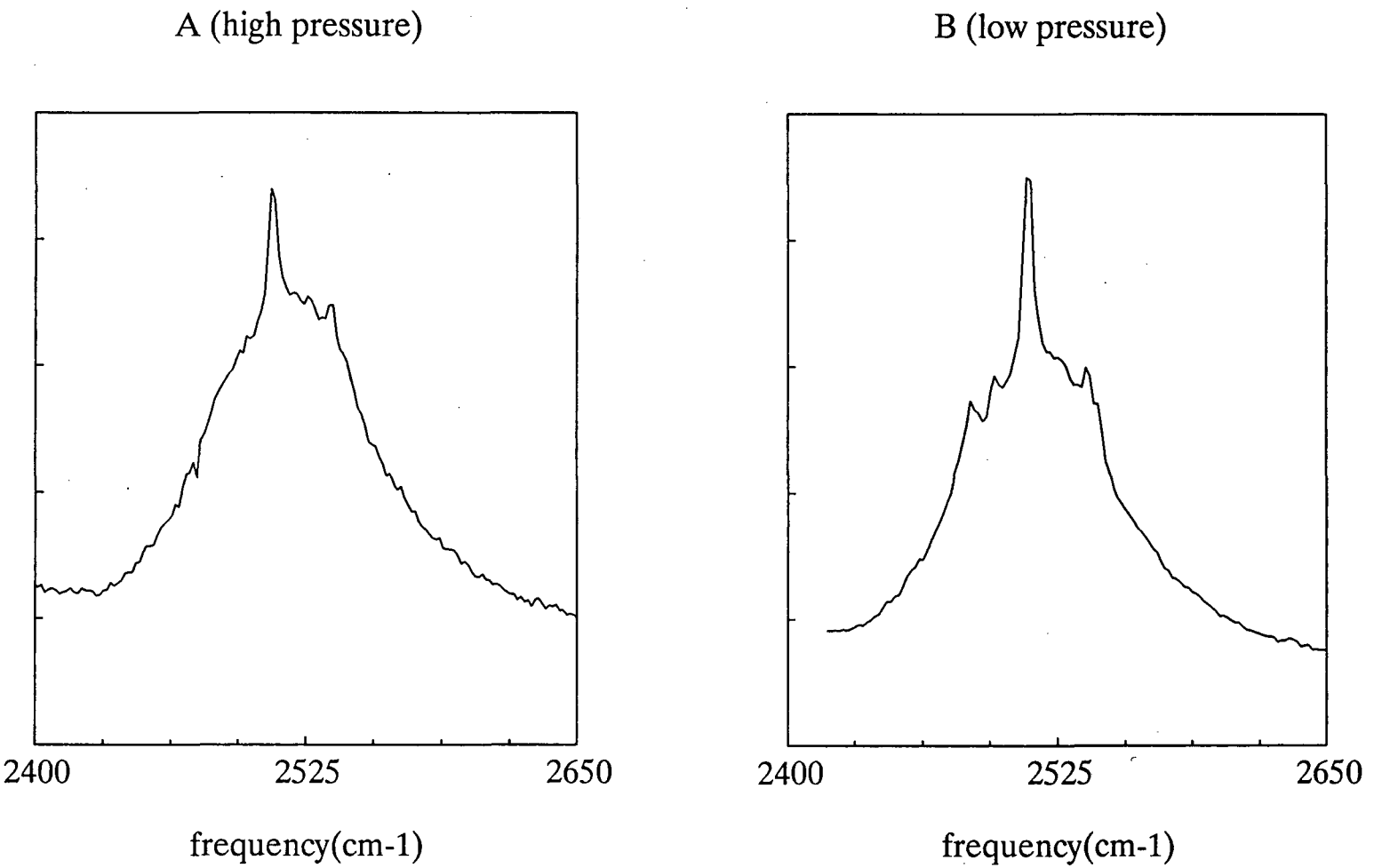
A (high pressure)
B (low pressure)
2400
2525
2650
frequency(cm-1)
2400
2525
2650
frequency(cm-1)

Figure 7

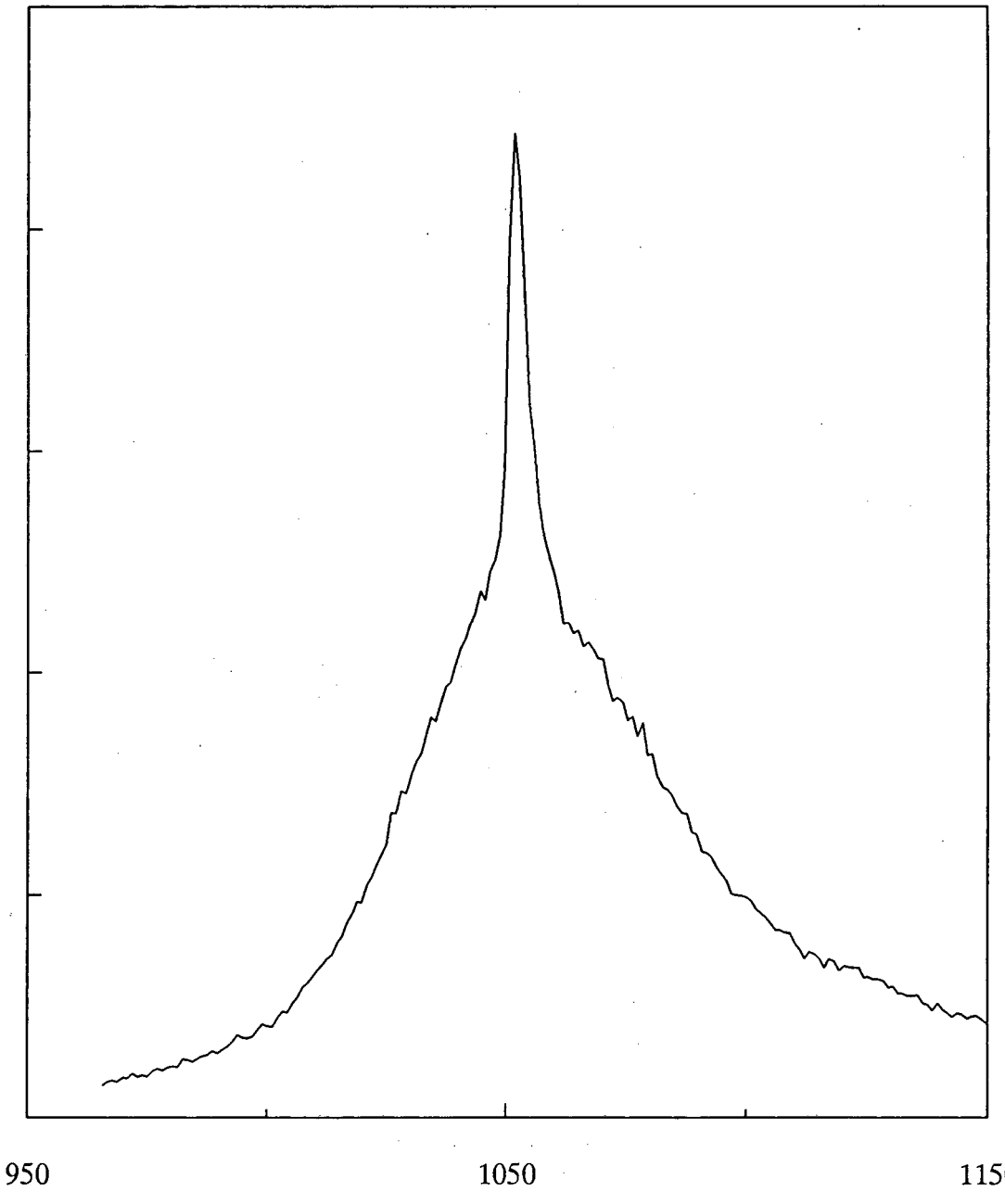

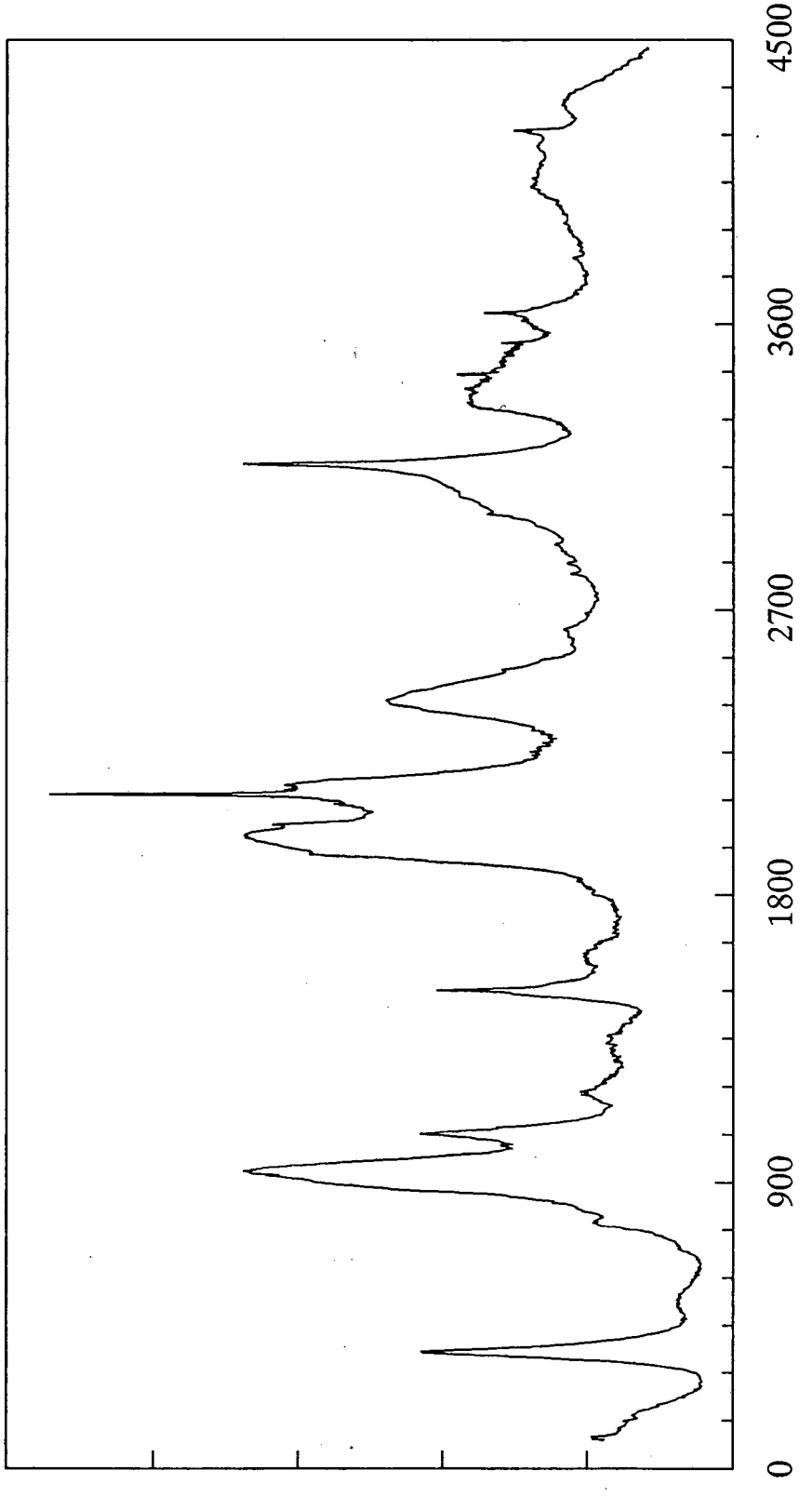


Figure 8

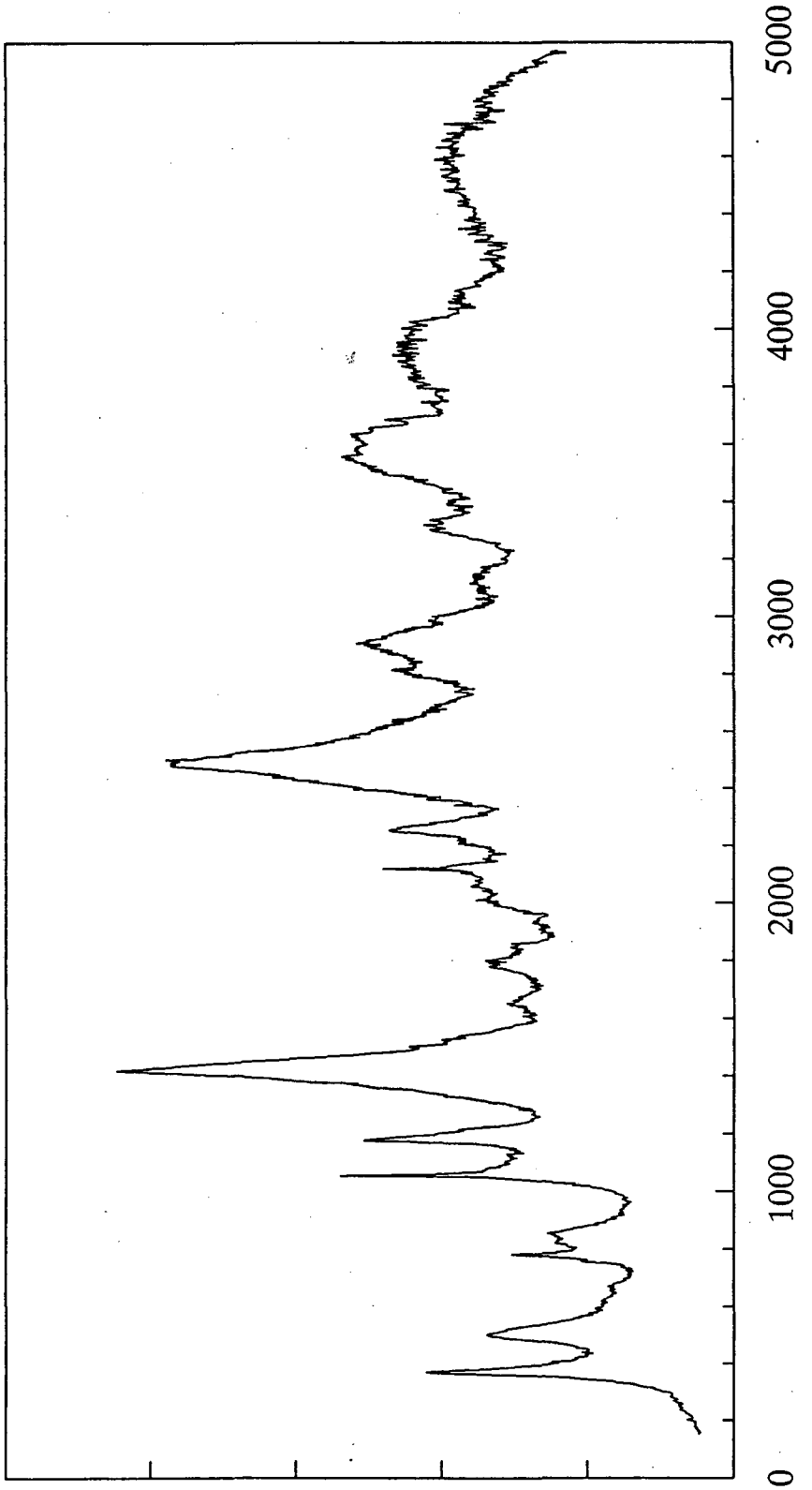


Figure 9

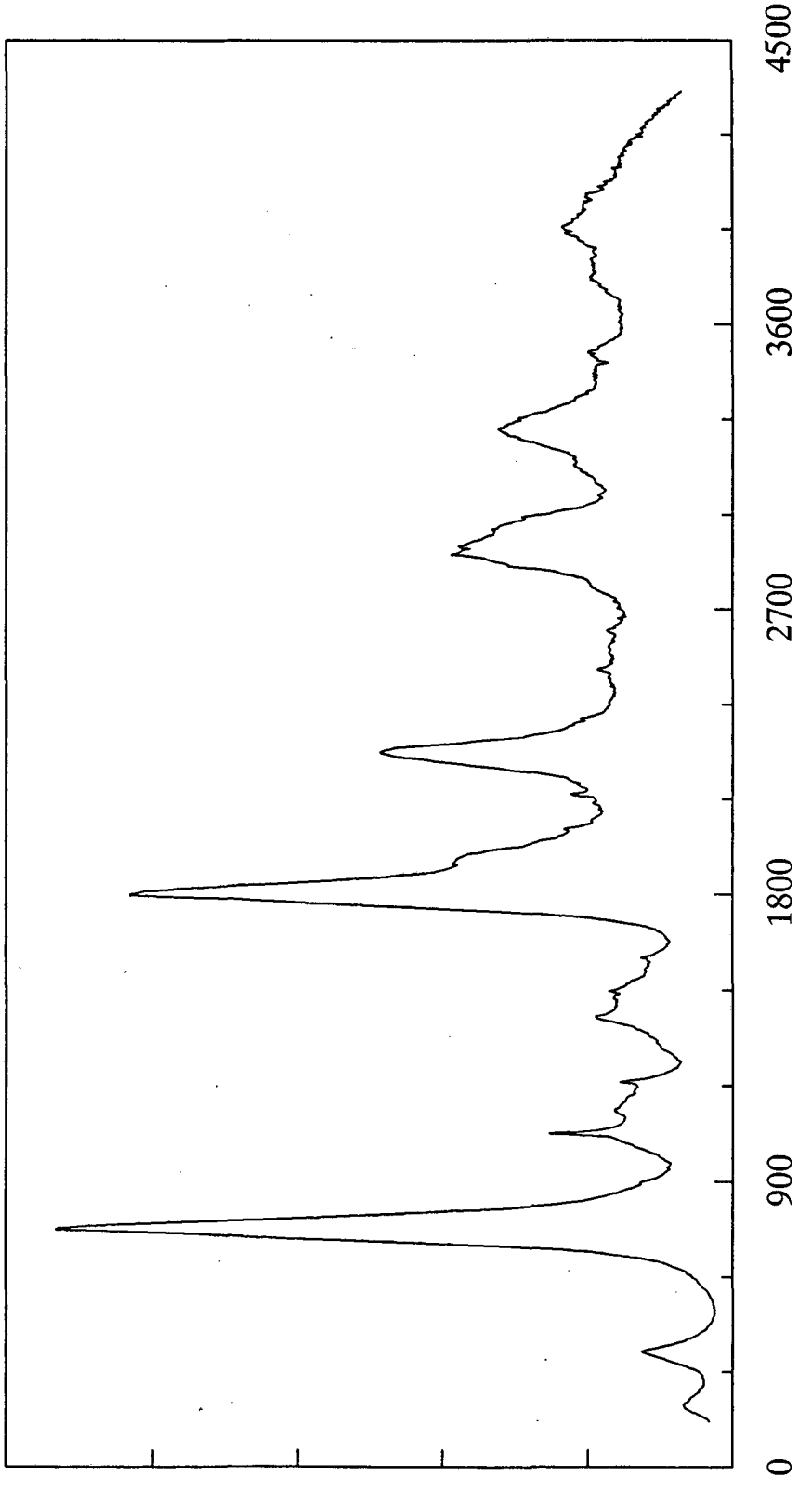


Figure 10

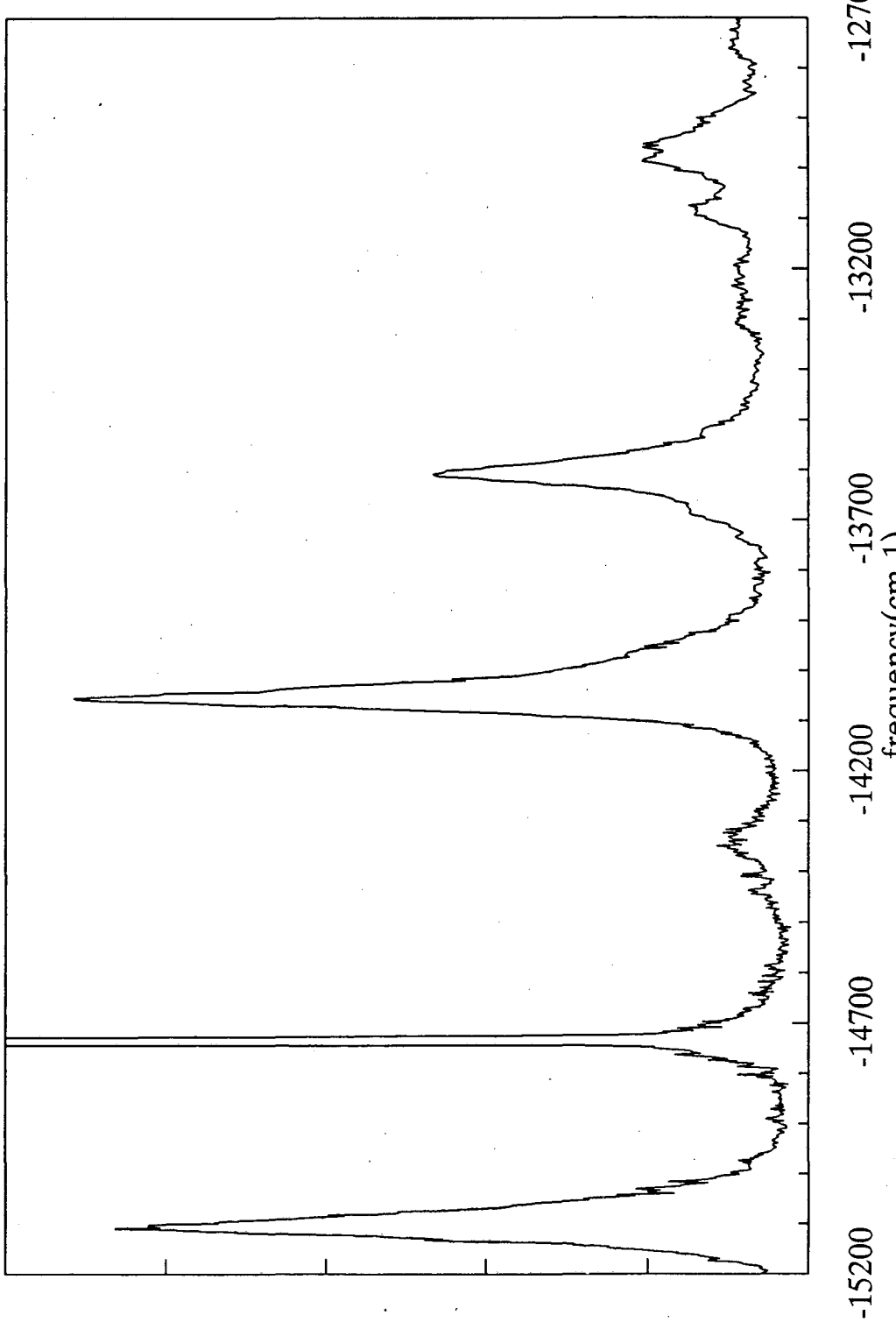


Figure 11

Figure 12
14742 cm-1 excitation

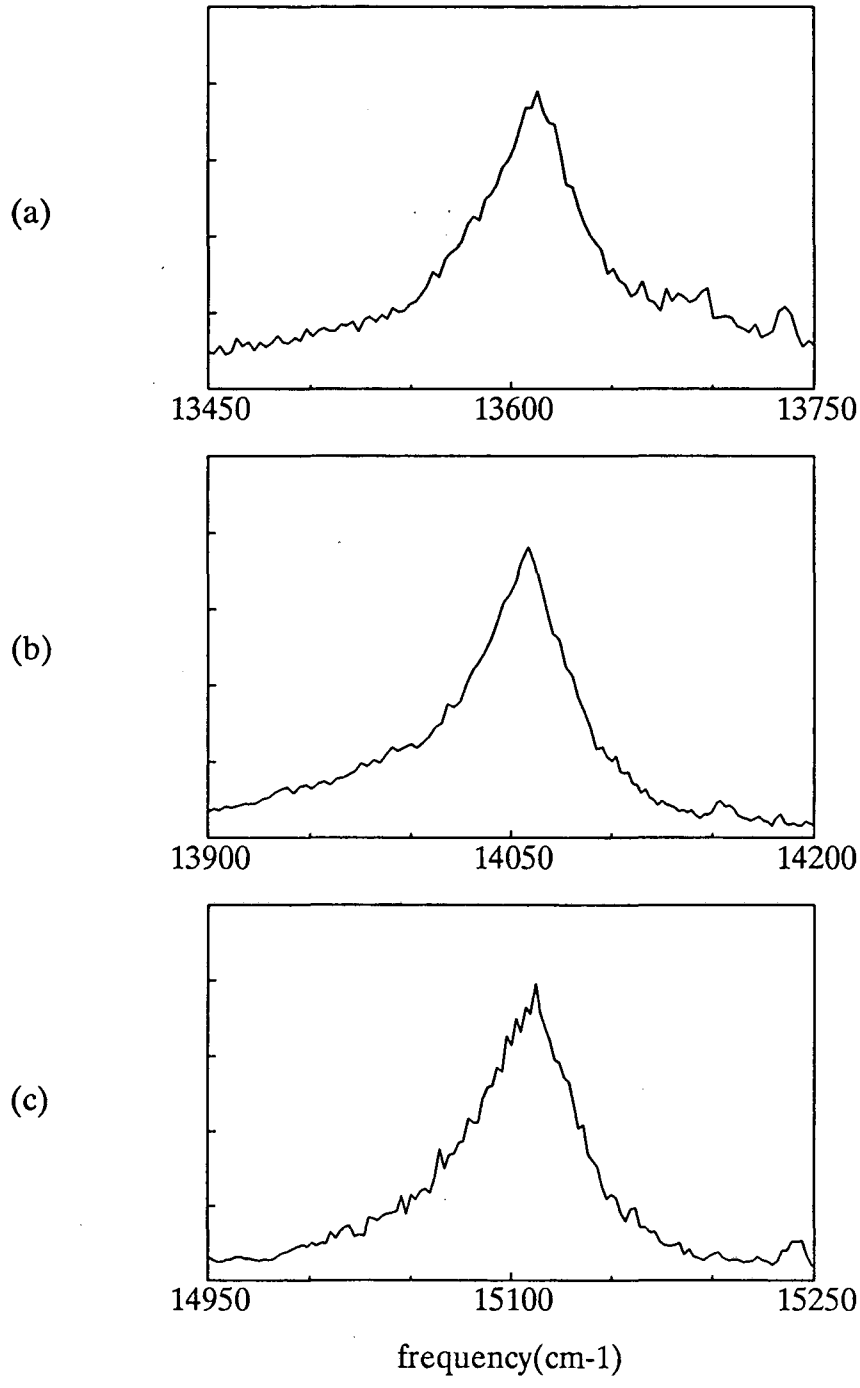

Figure 13

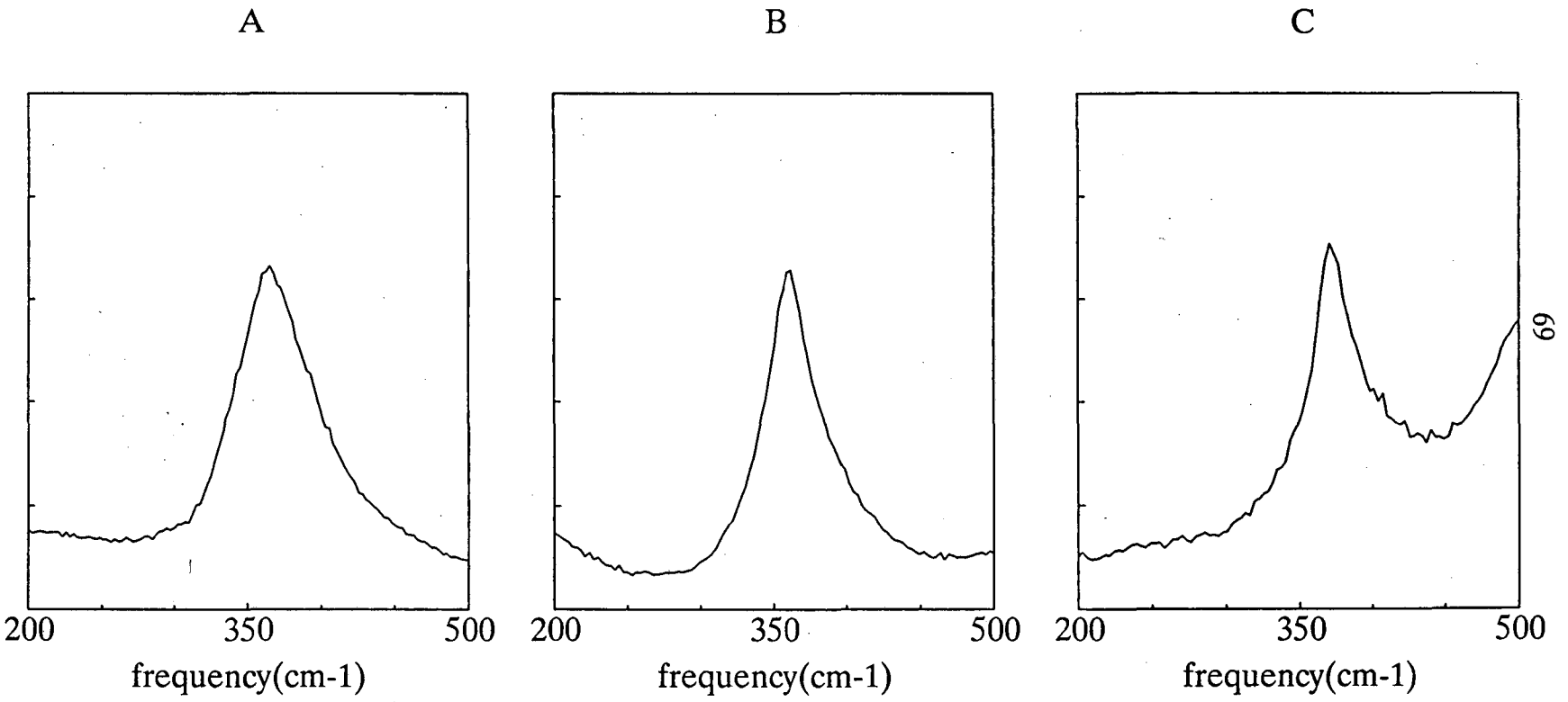
A
B
C
200
350
500
frequency(cm-1)
200
350
500
frequency(cm-1)
200
350
500
frequency(cm-1)

Figure 14

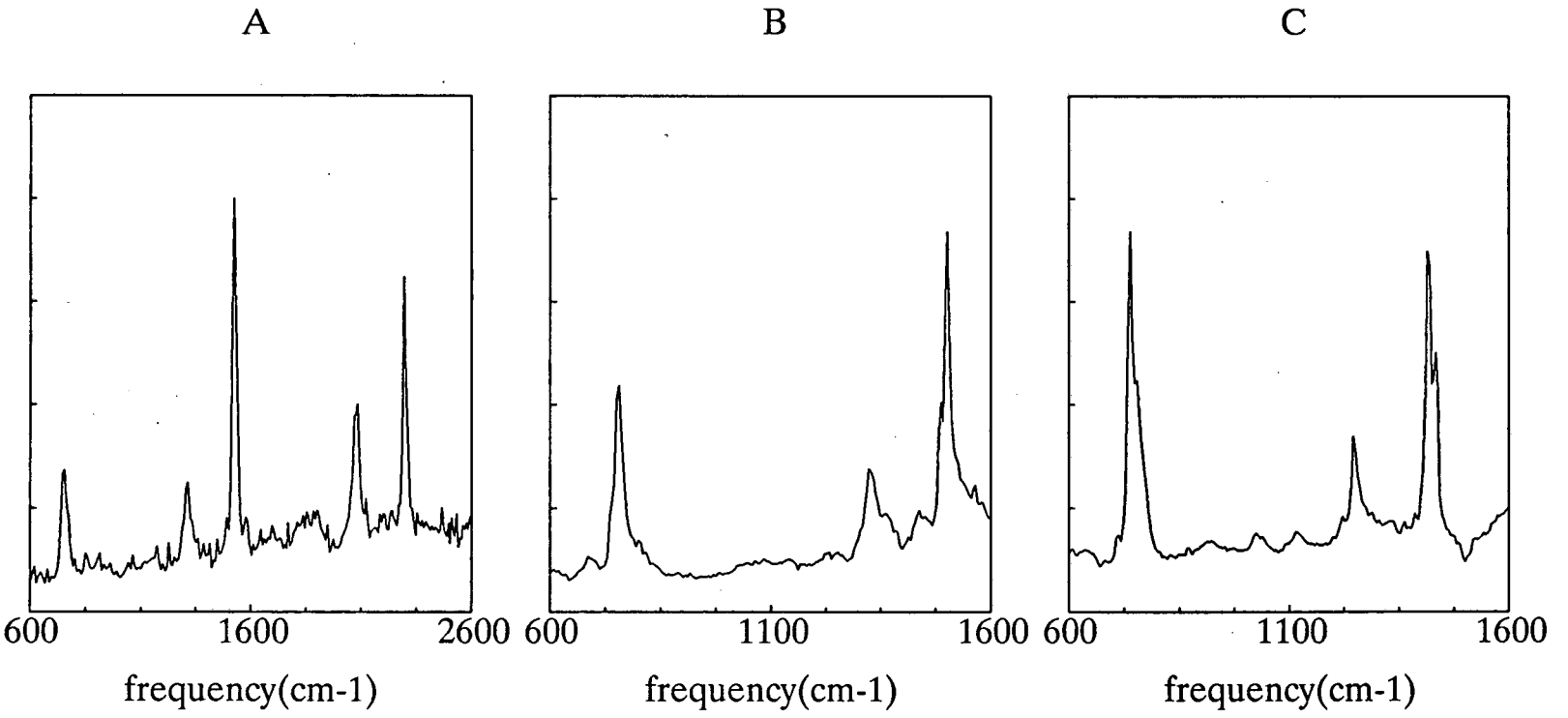
A
B
C
600
1600
2600
600
1100
1600
600
1100
1600
frequency(cm-1)
frequency(cm-1)
frequency(cm-1)

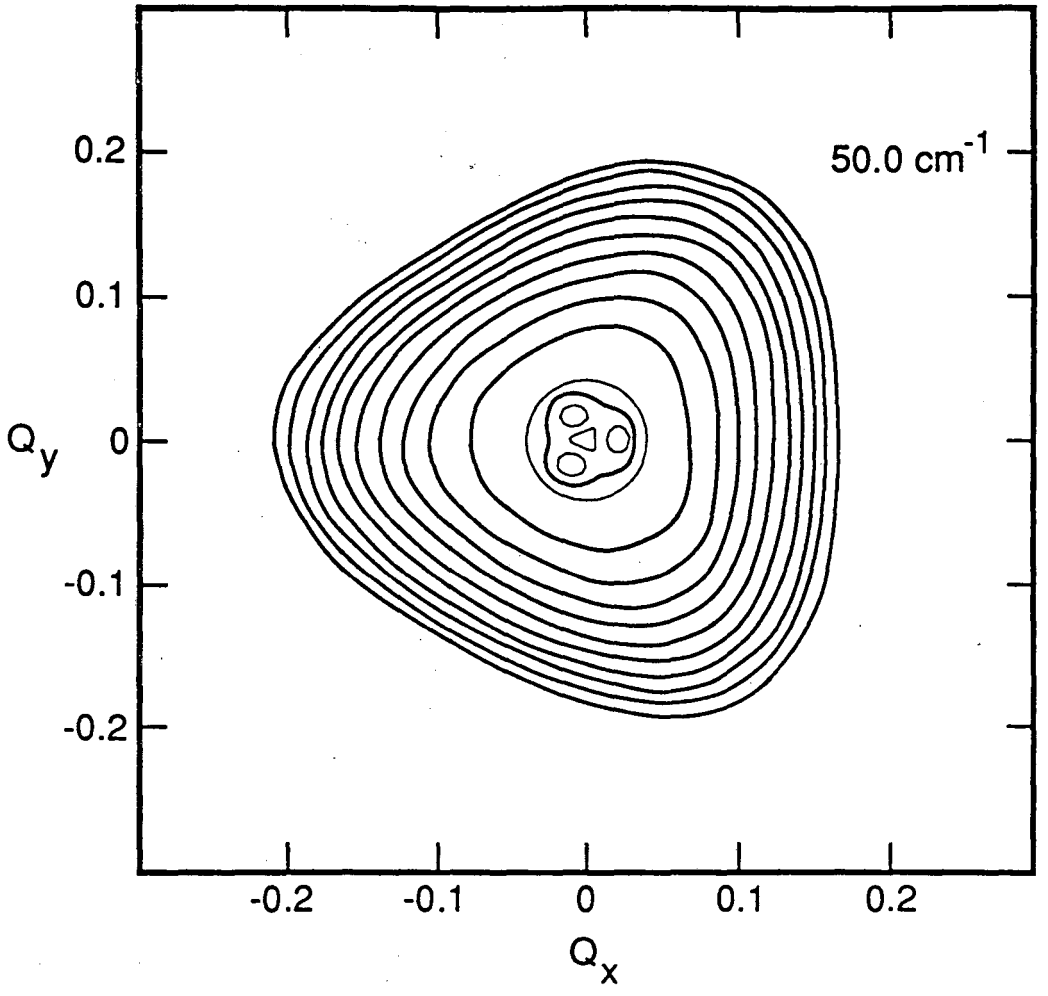


Figure 15

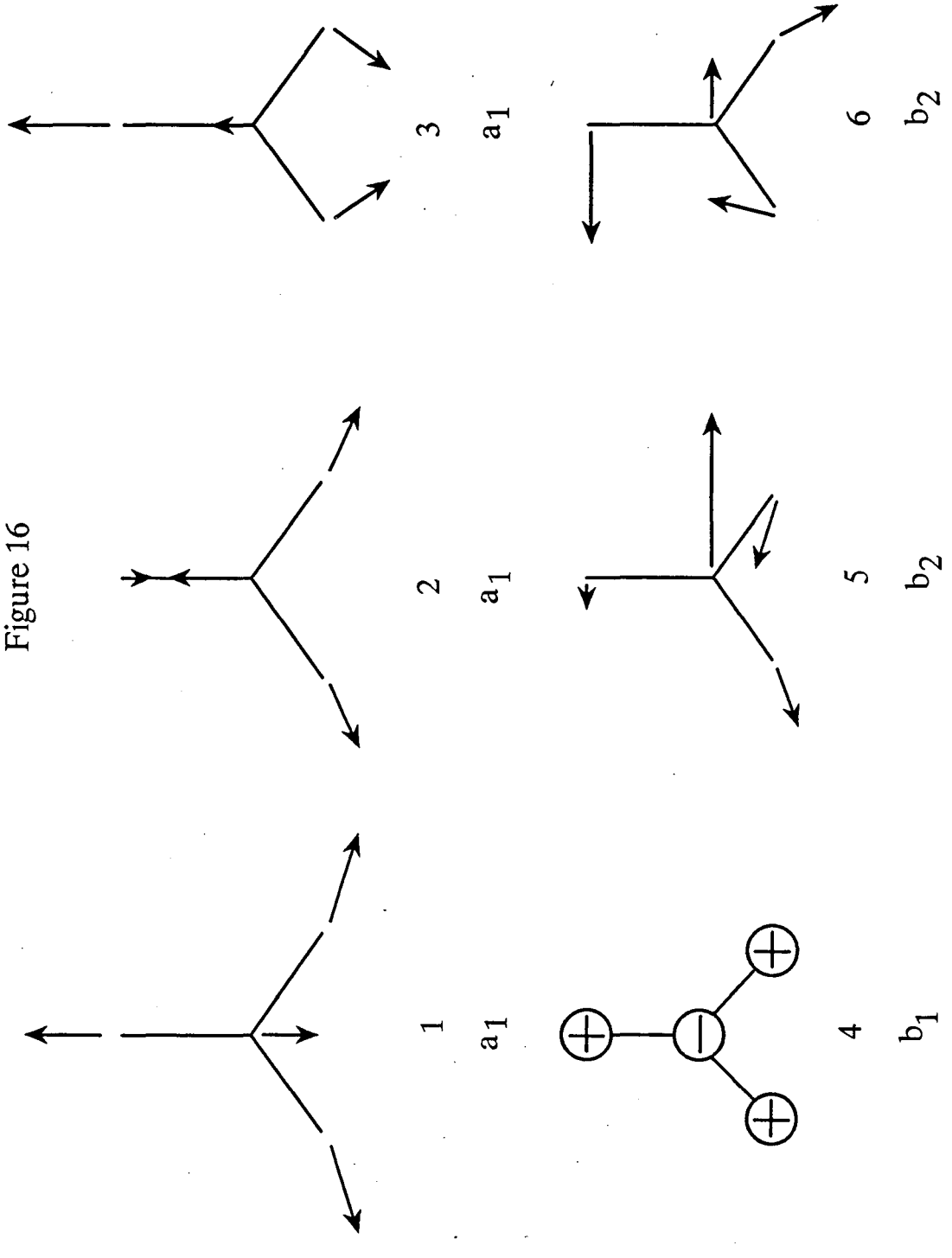


Figure 16

Figure 17

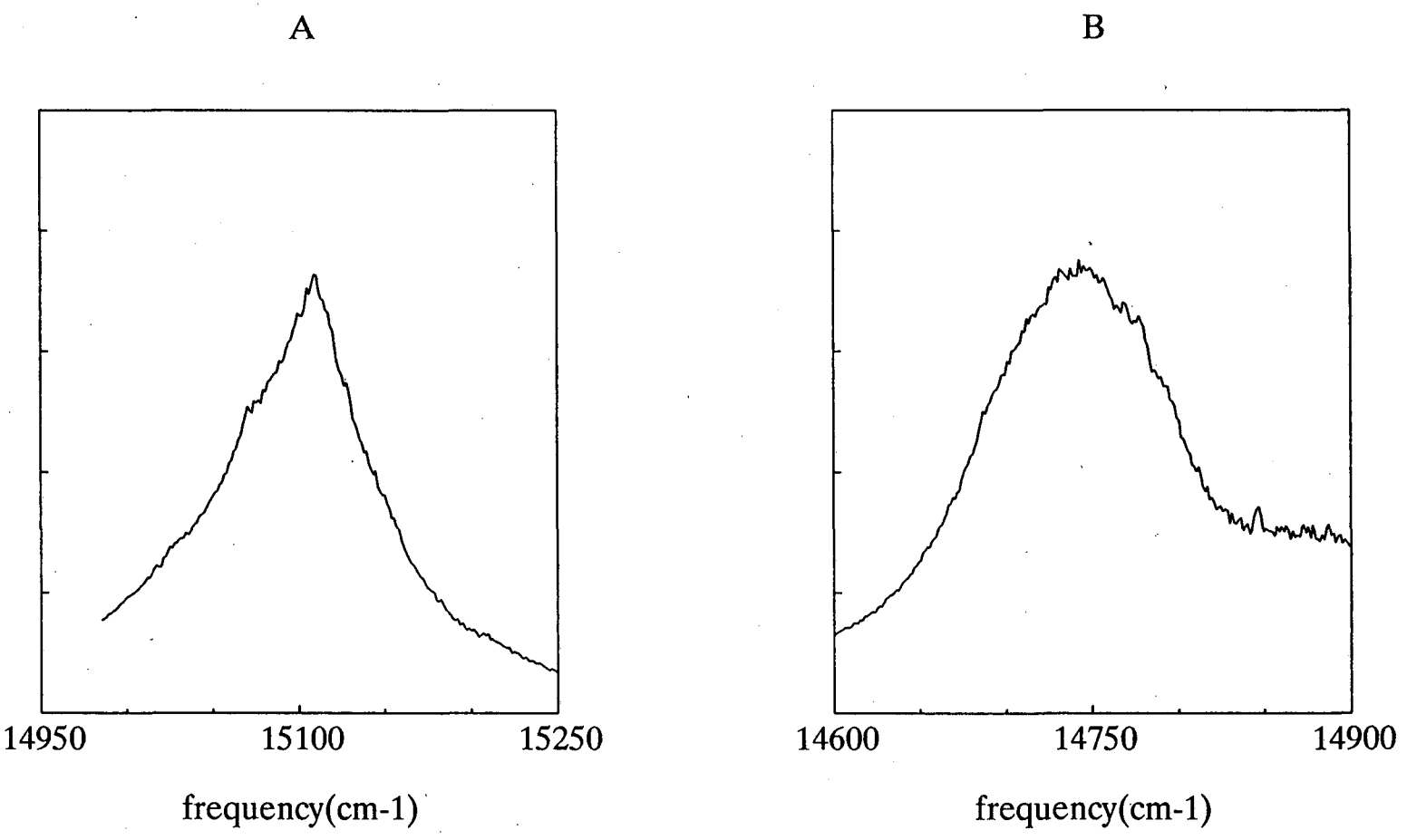
A
B
14950
15100
15250
frequency(cm-1)
14600
14750
14900
frequency(cm-1)

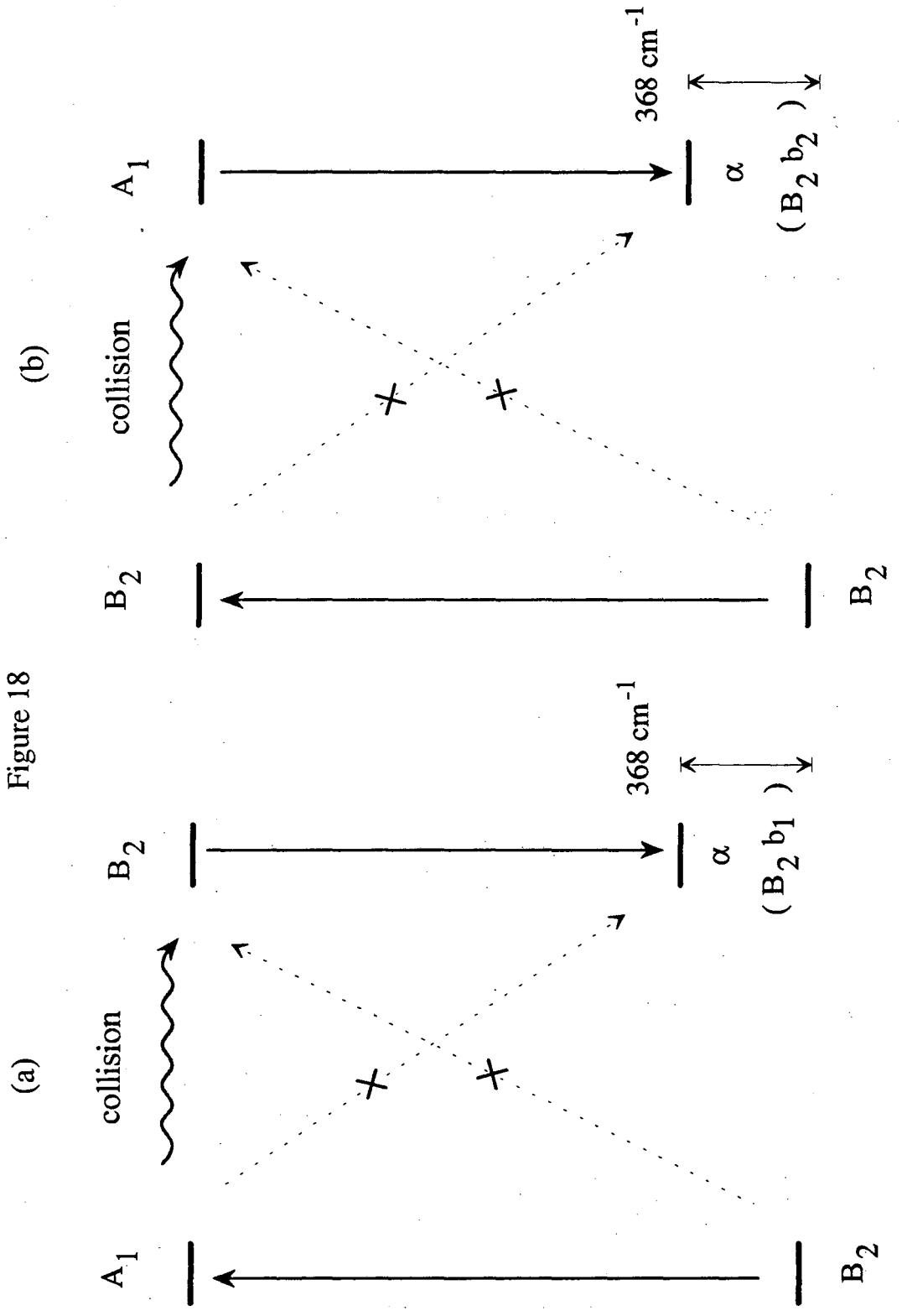
(a)
collision
A1
B2
B2
α
(B2 b1)
368 cm-1
(b)
collision
B2
B2
A1
α
(B2 b2)
368 cm-1

Figure 18

## Chapter 2. Photodissociation and fluorescence spectroscopy of $NO_3$ in a molecular beam

### Abstract

Nitrate radicals are produced in a molecular beam for the first time. The laser induced fluorescence excitation spectrum is obtained, which reveals new bands around 662 nm. The photodissociation of $NO_3$ is studied using time-of-flight detection. This experiment was performed in the Y. T. Lee group's molecular beam machine. Translational energy distributions are obtained for the dissociation products between 532 and 662 nm under collision free conditions. Within this wavelength range, several channels are observed: $NO_2(X\ ^2A_1) + O(^3P)$, $NO(^2\Pi) + O_2(^3\Sigma_g^-)$, and $NO + O_2(^1\Delta_g)$. The branching ratios are strongly wavelength dependent. The enthalpy of formation of $NO_3$, based on product translational energy distributions and the observed wavelength threshold for $NO_2 + O$, is 19.5 ± 1.7 kcal/mol (298 K).

# I. Introduction

## The goals of the experiments

If $NO_3$ could be generated in the molecular beam, some new experiments may reveal valuable information on the molecular properties of $NO_3$.

Our experimental goals in this study were:

1. Generation of $NO_3$ in cold jet in high concentration.
2. To record the LIF spectrum.
3. To obtain the wavelength dependent time-of-flight spectra of the photofragments.
4. Determination of the relative quantum yields for $NO_2 + O$ and $NO + O_2$ channels by analyzing the time-of-flight spectra.
5. Determination of the heat of formation of $NO_3$.

## A. Generation of $NO_3$ in the cold jet

The cooling of molecules in a supersonic free-jet expansion is one of the most widely used techniques in spectroscopy today. The dramatic simplification of spectra on cooling has applications in many areas such as high resolution spectroscopy, translational spectroscopy, photophysics, and analytical chemistry.

However, free-jet expansion has largely been confined to stable molecules and their van der Waals complexes with buffer gas molecules (or atoms), which are easy

to prepare. Comparable work on transient species has only recently started to appear. Several ingenious techniques for the generation of transient species have been recently developed:

1.Laser photolysis of stable precursors has been used to generate free radicals.[1,2]

2.Electron impact[3,4] and electrospray[5] have been used to produce a continuous jet rich in ions.

3.Multiphoton ionization[6,7]

4.Flash pyrolysis[8]

5.Pulsed electric discharge[9]

6.Laser ablation[10]

7.Continuous jet : Hg-photosensitized reactions inside the throat of a Campargue-type continuous free jet[10,11]

8.The corona-excited supersonic expansion (CESE) method of Engelking produces streams of vibrationally or electronically hot radicals and ions.[12]

Although most of the above techniques for the production of transient species have proven to be extremely useful, each method has some advantages and disadvantages. The pulsed techniques is not very effective in using the cw standing wave and ring dye lasers, which provides very high resolution. The photolysis and pyrolysis methods need suitable precursors, and the mercury photosensitization technique is applicable only to a limited number of species. The corona discharge

technique is limited to emission work. Therefore the most appropriate method should be chosen considering the specific species to be generated.

**B. The excited state of $NO_3$**

The visible absorption spectrum of $NO_3$ was first studied by Sprenger[13] as a function of ozone and nitrogen pentoxide concentration. However, no absorption cross section could be determined. Jones and Wulf[14] also studied the visible $NO_3$ spectrum, where $NO_3$ is produced by reaction of ozone with $NO_2$. This work was later reinvestigated by Ramsay[15] under high dispersion who concluded that the observed diffuseness indicated predissociation. He identified a short progression beginning with the strong 0-0 transition at 662.6 nm (15096 $cm^{-1}$) as a symmetric stretch with approximately 950 $cm^{-1}$ intervals, extending to 559.0 nm (17893 $cm^{-1}$). Some 15 or more weaker bands were also observed but unassigned.

$NO_3$ formed in X-irradiated urea nitrate crystal[16] and UV-irradiated cerric nitrate solution[17] exhibited a second absorption system, with a maximum in the vicinity of 330.0 nm. That observation has not been verified in the gas phase. Ravishankara and Mauldin[18] and Sander[19] have observed a strong temperature dependence with the absorption cross section of $NO_3$ at 662 nm increasing with decreasing temperature, while Cantrell et al.[20] observed no apparent temperature effect within the uncertainty of the determinations. The most recent measurement[19]

reported about 2 X $10^{-17}$ $cm^2$/molecule for the absorption coefficient of $NO_3$ at 662 nm at room temperature.

The absorption spectrum of $NO_3$, obtained by Marinelli et al.[21] at room temperature shows that the absorption is diffuse even with very high resolution (0.005 $cm^{-1}$). Nelson et al.[22] attributed the diffuseness of the absorption spectra to the extensive vibronic perturbation by nonemitting nearby vibronic levels. Marinelli et al. reported that the spectrum could be fitted with the overlap of the two Lorentzian lines.[21] The fluorescence excitation spectrum obtained at room temperature in a flow cell is presented in Figure 1,[23] the shape of which is very similar to that of the absorption.

From the ab initio calculation at the experimental geometry obtained from Ishiwata et al.'s analysis of IR spectrum[24] Kim et al.[24] found that the electronic state at 15108 $cm^{-1}$ belonged to $^2E'$ symmetry. However, the state should be split according to the Jahn-Teller theorem, which dictates that any nonlinear molecular system which is degenerate at a certain point of nuclear configuration is unstable and undergoes distortion to lower point group symmetry.

One of the goals in this experiment was to resolve some discrete features in the LIF spectra and then to determine the magnitude of the Jahn-Teller splitting by cooling $NO_3$ in the molecular beam.

**C. The photodissociation of $NO_3$**

The photodissociation of $NO_3$ is potentially important in the balance of ozone in the troposphere and lower stratosphere.[25] It has been known that $NO_2$ and ground state oxygen atom, $O(^3P)$ are energetically possible products of photodissociation for the photon wavelengths less than about 580 nm, although recently different values for the thermodynamic threshold were reported.[26] NO and $O_2$ molecules could be produced at any wavelengths below 8.0 $\mu$m.

When the photolysis products are NO and $O_2$, the net effect is catalytic destruction of ozone:

$$NO_3 + h\nu \rightarrow NO + O_2$$

$$NO + O_3 \rightarrow NO_2 + O_2$$

$$NO_2 + O_3 \rightarrow NO_3 + O_2$$

Net: $2\ O_3 + h\nu \rightarrow 3\ O_2$

The other channel leads to no net chemical reaction:

$$NO_3 + h\nu \rightarrow NO_2 + O$$

$$O + O_2 + M \rightarrow O_3 + M$$

$$NO_2 + O_3 \rightarrow NO_3 + O_2$$

Net: Null reaction

Graham and Johnston[27] found out that both NO + $O_2$ and $NO_2$ + O occurred as products of $NO_3$ photolysis, using broadband fluorescent photolytic lamps of different colors. While the wavelength distribution of the quantum yields was not determined, Graham was able to fit his data to photochemically active bands with synthetic shapes. The average quantum yield for NO + $O_2$ production was found to be 0.22 ± 0.05 at 520 < λ < 640 nm and for $NO_2$ + O, a value of 0.78 ± 0.16 at 470 < λ < 600 nm. Below 580 nm, the primary quantum yield appeared close to unity.

Magnotta and Johnston[28] studied tunable laser flash photolysis of $NO_3$ generated by thermal decomposition of $N_2O_5$ in a flow cell. Resonance fluorescence detection of O ($^1$P) and NO photoproducts confirmed the occurrence of both $NO_2$ + O and NO + $O_2$ as primary photodissociation products. The quantum yield for $NO_2$ + O was unity at 580 nm, remained constant at 0.8 below 560 nm and dropped to zero at 635 nm. The NO + $O_2$ quantum yield peaked at 0.4 at 594 nm, and dropped to zero at λ > 635 nm and λ < 580 nm. They did not attempt to explain the formation of $NO_2$ + O at wavelengths longer than the then accepted threshold of 580 nm.

However, recent interpretation of their data by another study[22] suggested that the dissociation observed above 580 nm was collisionally induced. The mechanism of the dissociation, i.e., whether it was direct or via internal conversion, collisional or collision free, remained unanswered, as did the identity of the electronic state(s) of the $O_2$ photoproduct.

Siegbahn[29] calculated the ab initio barrier height for the NO + $O_2$ product channel. The calculation, constrained to $C_{2v}$ symmetry, indicated that a barrier as high as 145 kcal/mol (50750 $cm^{-1}$) existed on the ON-$O_2$ surface. Even a barrier of half that height would preclude the possibility of the production of NO + $O_2$ from photolysis by visible light.

**D. The thermochemistry of $NO_3$**

The heat of formation of $NO_3$ has recently been reevaluated by Cantrell et al.,[26] by vapor pressure and chemical equilibrium constant measurements. Their value of 15.39 ± 0.72 kcal/mol at 298 K indicates that $NO_3$ is more stable than was previously believed. This value, together with the well known values for heats of formation of $NO_2$ and O,[30] yields a wavelength threshold of 564 nm for formation of $NO_2$ + O, substantially shorter than the wavelength at which Magnotta observed maximum quantum yield for $NO_2$ photoproduction. This result, if correct, would indicate that a large fraction of the photodissociation products observed by Magnotta and Johnston[28] were formed by collisional processes.

Several chemical species are energetically possible as photodissociation products in the region of strong $NO_3$ visible absorption. Adopting the JANAF value for the heat of formation of $NO_3$ as 17.0 kcal/mol,[31] if one product is the ground

vibrational state of NO ($^2\Pi_{3/2,1/2}$) then the calculated maximum wavelengths for various excited $O_2$ products are:

| $O_2$ | $\lambda_{cutoff}$(nm) | ($cm^{-1}$) |
|---|---|---|
| $^3\Sigma_g^-$ | 8000 | (1250) |
| $^1\Delta_g$ | 1100 | (9095) |
| $^1\Sigma_g^+$ | 700 | (14290) |
| $^3\Sigma_u^+$ | 270 | (37040) |

A correlation diagram of $NO_3$ and its photodissociation products is illustrated in Figure 21, which is adapted from Nelson, et al.[22] Dissociation into NO + $O_2$ is shown to the right and into $NO_2$ + O is given to the left.

**E. Translational spectroscopy (time-of-flight/MS detection)**

The photofragmentation translational spectroscopic method is one of the very effective ways to study the photo-dissociation of molecules. The supersonic molecular beam source, which provides molecules with rotational and translational temperatures below a few degrees Kelvin, makes it possible to study the photodissociation processes under isolated conditions.

When photolyzing laser is fired, only dissociation products, which can recoil away from the beam direction, are observed in the mass spectrometric detector. By

measuring the arrival time distribution of the neutral photofragments over a calibrated flight length as a function of detector angle away from the beam direction, the translational energy distribution and angular distribution of the photoproducts can be obtained.

Because of total energy conservation, the product internal energy distribution can be obtained directly from the translational energy distribution. For dissociation of $NO_3$ into $NO_2$ + O, the following relation should hold:

$$E_{photon} + E_{int}(NO_3)$$
$$= D_0(O-NO_2) + E_{trans}(NO_2) + E_{trans}(O) + E_{int}(NO_2) + E_{int}(O) \qquad (1)$$

where $E_{int}$ and $E_{trans}$ are the internal energy and the translational energy of the corresponding species, $E_{photon}$ is the energy of the incident photon, and $D_0$ is the bond dissociation energy.

Also by measuring the maximum release of translational energy of the photoproducts, i.e. the translational energy corresponding to production of ground state products, the heat of formation of molecules can be obtained.

## II. Experimental

### A. Generation of $NO_3$

For $NO_3$, all the experimental studies in the past, whether it was a kinetics, spectroscopic, or photodissociation study, were limited to flow cell systems at room temperature where $NO_3$ was made by reaction of $NO_2 + O_3$, $F + HNO_3$, $Cl + NO_3Cl$, or the dissociation of $N_2O_5$. It was hoped that the cold jet would simplify the complex optical spectrum of $NO_3$ and reveal some new information.

The primary purpose of this experiment was to study the photolysis of $NO_3$ by using the time-of-flight/mass spectrometer detection, for which the molecular beam was necessary. Also the laser induced fluorescence (LIF) excitation spectroscopy was planned.

There are 3 possible methods to generate $NO_3$ in a molecular beam.

1. Photolysis of $NO_3Cl$ by 248 nm excimer laser.
2. Expansion of the reaction mixture of $NO_2 + O_3$.
3. Pyrolysis of $N_2O_5$.

For method 1, the initial quantum yield of $NO_3$ after 248 nm photolysis of $NO_3Cl$ is known to be close to 1.[32] However, the photolysis method can generate only pulsed jet of $NO_3$, while the pyrolysis can generate continuous beam of $NO_3$. The photolysis needs a high power laser to photolyze the precursor, while the

pyrolysis can be done just by wrapping a heating wire around the nozzle. The photodissociation process deposits a large fraction of the available excess energy in vibrational energy of $NO_3$.[32] Since the jet does not provide effective cooling on the vibrational degrees of freedom, it would result in a high vibrational temperature.

Also the pulsed beam showed frequent problems when corrosive species (such as $NO_2$, $N_2O_5$) were running. The tip which closed the nozzle had to be replaced often, while the continuous jet was very stable and required little maintenance for the jet expansion part. The pyrolysis method was considered to have some advantages over the photolysis in those aspects.

The expansion of $NO_2$ + $O_3$ (method 2) would not give a very high concentration of $NO_3$. With that reaction the highest concentration of $NO_3$ which can be achieved before supersonic expansion is on the order of 10 mTorr according to a chemical kinetics calculation by the computer program ACUCHEM.[33] After expansion the concentration would be reduced by a factor of 1000. For the time-of-flight/mass spectrometer detection, 10 mTorr of $NO_3$ before expansion would be close to the limit of the detectability for the photofragments.

By the ACUCHEM chemical kinetics calculation, the time behavior of $N_2O_5$ $\rightarrow$ $NO_3$ + $NO_2$ reaction system was studied for different reaction temperatures. The main reactions which occur in the system are listed below.

1. $N_2O_5 \rightarrow NO_2 + NO_3$

2. $NO_2 + NO_3 \rightarrow N_2O_5$

3. $NO_2 + NO_3 \rightarrow NO + O_2 + NO_2$

4. $NO + NO_3 \rightarrow NO_2 + NO_2$

5. $NO_3 + NO_3 \rightarrow O_2 + NO_2 + NO_2$

The reaction rates for these reactions have been well studied and the most recent values reported along with the NASA recommended values were used[33] to obtain an estimation of the time behavior of the concentrations of $NO_3$ and other important species. The details of the chemical kinetics calculation results are shown in Appendix.

The calculation shows:

1.As the temperature of the nozzle is increased, the heating time when $NO_3$ reaches maximum concentration gets shorter.

2.When the nozzle temperature is 600 K, the maximum concentration of $NO_3$ is about 1.5 X $10^{17}$ molecules/cc when the heating time is between 10 $\mu$sec and 100 $\mu$sec.

3.The major species in the pyrolysis of $N_2O_5$ are $NO_2$ and $NO_3$ at 50 $\mu$sec heating time, 600 K.

The reaction time was determined by the length of the heating zone. The minimum length of the heating zone was limited by the diameter of heating wire, and the minimum reaction time (heating time) practically possible was about 100 $\mu$sec.

**B. Procedure**

The Time-of-flight (TOF) mass spectrum of photofragments and the laser induced fluorescence was measured in a molecular beam apparatus in Y. T. Lee group. The molecular beam photofragmentation apparatus has been previously described in detail.[35]

$N_2O_5$ is prepared following Schott and Davidson's method[36] as follows. Part of the stream of high purity oxygen was bubbled through a trap containing $NO_2$. This stream was merged with the $O_3/O_2$ stream coming from the ozonator. The flow of $O_2$ through the $NO_2$ was adjusted such that $O_3$ was in excess, as evidenced by the disappearance of the brown $NO_2$ color after the mixing tee. The $N_2O_5/O_3/O_2$ mixture was passed through a trap held at 196 K where $N_2O_5$ was deposited as thin

white needle-like crystals. Production of $N_2O_5$ in this manner is known to produce a large (10 - 20 %) impurity of $HNO_3$, formed in the reaction of $N_2O_5$ and $H_2O$.

The gas mixture was formed by flowing the carrier gas (He or Ar) through a glass container filled with solid $N_2O_5$, which is maintained at $-10° \sim -25°C$ (4 – 20 Torr of $N_2O_5$ vapor pressure). $NO_3$ was generated by heating the tip of nozzle made of stainless steel and expanded through 0.020" diameter hole at a total stagnation pressure of 90 – 150 Torr.

The nozzle was heated to about 500 – 700 K. Initially the heating zone was 1 inch long, however, by reducing the length of heating zone (reducing reaction time), a higher concentration of $NO_3$ was achieved. Therefore, only the nozzle tip (final 0.15") was heated in the final design of the nozzle. A small copper sleeve was soldered to the end of the nozzle and one turn of Thermocoax wire, wrapped and soldered to the sleeve, was heated by DC current. A 6" long water cooled copper block soldered to the tube at 1 mm behind the heating zone maintained other part of the nozzle cool and kept the heating time short enough.

The $NO_3$ concentration was monitored by the laser induced fluorescence intensity at 662 nm excitation or the $NO_3^+$
(m/e = 62) count rate of the mass spectrometer, which was looking at the beam direction (0°) through a 0.003" diameter pinhole. Since $NO_3$ showed a strong $NO_3^+$ signal and the $NO_3^+$ signal from the fragmentation of $N_2O_5$ was very low, the mass-spectrometric detection of $NO_3^+$ was a convenient way to optimize experimental conditions before taking the time-of-flight spectrum.

The beam was collimated by 2 skimmers, and after passing through a pressure reducing differential chamber, it was crossed by the photolyzing laser beam. A liquid nitrogen cooled copper cold finger was placed between the second skimmer and the photolysis region inside the main chamber so that the mass spectrometer would always face a cold surface during the angular scans thereby reducing the background noise at the product mass. Since the beam also contained large quantities of $NO_2$, NO, $O_2$, and $N_2O_5$, all of which could generate large background at the $NO^+$, $NO_2^+$, and $O_2^+$ detection, beam collimation was very crucial in this experiment.

Only $NO_3$ and $NO_2$ absorb significantly at the photolysis wavelengths among the species generated by the pyrolysis of $N_2O_5$, but $NO_2$ does not dissociate by single photon absorption in this wavelength range. Only dissociation products, which can recoil away from the beam direction, are observed in the mass spectrometric detector, which is facing the beam/laser intersection region but is located away from the beam direction.

Parallel experiments were run with 5 % $NO_2$/He mixtures to confirm the above argument. No dissociation signal was observed when $NO_2$/He was running. Formation of NO + O was observed only at 532 nm when the laser was tightly focussed, confirming that no signal is coming from $NO_2$ 2 photon absorption-dissociation in our experiments.

The beam source chamber was maintained at 1 x $10^{-4}$ Torr by a VHS 10" diffusion pump (DP) backed by a liquid-nitrogen- trapped 250 CFM roots blower.

The beam was differentially pumped by two 4" DP's, the main chamber by two 10" DP's and large liquid nitrogen cooled cryopanels resulting in a main chamber pressure of 1 x $10^{-7}$ Torr with the beam running.

The $NO_3$ vibrational temperature was measured by LIF detection, which is described in detail in Results section. The vibrational temperature measurements indicated that no vibrational cooling resulted from supersonic expansion through the nozzle with 0.020" channel length ($T_{vib}$ = 600 K). Use of a second nozzle with 0.080" channel length reduced the vibrational temperature to 450 K, due to the increased number of collisions on expansion.

Additional vibrational cooling was accomplished by cooling down the plate and nozzle orifice to 300 K by spot welding six thin nickel wires, soldered to a water cooled 0.125" diameter copper tube, to the plate surface. This arrangement achieved a vibrational temperature of 300 K.

The velocity distribution of the molecular beam was measured by spinning a slotted stainless steel disk at 320 Hz in front of the detector. The mean velocity was 1900 m/s and the full width at half maximum spread was about 6 % for the first nozzle described above. The beam velocity was periodically checked by monitoring the depletion of $NO_3^+$ parent ion signal with the detector at 0° from the beam direction with the laser on.

The photodissociation fragments were detected by a mass spectrometer rotatable in the plane of the laser and the molecular beam. It consisted of a triply differentially pumped Brinks type[38] electron bombardment ionizer, quadrupole mass

filter, and a Daly type ion counter.[39] Only the 3 X 3 mm zone centered at the interaction region could be viewed by the detector due to geometrical arrangement. A multichannel scaler with 1 μsec dwell time was triggered by the laser pulse with less than 1 μsec delay and a LSI/11 minicomputer controlled the data acquisition. Data from 15,000 laser pulses were averaged at each detector angle. The distance from the interaction region to ionizer was 20.8 cm, and the detector was operated at unit mass resolution for all the experiments.

Laser output (2–40 mJ pulses, 7 ns duration, 1 $cm^{-1}$ linewidth) from a Quanta Ray DCR–2A YAG pumped dye laser (PDL 1) was focussed to a 3 X 4 mm spot at the interaction region. For some experiments a Lambda Physik dye laser (FL 2002) pumped by an excimer laser (EMG 103) was used. It had a higher repetition rate (50 Hz) than the YAG pumped dye laser (10 Hz), however, the maximum power was only 10 mJ per pulse. For fluorescence experiments saturation occurred with laser power higher than 5 mJ/pulse, while for the photodissociation saturation was not observed even with 40 mJ/pulse.

For most experiments, the laser was polarized parallel and propagated perpendicular to the molecular beam direction. However, no difference in TOF signal was observed when polarization was changed to be perpendicular to the plane made by the laser and the molecular beam by changing the optical path.

For laser power dependence measurements, the dye laser output was controlled by varying the YAG pump energy. Laser output power was continuously monitored by a Scientech Joulemeter after the beam exited the main chamber.

A red sensitive RCA 31034A photomultiplier was used for LIF detection. The photocathode was placed 5 cm below the interaction region with the long side parallel with the molecular beam direction. A colored glass filter (Corning CS 7-69 for 698 nm excitation and CS 7-59 for other wavelength excitation) shielded the detector from scattered laser light. The signal from the PMT was amplified by a homemade 120 gain amplifier. The amplified signal was sent to an SRS gated integrator/boxcar, digitized and stored by an IBM AT computer equipped with DT2810A D/A board. The boxcar integrator sampled the fluorescence signal at 1 $\mu$sec delay time and 15 $\mu$sec gate width. The PMT bias voltage was kept typically at $-1300$ V.

## III. Results

### A. Excitation spectroscopy of $NO_3$

In Figure 2 A and 2 B the excitation spectra of $NO_3$ taken in low resolution are presented. He buffer was used in expansion. Figure 2 A is obtained with low laser power($<$ 2 mJ/pulse) and 3rd nozzle which provided 300 K vibrational temperature. Figure 2 B is obtained with high laser power ($\sim$ 20 mJ/pulse) and the vibrational temperature in the molecular beam in higher than 450 K. Depending on the experimental condition and the dye laser power curve the relative intensities of the fluorescence peaks show slight changes.

Although the absorption cross section for $NO_2$ is about 2 orders of magnitude smaller than that of $NO_3$ in this frequency range, the calculated concentration of $NO_2$ is about 100 times greater than that of $NO_3$, when it is about 0.1 torr (Appendix). The fluorescence from $NO_2$ is the major source of noise. Comparing the $NO_3$ LIF spectra with the $NO_2$ LIF spectrum in Figure 3, which is obtained for similar expansion conditions, it appears that the peaks seen at 613 ~ 618, 620, 640 ~ 650 nm are due to $NO_2$.

The dye laser power curve measured for DCM dye in the YAG pumped dye laser is presented in Figure 4. Since the power dependence test showed saturation effects at energies higher than 5 mJ/pulse for 623 and 662 nm absorption peaks, the laser energy was kept less than 2 mJ/pulse for most of the fluorescence experiments.

Figure 2 A and 2 B clearly show the existence of at least 3 states lying very closely between 623.0 and 629.0 nm. Compare the excitation spectrum with the room temperature spectrum in Figure 1. Nelson assigned 820 $cm^{-1}$ as an upper state vibrational frequency,[34] which corresponds to 628.0 nm in excitation wavelength. The small shoulders at 621.0, 622.0, 623.5, and 631.0 nm are seen repeatedly in other spectra, and they do not overlap with $NO_2$ peak positions seen in Figure 3.

In Figure 5 the magnified $NO_3$ excitation spectrum around 662 nm is shown. The spectra in Figure 5 A, B, C, I, and J were acquired with He buffer gas, and Figure 5 D, E, F, G , and H with Ar buffer gas. For Figure 5 A, B, G, H the laser power was kept low to avoid saturation (less than 2 mJ/pulse). For Figure 5 C, D, E, F, I, J laser power was high (maximum 15 mJ/pulse). The backing pressure of the

buffer gas was adjusted to about 150 mTorr for He and 90 Torr for Ar. It was collected for longer time and at slower scan speed than the spectra in Figure 2. The linewidth of the laser was 1 $cm^{-1}$, which limited the resolution of the spectrum. In Table I the experimental conditions for each spectrum are summarized.

The spectrum around 661.9 nm shows many discrete features which were not seen in room temperature spectra (See Figure 1). The position of the maximum fluorescence is 661.9 nm (15109 $cm^{-1}$), which coincides with the absorption peak position observed at room temperature.

The peaks at 665.2, 664.4, 663.2, 662.7, 662.0, 660.8, 660.1, and 659.5 nm are observed repeatedly, and there is no significant $NO_2$ peak between 658 to 666 nm. It appears that they are real absorption peaks of $NO_3$. At 661.6 nm, a peak is observed with high laser pulse energy (15 mJ/pulse). When low pulse energy (2 mJ/pulse) was used for excitation, the peak shape was changed, which is probably due to the saturation effect of the peak at 661.9 nm.

In Figure 7 the magnified spectrum around 678.0 nm is shown. The maximum intensity is at 678.4 nm, and a shoulder is observed at 677.4 nm. The spectrum was obtained by subtracting the $NO_2$ peaks from the total spectrum.

In Figure 6 the $NO_3$ excitation spectra obtained with different buffer gases are compared. Figure 6 A was obtained with Ar buffer gas and 6 B with He. Lambda Physik excimer pumped dye laser with 1 $cm^{-1}$ linewidth was used for excitation. Figure 6 A (Ar buffer) shows better resolved structure than Figure 6 B (He buffer),

although the intensity of the fluorescence signal is 3 times stronger with He buffer gas.

The change of the buffer gas affects the conditions of the pyrolysis reaction system. When the nozzle was changed to a different design which allowed shorter pyrolysis time and more vibrational cooling, the effect of changing buffer gas was not observed.

**B. Photodissociation**

The time-of-flight spectra were taken at laser wavelengths which covered most of the major $NO_3$ absorption peaks in the range of 532 nm ~ 662 nm ( 532, 580 ~ 604 at 2 nm interval, 605, 623, 637, 662). Photodissociation product signal was observed at m/e = 46 ($NO_2^+$), m/e = 32 ($O_2^+$), m/e = 30 ($NO^+$), and m/e = 16 ($O^+$).

**590 nm excitation**

At 590 nm excitation both dissociation channels were observed, and hence the most extensive data were acquired at 590 nm photolysis. Two different dissociation channels are possible when $NO_3$ is excited at 590 nm. Figure 8 shows the time-of-flight spectrum of $NO^+$ (m/e = 30) at 10°, where the photofragments from two different channels are well separated. The fast peak seen at 75 $\mu$sec is $NO^+$ from the NO + $O_2$ channel; the slow peak at 120 $\mu$sec is $NO^+$ daughter ion generated

from the fragmentation of $NO_2$ by the electron bombardment ionization. The $NO_2$ is from $NO_2$ + O channel.

The $NO_2^+$ (m/e = 46) time-of-flight spectrum is presented in Figure 9, where an identical peak to the slow $NO^+$ peak, only shifted by slightly longer transmission time through the ion optics, is observed. This spectrum confirms that the slow peak resulted from the $NO_2$ + O channel. Likewise, the existence of a similar peak in the $O_2^+$ (m/e = 32) TOF spectrum (Figure 10) corresponding to the momentum matched $O_2$ fragment confirms that the fast peak is due to NO + $O_2$ channel.

To explore the anisotropy of the photofragmentation, the laser polarization was changed from vertical to horizontal at 2 mJ and 20 mJ pulse energies. Since it showed no detectible effect, it is concluded that both channels yield an isotropic product distribution in the center-of-mass coordinate system. An additional peak is observed between 12.5° and 20° at 120 μsec (Figure 11 A and B). It is probably due to the sequential 2 photon absorption of $NO_3$ producing $NO_2$ + O. This 2 photon channel will be discussed later. Since the $NO_2$ + O channel cannot have translational energy of more than 4 kcal/mol, the $NO_2$ product channel is observed only at angles less than 12.5°, while the NO + $O_2$ products can be seen at all detector angles with translational energies up to 45 kcal/mol. This is illustrated by the Newton diagram in Figure 12.

The center-of-mass translational energy distribution $P(E_T)$ for each photodissociation channel is obtained with forward convolution technique. An assumed $P(E_T)$ for a particular dissociation channel is transformed to a center of

mass velocity flux distribution. This center of mass velocity distribution is added vectorially to the beam velocity and transformed to a laboratory velocity flux distribution for a given detector angle using the appropriate Jacobian factor. Experimental factors are averaged over, including the beam velocity and angular dispersion, ionizer length, detector angular resolution, and multichannel scaler channel width. The trial $P(E_T)$ is iteratively adjusted until satisfactory fitting is obtained between the calculated and the observed TOF spectra. In this experiment an isotropic center-of-mass product angular distribution is assumed, as found in the anisotropy test.

The product translational energy distributions obtained by fitting the 590 nm dissociation time-of-flight data are shown in Figure 13. Two separate $P(E_T)$ distributions were used in fitting the NO + $O_2$ channel. A small shoulder is observed on the fast side of the NO time-of-flight spectra at all detected angles (See Figure 11). In $O_2^+$ time-of-flight spectra, a similar shoulder was observed (Figure 14). This fast shoulder are due to the formation of NO ($^2\Pi$) + $O_2$ ($^3\Sigma_g^-$). This conclusion is based on energy conservation (see equation (1)) since the product translational energy higher than 25 kcal/mol cannot provide enough energy for excitation to the $O_2$ ($^1\Delta_g$) state.

The slower component which is strong in intensity in the time-of-flight spectra (Figure 8, 11 A, and 11 B) falls completely within the translational energy range required by the conservation of energy for the NO + $O_2$ ($^1\Delta_g$) channel. From this observation, together with the existence of a shoulder in the fast edge noted above,

the major product from the photodissociation of $NO_3$ at 590 nm must be $O_2$ ($^1\Delta_g$). The two components in the NO + $O_2$ spectra were thus fitted by requiring that the slower peaks fall completely within the energy boundaries consistent with NO + $O_2$ ($^1\Delta_g$), i.e. $E_{tran,max}$ = 25.85 kcal/mol.

The branching ratio of the $NO_2$ + O channel to the NO + $O_2$ channel at 590 nm photolysis was obtained from the m/e = 30 ($NO^+$) time-of-flight data. The optimized fit of the data acquired at all detector angles gives an "apparent" branching ratio $R_{app}$ defined by equation (2):

$$R_{app} = \frac{\chi(NO+O_2)}{\chi(NO_2+O)} = 1.10 \qquad (2)$$

where the $\chi$'s are the integrated areas under the product $P(E_T)$ distributions for the two different chemical product channels, which is normalized for the Jacobian factors calculated by the computer program in carrying out the laboratory to center-of-mass coordinate transformations. The actual branching ratio R is related to the "apparent" ratio by the following expression:

$$R = R_{app} \times \frac{\sigma_{ion}(NO_2)}{\sigma_{ion}(NO)} \times \frac{F(NO^+/NO_2)}{F(NO^+/NO)} \qquad (3)$$

In equation (3), $\sigma_{ion}(NO_2)$ and $\sigma_{ion}(NO)$ are the ionization cross sections for $NO_2$ and NO, respectively. They are estimated using the following empirical correlation method of Center and Mandl[40] relating the peak ionization cross section ($\sigma_{ion}$ in Å$^2$) to molecular polarizability ($\alpha$ in Å$^3$):

$$\sigma_{ion} = 36\sqrt{\alpha} - 18 \qquad (4)$$

Molecular polarizabilities are approximated as the sum of the atomic polarizabilities. $F(NO^+/NO_2)$ is the fraction of $NO_2$ which yield $NO^+$ ion, a quantity which can be directly measured in this experiment. Although the fragmentation pattern of $NO_2$ is expected to depend strongly on the level of internal excitation, our fragmentation ratios agree well with published values[41] for room temperature $NO_2$.

From equation (3) we find that R = 1.01. Thus the yields of the two dissociation channels ($NO_2$ + O, NO + $O_2$) are equal at 590 nm within the calculational errors, which are estimated to be ± 20 %. The largest source of error is the uncertainty in the $P(E_T)$ for $E_{trans}$ < 1 kcal/mol, because we could not detect photo-dissociation products within 5° of the molecular beam direction. At smaller angles the background noise due to the molecules from the direct beam arriving at mass spectrometer is quite large, and prolonged exposure would contaminate the mass spectrometer.

Due to our inability of detecting the photoproduct at less than 5 degrees, where $NO_2$ + O is the dominant dissociation product, the relative quantum yield for $NO_2$ + O channel is likely to be estimated lower, i.e. our measured relative quantum yield for $NO_2$ + O channel would be the lower limit.

Now we conclude that at 590 nm:

$$NO_3 \rightarrow NO_2 + O \qquad \Phi_1 = 0.5 \pm 0.1$$

$$\rightarrow NO + O_2 \qquad \Phi_2 = 0.5 \pm 0.1$$

This calculation is based on several assumptions. First, we assume that photodissociation occurs within 3 $\mu$sec, i.e., before the excited $NO_3$ molecules fly out of the viewing range of the detector. Also it is assumed that $\Phi_1 + \Phi_2 = 1.0$ at 590 nm (i.e. no other channel exists). Considering the absence of the fluorescence below 600 nm under collision free conditions, the second assumption appears to be a reasonable one.

**Photodissociation at other wavelengths**

When the laser wavelength was changed from 590 to 584 nm, the NO + $O_2$ dissociation channel disappeared, as seen in Figure 15, where the time-of-flight spectra for $NO^+$ detected at 10° at different photolysis wavelengths are shown. The $O_2^+$ time-of-flight spectra showed similar behavior, as expected. The integrated signal intensity for the $NO_2$ + O channel (measured at m/e = 30 or 46) increased when the photolysis wavelength is changed from 590 to 584 nm. Since the absorption cross section was not known for rotationally cold $NO_3$, the data in Figure 15 was not normalized for the absorption cross sections. When the photolysis wavelength was changed to 532 nm, only the $NO_2$ + O dissociation channel was observed.

Although no significant change in signal intensity was seen on changing the polarization of the laser at 532 nm, we cannot rule out the possible existence of

effects whose magnitude is smaller than 20 %. In order to change the polarization we had to realign the laser, which made it difficult to notice a small difference.

Figure 16 shows the $NO^+$ time-of-flight spectra detected at 10° as the photolysis wavelength is changed from 590 nm to longer wavelengths (596 nm). Two major effects are noticed:

First, the relative quantum yield of the NO + $O_2$ channel (fast peak) compared to the $NO_2$ + O channel (slow peak) decreased. The decrease in the quantum yield of the NO + $O_2$ channel was also observed from the $O_2^+$ time-of-flight spectra.

Second, another peak showed up between the two peaks. When the photolysis wavelength was set at 596 nm, the three peaks nearly merged together. This third peak, which was also observed in $NO_2^+$ time-of-flight spectra (but not in $O_2^+$ time-of-flight spectra), is interpreted as the result of sequential two photon absorption of $NO_3$, producing of $NO_2$ + O. Two photon absorption by $NO_3$ does not produce NO + $O_2$ photo-products. Because the two photon process provides $NO_2$ fragments with substantially higher translational energy than the single photon process, they can be distinguished from one another.

The power dependence studies at 596 nm supports the claim that the third peak is due to a sequential two photon effect. At high laser power (60 mJ/pulse), the intensity of the third peak located in the middle was much higher (approximately

2 times) than that of the two single photon peaks, but decreased to a negligible magnitude when the laser power was reduced to 2 mJ/pulse.

After prolonged averaging for m/e = 32 ($O_2^+$) with the photolysis laser at 605 nm, a weak signal indicating the existence of the NO + $O_2$ channel was found. No $O_2^+$ photofragment signal was observed at 613, 623, 637, or 662 nm (the absorption peaks of $NO_3$), but the $NO_2$ + O dissociation channel from the single photon absorption could be seen with decreased intensity at photolysis wavelengths up to 637 nm. Figure 17 A shows the single photon wavelength dependence for the relative quantum yields of two channels. The time-of-flight spectra for these two channels were normalized using the measured 1:1 branching ratio at 590 nm.

**C. The heat of formation of $NO_3$**

Translational energies of the $NO_2$ and O products were obtained by analyzing the time-of-flight spectra at photolysis wavelengths of 532, 580, and 590 nm. Figures 18 and 19 show the time-of-flight spectra of 532 nm photolysis for m/e = 46 ($NO_2^+$) and m/e = 16 ($O^+$) with the detector angle set at 10° from the molecular beam direction. The translational momenta of the two fragments were the same, showing that they originated from $NO_3$. At all three photolysis wavelengths, the $P(E_T)$ has a maximum at zero energy, indicating that the translational energy release from the barrier for dissociation channel is less than 1.0 kcal/mole.

The fastest $NO_2$ fragment is assumed to be in the ground vibrational and rotational state. Since the photolysis wavelength is very close to the dissociation threshold and considering the nature of the process, i.e. $O-NO_2$ bond cleavage, this assumption seems to be reasonable.

In Figure 20 the product translational energy distributions for the fragmenting $NO_2$ + O pair at 532 nm and 590 nm photodissociation wavelength, obtained by fitting the time-of-flight spectra, are illustrated. At 532 nm the maximum translational energy was 7.0 ± 0.5 kcal/mol. At 590 nm photolysis, more than 80 % of the fragments were formed with translational energy less than 2.0 ± 0.5 kcal/mol; a small fraction of molecules had translational energy up to 3.5 ± 0.5 kcal/mol. At 637 nm $NO_2$ + O dissociation channel was observed, however, this wavelength corresponds to a hot band excitation from 368 $cm^{-1}$ to 16053 $cm^{-1}$ (623 nm). Thus the threshold for $NO_2$ + O dissociation channel should be 623 nm.

If the cooling were complete, i.e. all of the $NO_3$ molecules in the beam were in their ground vibrational and rotational state, the maximum product translational energy would give an upper limit to the bond dissociation energy. However, since the nozzle tip was heated to 500 – 700 K and the vibrational cooling for $NO_3$ molecule was not as effective as for rotation or translation, there is a possibility that the detected dissociation has originated from the dissociation of vibrationally hot $NO_3$.

The vibrational temperature of $NO_3$ in the beam was estimated by measuring the laser induced fluorescence (LIF) intensity. The initial design of the nozzle

resulted in a vibrational temperature of about 600 K. When a nozzle of improved design was employed, the vibrational temperature measured by LIF intensity decreased to about 300 K.

The vibrational frequencies for $NO_3$ and the expected equilibrium populations at two different temperatures are listed in Table II. Using the new nozzle, a second set of experiments was conducted at 590 nm. Dissociation products were still observed with translational energies up to 3.5 kcal/mol, while the contribution from the high energy tail decreased. From this observation the fast component seems to be originated from the photodissociation of vibrationally excited $NO_3$ radicals.

No significant change was observed for the dominant slower products with translational energy lower than 2 kcal/mol at 590 nm dissociation. Based on the vibrational temperature dependence studies, the maximum product translational energy from the dissociation of cold $NO_3$ at 590 and 532 nm is 2.0 ± 0.5 and 7.0 ± 0.5 kcal/mol, respectively. From equation (3) the bond dissociation energy is calculated to be 46.4 ± 0.5 and 46.7 ± 0.5 kcal/mol, respectively.

Sander[18] studied the temperature dependence of the $NO_3$ absorption spectrum. His result showed that when the temperature was decreased from 298 K to 230 K, the absorption cross section at 637 and 679 nm, which are hot band absorption, decreased by ~10 % from 22.5 X $10^{-19}$ to 20.1 X $10^{-19}$ and from 8.5 X $10^{-19}$ to 7.3 X $10^{-19}$, respectively. However, the absorption cross sections at 590, 580, and 532 nm increased from 64.7 X $10^{-19}$ to 71.8 X $10^{-19}$, from 36.3 X $10^{-19}$ to 39.9 X $10^{-19}$,

and from 21.9 X $10^{-19}$ to 22.0 X $10^{-19}$, which suggests that the three wavelengths used for dissociation here are not the hot band absorptions.

Although the above statements suggest that it is not likely, we cannot absolutely rule out the possibility that the highest translational energies are due to the dissociation of vibrationally hot $NO_3$ molecules with one quantum of 368 $cm^{-1}$. If the hot band absorption at 368 $cm^{-1}$ gave significant contribution to the dissociation signal, the upper limit to the $D_0(O-NO_2)$ would be 46.7 + 0.5 kcal/mol + 1.0 kcal = 48.2 kcal/mol. The lower limit would be the case when 590 nm photolysis produced the product with 3.5 ± 0.5 kcal/mol, which gives 44.4 kcal/mol.

From these estimations, $D_0$ is given as 46.6 ± 1.7 kcal/mol. The standard heat of formation of $NO_3$ ($\Delta_f H^0(NO_3)$) at 0 K can be calculated from the known values of heat of formation of $NO_2$ and O ($^3P$), resulting in $\Delta_f H^0(NO_3)$ = 21.0 ± 1.7 kcal/mol at 0 K. This corresponds to 19.7 ± 1.7 kcal/mol at 298 K, substantially higher than the result of Cantrell et al.,[26] who reported $\Delta_f H^0(NO_3)$ = 15.39 ± 0.72 kcal/mol at 298 K. Our result is a few kcals higher than the JANAF compilation value, but within the error limits (17.0 ± 4.8 kcal/mol).[31] It will change dramatically the equilibrium constants of some reactions with which $NO_3$ is involved. For example, by using this value, the equilibrium constant for $NO_3$ + HCl = $HNO_3$ + Cl becomes about 1000 times larger than calculated with Cantrell et al.'s heat of formation.

Very recently, Weaver et al.[40] estimated the heat of formation of $NO_3$ from the measured electron affinity of $NO_3$ and the heat of formation of $NO_3^-$. Their

value is 17.91 ± 0.79 kcal/mol, which agrees with the previous value of 17.0 ± 5.0 kcal/mol.[31]

Using the Cantrell et al.'s enthalpy of formation of $NO_3$, the wavelength threshold for the formation of $NO_2$ + O is 564 nm. If that were true, the dissociation signals we have seen should have come from the hot band contribution and when $NO_3$ is photolyzed with 532 nm, we should have seen a large increase in the slow $NO_2$ + O fragments signal, which was not observed.

## IV. Discussion

### A. Excitation spectroscopy of $NO_3$

It was expected before the experiment that the excitation spectrum would show a couple of discrete peaks when the temperature of $NO_3$ was cooled down, due to Jahn-Teller splitting.[41] How can we explain the appearance of 7 peaks observed around 15109 $cm^{-1}$ (Figure 5)?

One possible explanation is that the hot band contribution might be involved in this spectrum. Nelson et al.[34] assigned the 644 nm (15532 $cm^{-1}$) absorption peak as a fundamental vibration of the excited states, although the location of this transition overlaps the hot band transition from 368 $cm^{-1}$ to the state at 16053 $cm^{-1}$. This vibrational mode is 423 $cm^{-1}$ in frequency and considered to correspond to the same normal mode as 368 $cm^{-1}$ for the ground state. Then the Franck-Condon

factor would be favorable for the transition from the 368 $cm^{-1}$ state to the excited 644 nm (15532 $cm^{-1}$) state. The measured vibrational temperature in the beam was 300 K, at which the population of the $NO_3$ in the 368 $cm^{-1}$ vibrational state is about 10 % when it is non-degenerate and 20 % when it is degenerate.

It is possible that the Jahn-Teller coupling, either dynamic or static,[42] affects the energy levels of excited state $NO_3$ in a very complex way. Also Spin-orbit coupling and the complexity of the ground state structure may contribute to the excitation spectrum.

The existing data are in the process of analysis. Obviously, additional experimental information would be very useful. The best information would be obtained from high resolution spectroscopy by the ring dye laser which can provide 1 MHz line width. Although the Doppler width of about 30 Mhz would be the limiting factor in resolution, it may be reduced further if the signal is strong enough.

In this experiment the backing pressure was maintained only at 150 Torr at highest. The mass spectrometer detection system could not be operated at higher backing pressure, which would result in higher main chamber pressure. By increasing the backing pressure to a few atm, a very cold beam can be obtained. Also pulsed pyrolysis may be employed, to generate a pulsed $NO_3$ beam.

**B. Measurement of vibrational temperature.**

$NO_3$ shows 0-0 transition at 662 nm (15109 $cm^{-1}$) and a hot band absorption at 678.4 nm (14745 $cm^{-1}$), which corresponds to the transition from 368 $cm^{-1}$ to

15109 $cm^{-1}$. By comparing the intensities of the fluorescence peak excited by 662 and 678 nm with measured absorption cross sections for those wavelengths at certain temperature, the vibrational temperature can be calculated. The absorption cross sections for $NO_3$ at different temperatures[19] are listed below.

| Temperature(K) | $\sigma$ at 662 nm X $10^{19}$ ($cm^2$/molecule) | $\sigma$ at 679 nm X $10^{19}$ ($cm^2$/molecule) | $\sigma_{662} / \sigma_{679}$ |
|---|---|---|---|
| 298 | 228.0 | 8.5 | 26.8 |
| 230 | 266.9 | 7.3 | 36.6 |

It should be mentioned that Cantrell et al.[43] obtained no temperature dependence in absorption cross section of 662 nm, which is contrary to Sander's observation.

Several nozzles of different design were used in the experiment. With the first nozzle, the ratio of the fluorescence intensity at 662 nm to that at 679 nm, normalized by laser power, was 12.7. This indicates there is significantly higher population at the vibrational state 368 $cm^{-1}$ above the ground state than at 298 K. By improving the nozzle design we were able to increase the ratio $\sigma_{662}/\sigma_{679}$ up to 30. Refering to the above table, the vibrational temperature was estimated to be close to room temperature with this nozzle.

**C. Photodissociation of $NO_3$**

Our results indicate that $NO_3$ photodissociates on absorption of a single photon to form $NO_2$ + O (623 – 532 nm) and NO + $O_2$ (602 – 586 nm) in collision free conditions. Magnotta and Johnston[28] observed both channels in the study of photodissociation of $NO_3$ using laser photolysis in flow cell. Their experiments were performed at 10 Torr which allowed thousands of collisions in the lifetime of the $NO_3$ excited state. Nelson et al. suggested the dissociation observed above 580 nm was collisionally induced.[22] One of the motivation of this time-of-flight study was to reinvestigate the photodissociation of $NO_3$ in collision free conditions.

They were able to measure the absolute quantum yield for both channels ($NO_2$ + O, NO + $O_2$), while we could only obtain the relative quantum yields (Figure 17 A). Their measured absolute quantum yield for both channels are presented in Figure 17 B. Our measured values for relative quantum yield for each channel show a little higher values for the relative quantum yield of NO + $O_2$ channel than their values, although the wavelength dependence of the quantum yields looks very similar to their measurements.

The quantum yield for NO + $O_2$ reaches its maximum value of 0.5 at 590 nm, where at least 5 % of the $O_2$ molecules are formed in the $^3\Sigma_g^-$ ground electronic state. From the analysis of the time-of-flight spectra, more than 50 % of $O_2$ photoproducts are believed to be in the $^1\Delta_g$ excited state. Considering the absence of a slow $O_2$ signal ($E_{trans}$ < 5 kcal/mole ), $O_2$ ($^1\Sigma_g^+$) does not seem to be the product of the dissociation.

Since the two components in the NO + $O_2$ TOF data are not very well resolved, quantitative estimation of the relative quantum yields of the two $O_2$ electronic states as a function of wavelength is not possible. Based on the shape of the NO + $O_2$ time-of-flight spectra, it appears that no drastic change in relative quantum yield occurs in wavelength range 602 – 586 nm, where NO + $O_2$ dissociation channel was observed. This suggests that both processes leading to two different electronic states of $O_2$ ($^3\Sigma_g^-$ and $^1\Delta_g$) have similar barrier heights.

It is very interesting that the photodissociation of $NO_3$ into NO + $O_2$ is observed in a very narrow wavelength range (602 – 586 nm). In contrast, $NO_2$ + O is observed at all wavelengths studied shorter than 637 nm. At 590 nm (16953 $cm^{-1}$), $NO_3$ is excited only 5 kcal/mol (1750 $cm^{-1}$) above the (0,0) band origin (662 nm, 15111 $cm^{-1}$). Formation of NO + $O_2$ involves bond rearrangement and is expected to require bond distortion greater than that provided by 5 kcal/mol of vibrational excitation. This suggests that formation of NO + $O_2$ involves internal conversion of electronically excited $NO_3$ to vibrationally hot ground state (or lower electronic states). Siegbahn[29] calculated a barrier height of more than 120 kcal/mol for the $C_{2v}$ constrained dissociation process of $NO_3$ to ground state NO + $O_2$ ($^3\Sigma_g^-$). Since we detected photodissociation of $NO_3$ to NO + $O_2$ at about 602 nm (16615 $cm^{-1}$), the barrier actually lies less than 47.5 kcal/mol above $NO_3$.

The disappearance of $NO_3 \rightarrow$ NO + $O_2$ at wavelengths shorter than 584 nm suggests a possible kinetic competition with the $NO_2$ + O channel. The NO + $O_2$ quantum yield decreases sharply when the photolysis wavelength is changed to

wavelengths shorter than 590 nm. A simple and plausible explanation for this observation could be that the vibrationally hot $NO_3$, produced by internal conversion, also dissociates to $NO_2$ + O. The apparent equal quantum yields for the two channels at 590 nm suggests that the two dissociation channels have the same rate constant if both channels dissociate from the common precursor.

However, the existence of the $NO_2$ + O channel both at longer and shorter wavelengths than the NO + $O_2$ dissociation region indicates that $NO_3$ photodissociation cannot be explained in terms of simple kinetic competition between the two dissociation channels. Another possible mechanism might be either a crossing of the potential energy surface between 582 and 605 nm or the participation of two different electronic states in the excitation process. Due to a Jahn-Teller distortion, the excited states of $NO_3$ around this region would have $C_{2v}$ symmetry, $^2B_2$ and $^2A_1$.

At excitation wavelengths longer than 605 nm, fluorescence is observed, which competes with the dissociations. The fluorescence is not observed at wavelengths shorter than 605 nm, suggesting that dissociations dominate radiative processes in that region. An experiment is being studied in Y. T. Lee group to find out the rate of $NO_3 \rightarrow NO + O_2$ photodissociation, by detecting NO photoproduct with picosecond laser.

More detailed analysis of the data and study of the possible dissociation mechanisms is being worked on currently and will be reported soon.

*Acknowledgements*

It is a great pleasure to acknowledge the support by Prof. Y. T. Lee and his coworker in carrying out the Translational Spectroscopy of the photofragmentation of $NO_3$. This work is done under the direction of Prof. Y. T. Lee, using his molecular beam machine. Floyd Davis is a graduate student in Prof. Lee group, who have been responsible for much of the effort in performing time-of-flight experiments. He taught the author about the techniques and principles of the translational spectroscopy, came up with numerous exciting ideas to solve difficult problems, and prepared a draft article for publication. Part of the photodissociation section including the heat of formation determination in this chapter used some of the contents of the article prepared by him. This work was supported by the Director, Office of Energy Research, Office of Basic energy Sciences, Chemical Sciences Division of the U.S. Department of Energy under Contract No. DE-AC03-76SF00098. This DOE support also covers the research done in Prof. Lee group.

## Appendix

### Chemical kinetics calculation of $NO_3$ by ACUCHEM

$NO_3$ Production(600K) from $N_2O_5$, [He] = 120 Torr (= 60 torr of $N_2$).

| Time(sec) | $N_2O_5$ | $NO_2$ | $NO_3$ | NO | O2 |
|---|---|---|---|---|---|
| 0.000E+00 | 1.750E+17 | 3.500E+15 | 1.000E+12 | 1.000E+11 | 1.000E+14 |
| 1.000E-06 | 1.357E+17 | 4.282E+16 | 3.930E+16 | 4.443E+12 | 1.078E+14 |
| 2.500E-06 | 9.329E+16 | 8.534E+16 | 8.156E+16 | 2.165E+13 | 1.883E+14 |
| 5.000E-06 | 5.226E+16 | 1.271E+17 | 1.219E+17 | 3.706E+13 | 5.551E+14 |
| 7.500E-06 | 3.226E+16 | 1.482E+17 | 1.407E+17 | 4.401E+13 | 1.145E+15 |
| 1.000E-05 | 2.265E+16 | 1.593E+17 | 1.489E+17 | 4.755E+13 | 1.860E+15 |
| 2.500E-05 | 1.395E+16 | 1.776E+17 | 1.479E+17 | 5.325E+13 | 6.701E+15 |
| 5.000E-05 | 1.356E+16 | 1.937E+17 | 1.327E+17 | 5.805E+13 | 1.451E+16 |
| 7.500E-05 | 1.309E+16 | 2.086E+17 | 1.186E+17 | 6.254E+13 | 2.176E+16 |
| 1.000E-04 | 1.249E+16 | 2.226E+17 | 1.059E+17 | 6.673E+13 | 2.846E+16 |
| 2.500E-04 | 7.863E+15 | 2.862E+17 | 5.150E+16 | 8.580E+13 | 5.796E+16 |
| 5.000E-04 | 2.554E+15 | 3.340E+17 | 1.427E+16 | 1.001E+14 | 7.924E+16 |
| 7.500E-04 | 7.108E+14 | 3.482E+17 | 3.805E+15 | 1.044E+14 | 8.539E+16 |
| 1.000E-03 | 1.897E+14 | 3.520E+17 | 1.004E+15 | 1.055E+14 | 8.706E+16 |
| 2.500E-03 | 6.284E+10 | 3.534E+17 | 3.313E+11 | 1.059E+14 | 8.765E+16 |
| 5.000E-03 | 9.892E+04 | 3.534E+17 | 5.215E+05 | 1.059E+14 | 8.765E+16 |
| 7.500E-03 | 1.555E-01 | 3.534E+17 | 8.200E-01 | 1.059E+14 | 8.765E+16 |
| 1.000E-02 | 2.157E-07 | 3.534E+17 | 1.137E-06 | 1.059E+14 | 8.765E+16 |
| 2.500E-02 | 1.097E-09 | 3.534E+17 | 5.785E-09 | 1.059E+14 | 8.765E+16 |
| 5.000E-02 | 4.937E-11 | 3.534E+17 | 2.603E-10 | 1.059E+14 | 8.765E+16 |
| 7.500E-02 | 1.000E-30 | 3.534E+17 | 1.000E-30 | 1.059E+14 | 8.765E+16 |
| 1.000E-01 | 1.000E-30 | 3.534E+17 | 1.000E-30 | 1.059E+14 | 8.765E+16 |
| 2.500E-01 | 1.000E-30 | 3.534E+17 | 1.000E-30 | 1.059E+14 | 8.765E+16 |
| 5.000E-01 | 1.000E-30 | 3.534E+17 | 1.000E-30 | 1.059E+14 | 8.765E+16 |

Rate constants:

1) $N_2O_5 \rightarrow NO_2 + NO_3$ / 0.2550E+06 ($cm^{-3}$ $molecule^1$ $s^{-1}$)

2) $NO_2 + NO_3 \rightarrow N_2O_5$ / 0.1340E-12 ($cm^3$ $molecule^{-1}$ $s^{-1}$)

3) $NO_2 + NO_3 \rightarrow NO + O_2 + NO_2$ / 0.9000E-14 ($cm^{-3}$ $molecule^1$ $s^{-1}$)

4) $NO + NO_3 \rightarrow NO_3 + NO_3$ / 0.3000E-10 ($s^{-1}$)

5) $NO_3 + NO_3 \rightarrow O2 + NO_2 + NO_2$ / 0.3980E-14 ($cm^{-3}$ $molecule^1$ $s^{-1}$)

The rate constants are calculated at the experimental pressure and temperature using the values in Ref. 34.

**References**

1. M. Heaven, T. A. Miller, and V. E. Bondybey, Chem. Phys. Lett. **84**, 1 (1981).

2. D. E. Powers, J. B. Hopkins, and R. E. Smalley, J. Phys. Chem. **85**, 2711 (1981).

3. B. M. DeKoven, D. H. Levy, H. H. Harris, B. R. Zegarski, and T. A. Miller, J. Chem. Phys. **74**, 5659 (1981).

4. M. A. Johnson, J. Rostas, and R. N. Zare, Chem. Phys. Lett. **92**, 225 (1982).

5. M. Yamashita and J. B. Fenn, J. Phys. Chem. **88**, 4451 (1984).

6. M. Heaven, T. A. Miller, and V. E. Bondybey, J. Chem. Phys. **76**, 3831 (1982).

7. T. A. Miller and V. E. Bondybey, eds., in: Molecular spectroscopy, structure and chemistry ( North-Holland, Amsterdam, 1983) p.201.

8. P. Chen, S. D. Colson, W. A. Chupka, and J. A. Berson J. Phys. Chem. **90**, 2319 (1986).

9. S. Sharpe and P. Johnson, Chem. Phys. Lett. **107**, 35 (1984).

10. K. Obi, Y. Matsumi, Y. Takeda, S. Mayama, H. Watanabe, and S. Tsuchiya, Chem. Phys. Lett. **95**, 520 (1983).

11. S. Mayama, S. Hiraoka, and K. Obi, J. Chem. Phys. **80**, 7 (1983).

12. P. C. Engelking, Rev. Sci. Instrum. **57**, 2274 (1986).

13. G. Sprenger, Z. Elektrochem. **37**,674 (1931).

14. E. J. Jones and O. R. Wulf, J. Chem. Phys. **5**, 873 (1937).

15. D. A. Ramsay, Proc. Colloq. Spectrosc. Int. **10**, 583 (1962).

16. G. W. Chantry, A. Horsfield, J. R. Norton, and D. H. Whiffen, Mol. Phys. **5**, 589 (1962).

17. L. Dogliotti and E. Hayon, J. Phys. Chem. **71**, 3802 (1967).

18. A. R. Ravishankara and R. L. Mauldin, J. Phys. Chem. **89**, 3144 (1985).

19. S. P. Sander, J. Phys. Chem. **90**, 4135 (1986).

20. C. A. Cantrell, J. A. Davidson, R. E. Shetter, B. A. Anderson, and J. G. Calvert, J. Phys. Chem. **91**, 5858 (1987).

21. W. J. Marinelli, D. M. Swanson, and H. S. Johnston, J. Chem. Phys. **76**, 2864 (1982).

22. H. H. Nelson, L. Pasternack, and J. R. McDonald, J. Chem. Phys. **79**, 4279 (1983).

23. The spectrum is obtained by the same experimental set up as described in Chapter 1.

24. B. Kim, H. S. Johnston, D. A. Clabo, Jr., and H. F. Schaefer III, J. Chem. Phys. **88**, 3204 (1988).

25. H. S. Johnston, Science **173**, 517 (1971).

26. a) C. A. Cantrell, J. A. Davidson, A. H. McDaniel, R. E. Shetter, and J. G. Calvert, J. Chem. Phys. **88**, 4997 (1988).

    b) A. H. McDaniel, J. A. Davidson, C. A. Cantrell, R. E. Shetter, and J. G. Calvert, J. Phys. Chem. **92**, 4172 (1988).

27. R. A. Graham and H. S. Johnston, J. Phys. Chem. **82**, 254 (1978).

28. a) F. Magnotta and H. S. Johnston, Geophys. Res. Lett. **7**, 769 (1980).

b) F. Magnotta, Ph. D. Thesis, University of California, Berkeley and Lawrence Berkeley Laboratory report LBL-9981 (1979).

29. P. E. M. Siegbahn, J. Comput. Chem. **6**, 182 (1985).

30. The following values were adopted from Ref. 31 (0 K).

$\Delta_f H^0(NO_2)$ = 8.59 ± 0.2 kcal/mol, $\Delta_f H^0(O^3P)$ = 59.0 ± 0.02 kcal/mol.

31. M. W. Chase, Jr., C. A. Davis, J. R. Downy, Jr., D. J. Frurip, R. A. McDonald, and A. N. Syverud, JANAF Thermochemical Tables, 3rd. ed. (American Institute of Physics, New York, 1985).

32. B. Oh, Ph. D. Thesis, University of California, Berkeley (1988).

33. ACUCHEM, Computer program to solve chemical kinetics problem, written by Walter Braun and John T. Herron, Chemical Kinetics Division and David Kahaner, Scientific Computing Division National Bureau of Standards, Gaithersburg, Md 20899.

34. For each reaction the values in the following references are used.

(A). $N_2O_5 \rightarrow NO_2 + NO_3$ reaction : $K_{eq}$ in Ref. 26 (A) is used.

(B). $NO_2 + NO_3 \rightarrow N_2O_5$ :

C. C. Kircher, J. J. Margitan, and S. P. Sander, J. Phys. Chem. **88**, 4370 (1984).

(C). $NO_2 + NO_3 \rightarrow NO + O_2 + NO_2$ : Ref. 26 (A).

(D). $NO + NO_3 \rightarrow NO_2 + NO_2$ :

P. D. Hammer, E. J. Dlugokencky, and C. J. Howard, J. Phys. Chem. **90**, 2491. (1986).

(E). $NO_3 + NO_3 \rightarrow O_2 + NO_2 + NO_2$ : Ref. 28 (B).

35. H. H. Nelson, L. Pasternack, and J. R. McDonald, J. Phys. Chem. **87**, 1286 (1983).

36. Y. T. Lee, J. D. McDonald, P. R. LeBreton, and D. R. Hershbach, Rev. Sci. Instrum. **40**, 1402 (1969).

37. G. Schott and N. J. Davidson, J. Am. Chem. Soc. **80**, 1841 (1958).

38. G. O. Brink, Rev. sci. Instrum. **40**, 1402 (1966).

39. N. R. Daly, Rev. Sci. Instrum. **31**, 264 (1960).

40. R. E. Center and A. Mandl, J. Chem. Phys. **57**, 4104 (1972).

41. "Atlas of Mass Spectral data", E. Stenhagen, S. Abrahamson, and F. W. McLafferty, editors, Vol. 1 (Wiley, New York, 1969)

42. A. Weaver, D. W. Arnold, S. E. Bradforth, and D. M. Neumark, submitted to J. Chem. Phys.

43. H. A. Jahn and E. Teller, Proc. R. Soc. London, Ser. A **161**, 220 (1937).

44. G. Herzberg, "Electronic spectra of polyatomic molecules" (van Nostrand Reinhold, N.Y., 1966).

45. C. A. Cantrell, J. A. Davidson, R. E. Shetter, B. A. Anderson, and J. G. Calvert, J. Phys. Chem. **91**, 5858 (1987).

Table I. Experimental conditions for the fluorescence spectra in Figure 5. Some of the spectra are taken at the same conditions to check the reproducibility of the peaks (5A and B; D, E, and F; G and H; I and J).

| Figure | Data file | Buffer gas | Laser power | Dye |
|---|---|---|---|---|
| 5 A | k57d, k58a.dat | He | low | DCM |
| B | k57c.dat | He | low | DCM |
| C | kim1234.dat | He | high | DCM |
| D | k36c.dat | Ar | high | DCM |
| E | k36a.dat | Ar | high | DCM |
| F | k33b, k33c.dat | Ar | high | DCM |
| G | k44d, k44e.dat | Ar | low | LDS 698 |
| H | k44c.dat | Ar | low | LDS 698 |
| I | k37d, k37e.dat | He | high | DCM |
| J | k37b,k37c.dat | He | high | DCM |

Table II. Calculated $NO_3$ vibrational frequencies assuming $D_{3h}$ symmetry

| mode | vibrational frequency($cm^{-1}$) | $N(\nu_i)/N(\nu=0)$[a] | |
|---|---|---|---|
| | | 600 K | 300 K |
| $\nu_1$ | 1053 | 0.08 | 0.004 |
| $\nu_2$ | 762(degenerate) | 0.32 | 0.05 |
| $\nu_3$ | 1492 | 0.03 | $<0.001$ |
| $\nu_4$ | 368(degenerate) | 0.83 | 0.34 |

[a]The relative population $N(\nu_i)/N$(ground state) is calculated by the equation:

$N(\nu_i)/N(\text{ground state}) = g_i\exp(-\Delta E/kT)/g_0$,

where $g_i$ is the degeneracy of the vibrational state.

**Figure caption**

Figure 1. The laser induced fluorescence excitation spectrum of $NO_3$ at room temperature. Obtained in the experiments described in Chapter 1.

Figure 2. Fluorescence excitation spectra in the cold jet. He buffer gas was used in the expansion. (A) is obtained with low laser power (< 2 mJ/pulse) and 3rd nozzle which provided 300 K vibrational temperature. (B) is obtained with high laser power (~ 20 mJ/pulse) and the vibrational temperature in the molecular beam is higher than 450 K.

Figure 3. $NO_2$ LIF excitation spectrum in molecular beam. $NO_2$ was held at -40°C before expansion.

Figure 4. DCM dye power curve measured by Scientech Joule-meter. For YAG pumped dye laser.

Figure 5. LIF excitation spectra of $NO_3$. Details of the experimental conditions are listed in Table I. See text.

Figure 6. LIF excitation spectra of $NO_3$ around 678.0 nm. Obtained with He buffer gas. $NO_2$ fluorescence peaks are subtracted from the total spectrum. At 677.4 nm a shoulder is observed.

Figure 7. LIF excitation spectra of $NO_3$. (A) is obtained with Ar buffer gas, (B) is with He. The strong peaks between 640 and 648 nm are due to $NO_2$. Lambda Physik excimer pumped dye laser is used.

Figure 8. $NO^+$ (m/e=30) time-of-flight spectrum with 590 nm photolysis laser at 10° detection. Fast peak is due to NO + $O_2$ channel, slow peak is due to $NO_2$ + O channel.

Figure 9. $NO_2^+$ (m/e=46) time-of-flight spectrum with 590 nm photolysis laser at 10° detection. Corresponds to $NO_2$ fragment dissociated from $NO_2$ + O channel.

Figure 10. $O_2^+$ (m/e=32) time-of-flight spectrum with 590 nm photolysis laser at 10° detection. Corresponds to $O_2$ fragments dissociated from NO + $O_2$ channel.

Figure 11. $NO^+$ (m/e=30) time-of-flight spectrum with 590 nm photolysis laser detected at various angles. As the detection angle is increased, the peak corresponding to $NO_2$ fragments becomes weaker. See the Newton diagram in Figure 12.

Figure 12. Newton diagram for $NO_3 \rightarrow NO_2 + O$ at $E_c$ = 2 kcal/mol and 18.3 kcal/mol. To be detected at 12.5°, the $NO_2$ fragment should have at least 2 kcal/mol of translational energy (center-of-mass frame). To be detected at 40° $NO_2$ fragment should have at least 18.3 kcal/mol of $E_{trans}$.

Figure 13. Center-of-mass frame product translational energy distributions obtained by fitting the 590 nm dissociation time-of-flight spectra.

Figure 14. Time-of-flight spectrum of $O_2^+$ (m/e=32) with 590 nm photolysis laser at 35° detection. A shoulder is observed on the fast edge.

Figure 15 & 16.

time-of-flight spectra of $NO^+$ at 10° detection with different photolysis wavelength.

Figure 17 (A) Wavelength dependence for the relative quantum yields of two channels ($NO_2$ + O, NO + $O_2$). Circle represents $NO_2$ + O channel, cross for NO + $O_2$.

(B) Absolute quantum yield of two channels (NO + $O_2$, $NO_2$ + O). Obtained by Magnotta and Johnston[28] in flow cell experiment.

Figure 18. Time-of-flight spectrum for m/e = 16 ($O^+$) at 532 nm photolysis. The small component (dotted line) results from the fragmentation of the $NO_2$ fragment to $O^+$ in the electron bombardment ionizer. Solid line corresponds to the best fit to $P(E_T)$ in figure 20.

Figure 19. Time-of-flight spectrum for m/e = 46 ($NO_2^+$) at 532 nm photolysis, 10° detection. Same as Figure 18.

Figure 20. Product translational energy distributions for the $NO_3 \rightarrow NO_2$ + O at 532 and 590 nm photolysis.

Figure 21. An approximate correlation diagram of $NO_3$ and its photodissociation products. Dissociation into NO + $O_2$ is given to the right, and into $NO_2$ + O is given to the left. Both dissociations

are assumed to occur in the molecular plane.

Adapted from Nelson, et al.[22].

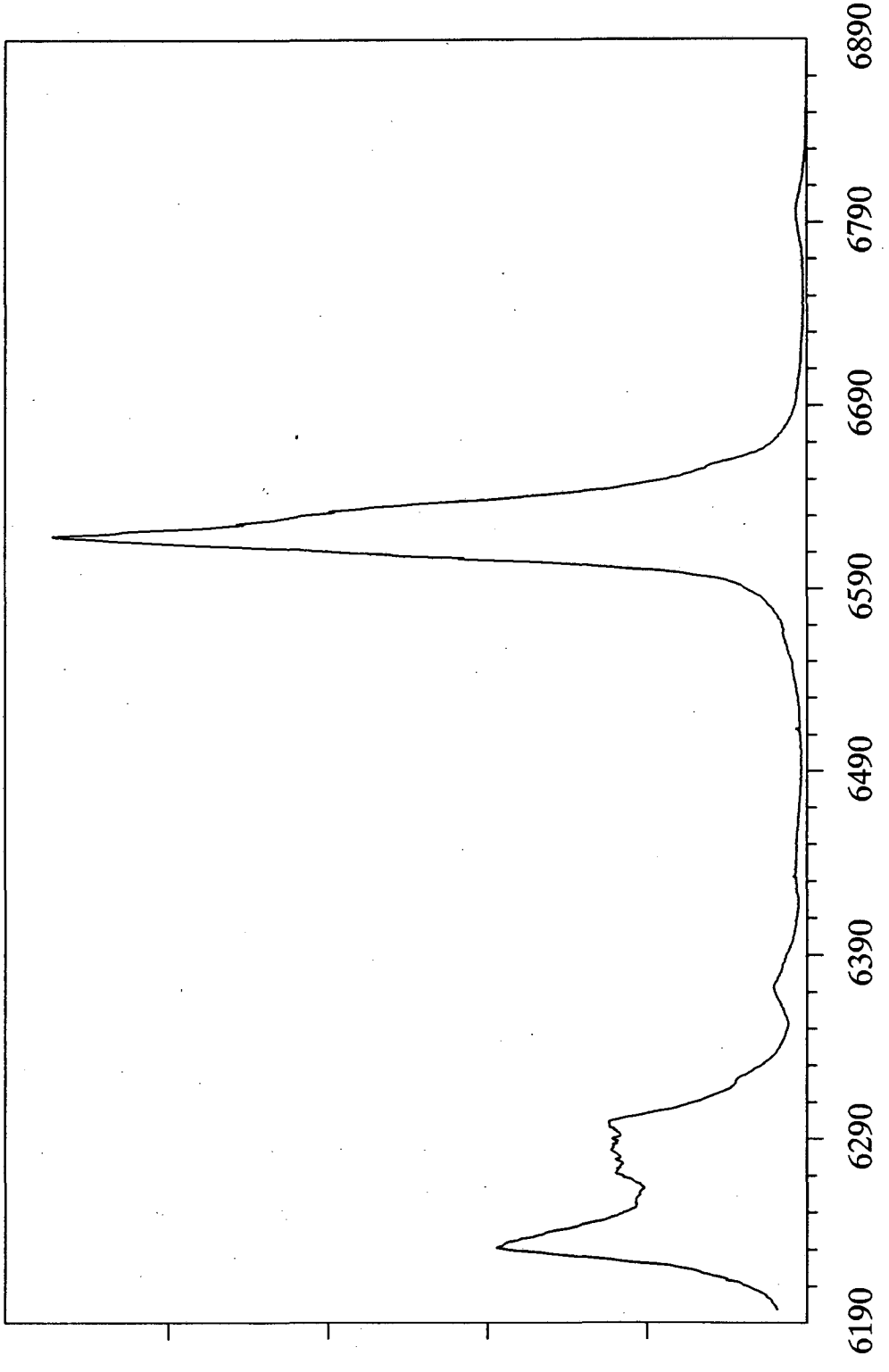


Figure 1

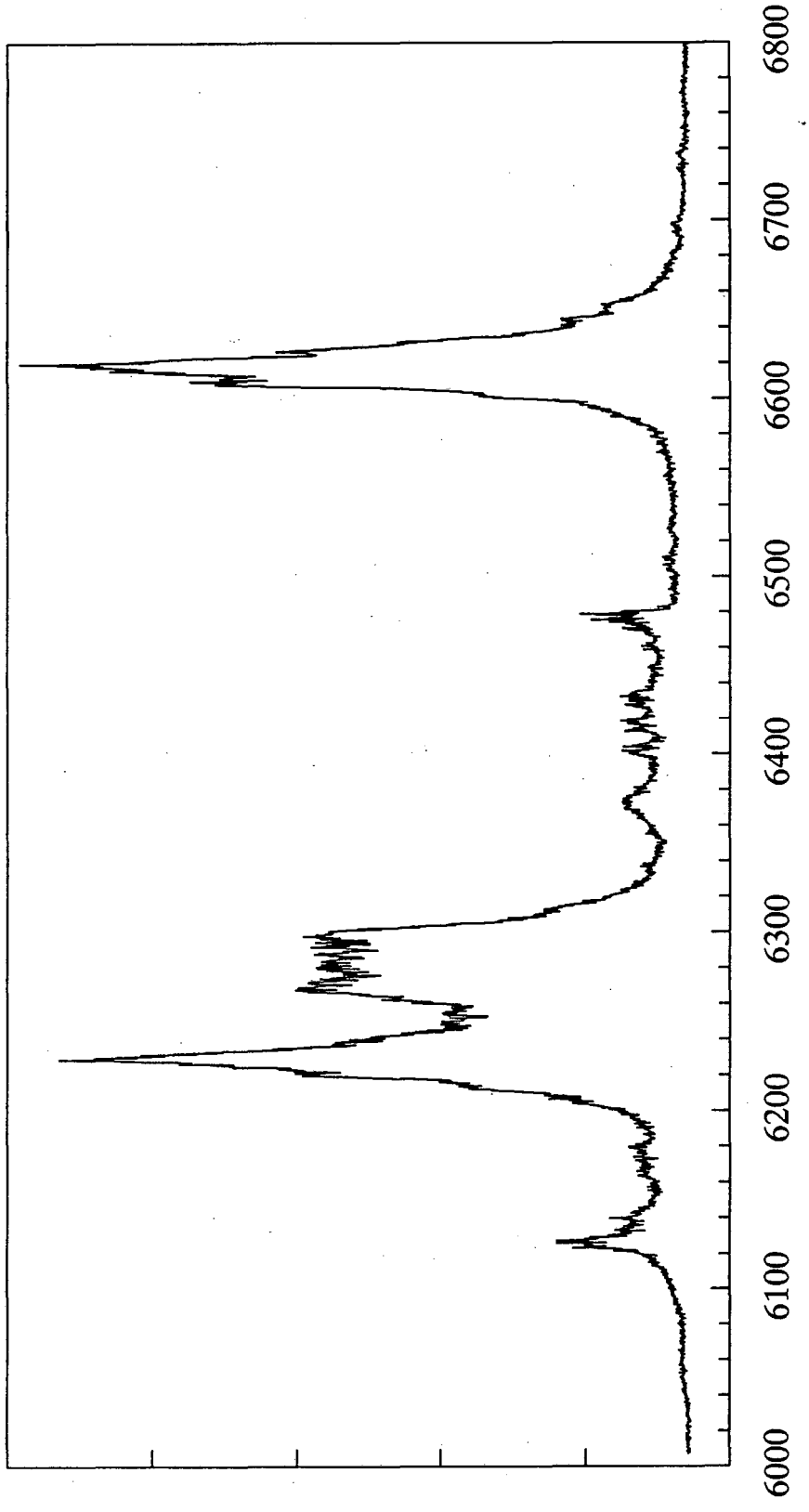


Figure 2 A

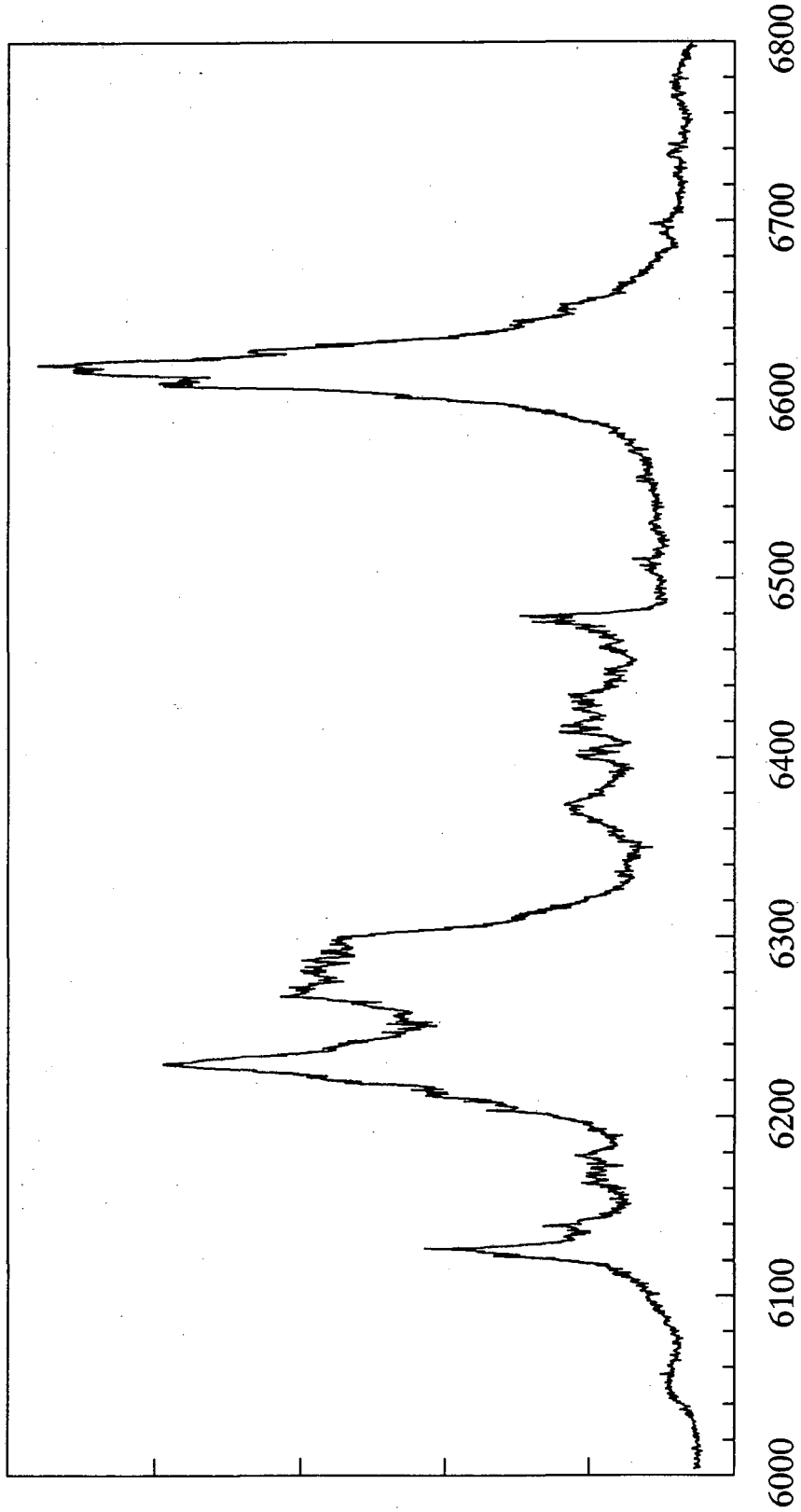


Figure 2 B

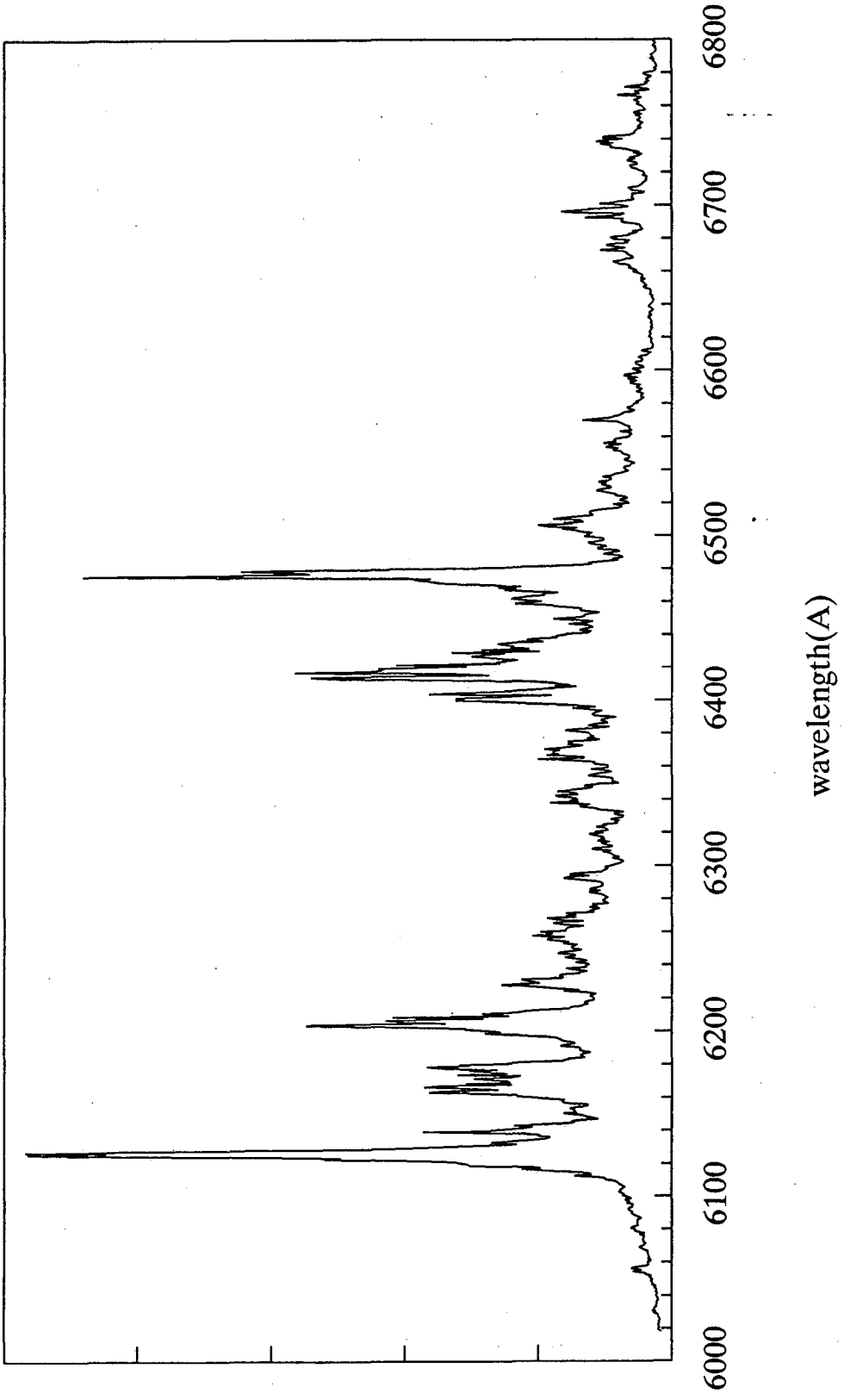


Figure 3

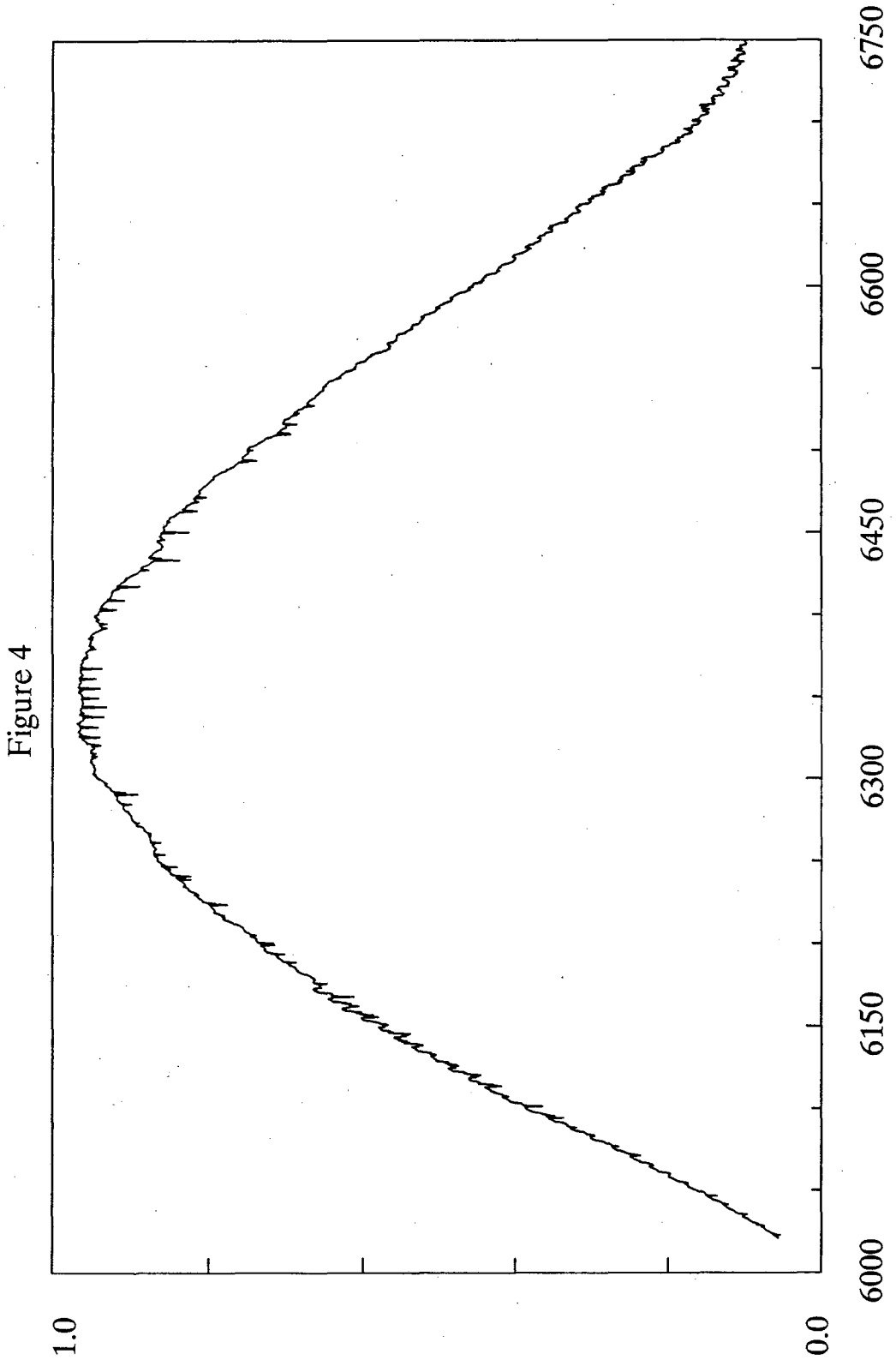


Figure 4

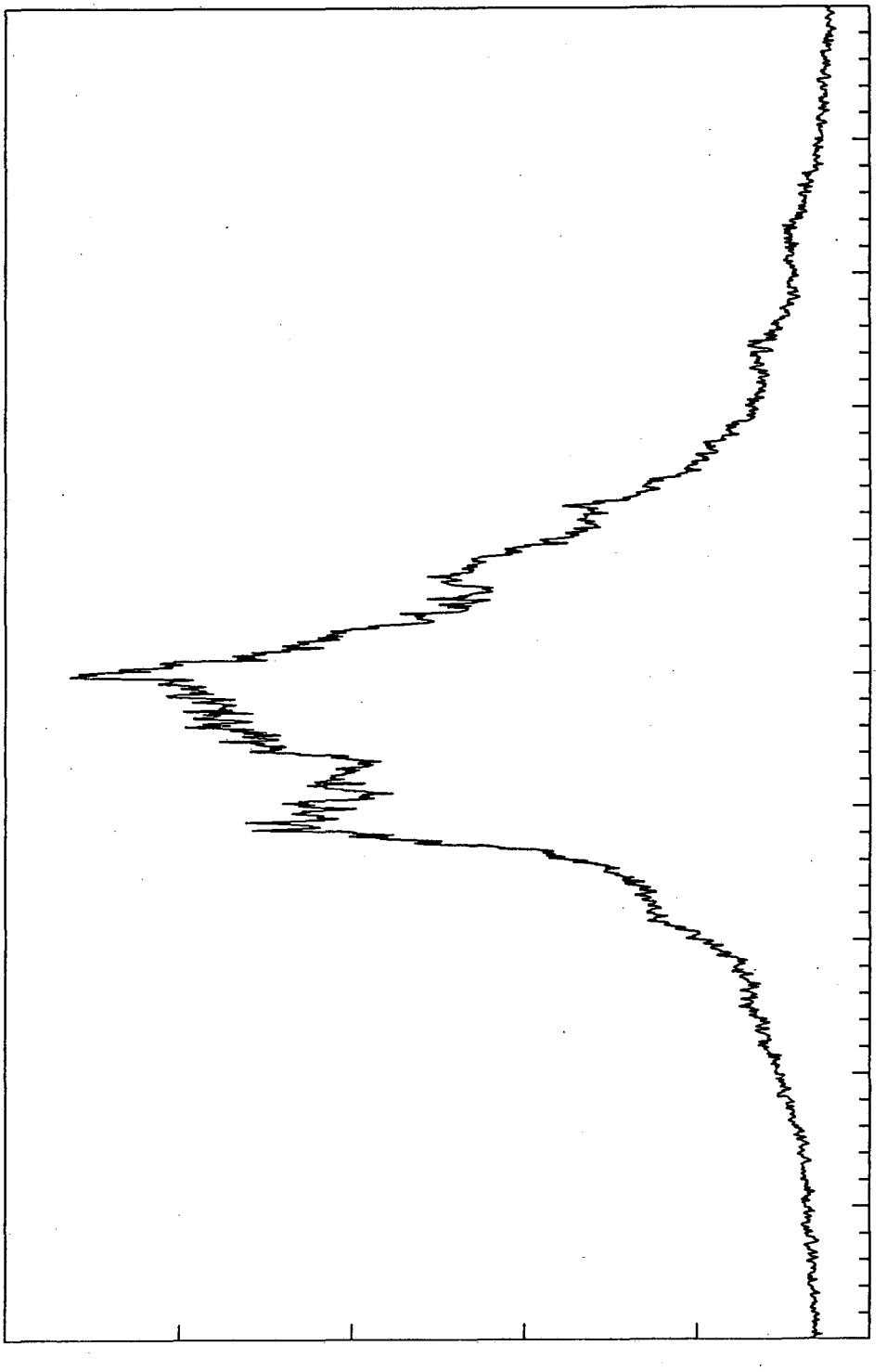
6570
6580
6590
6600
6610
6620
6630
6640
6650
6660
6670
wavelength(A)

Figure 5 A

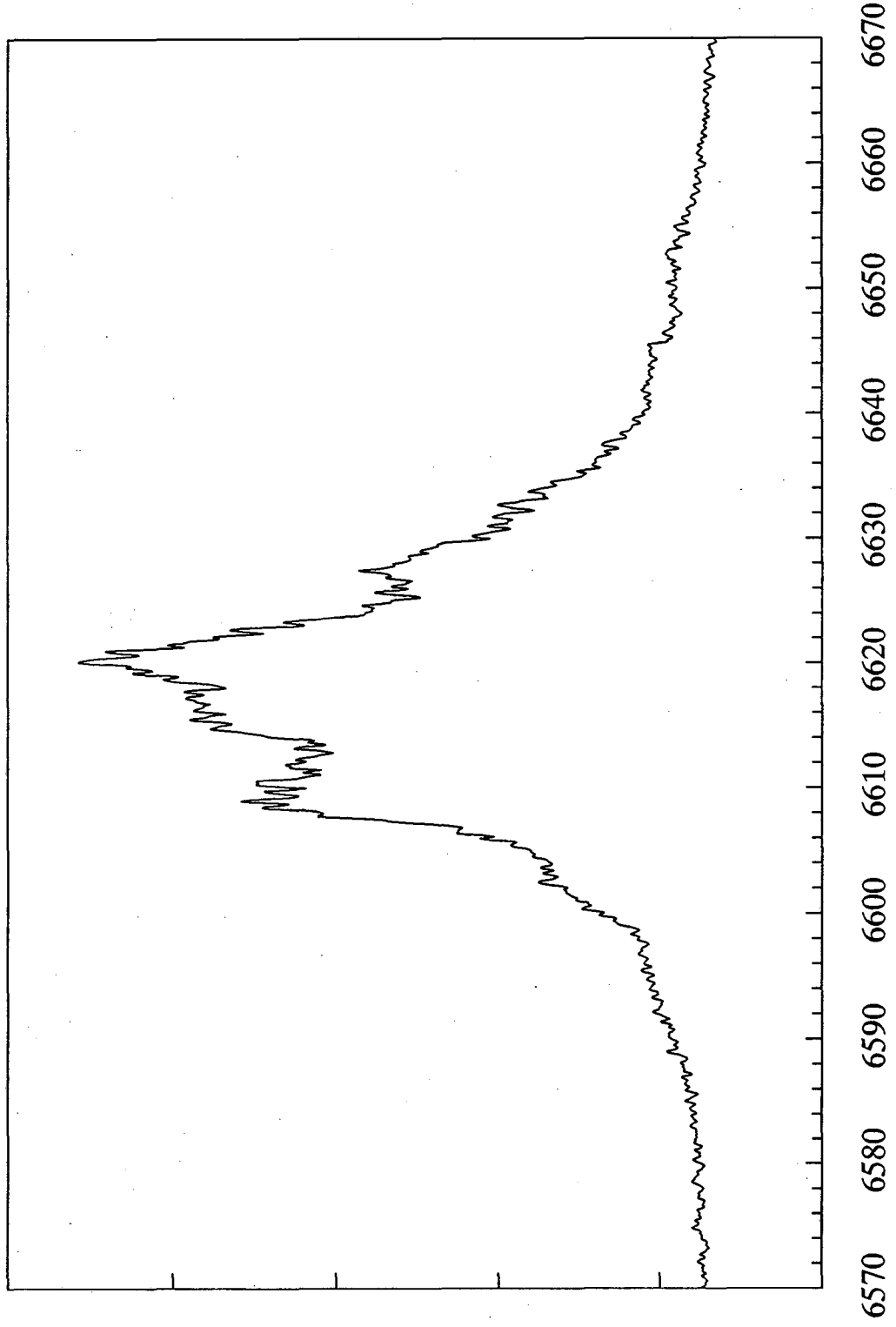
6570
6580
6590
6600
6610
6620
6630
6640
6650
6660
6670
wavelength(A)

Figure 5 B

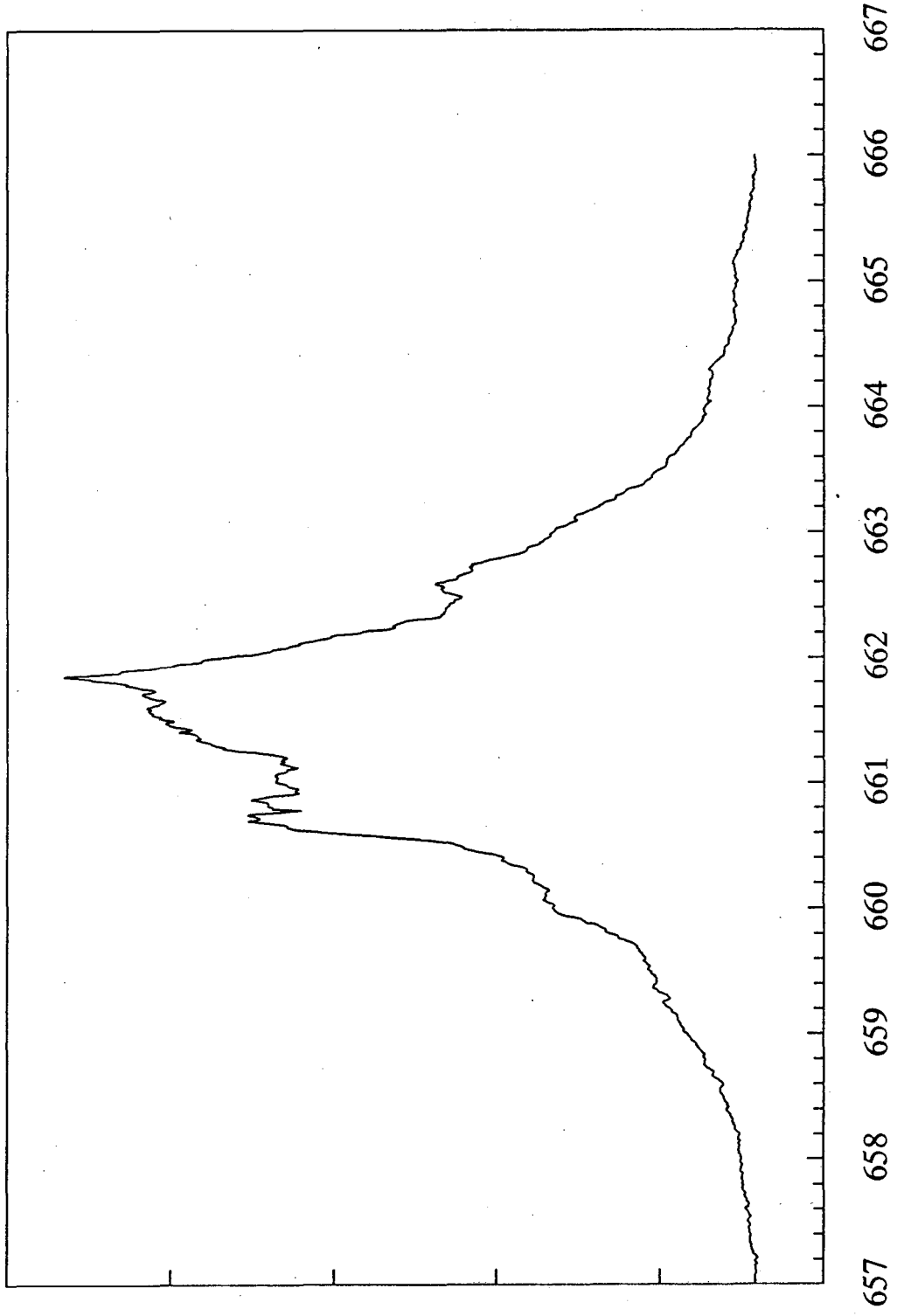


Figure 5 C

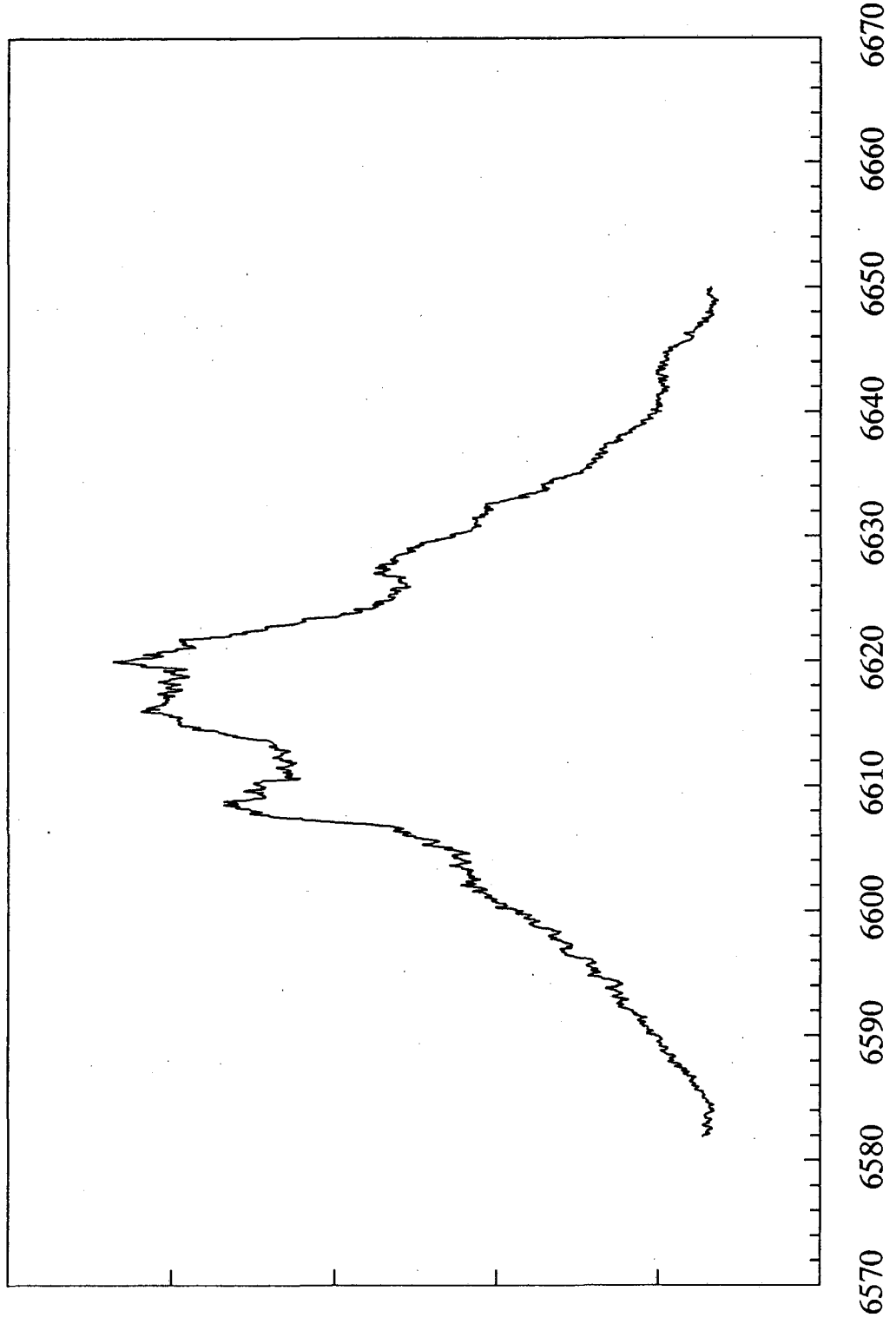
6570
6580
6590
6600
6610
6620
6630
6640
6650
6660
6670
wavelength(A)

Figure 5 D

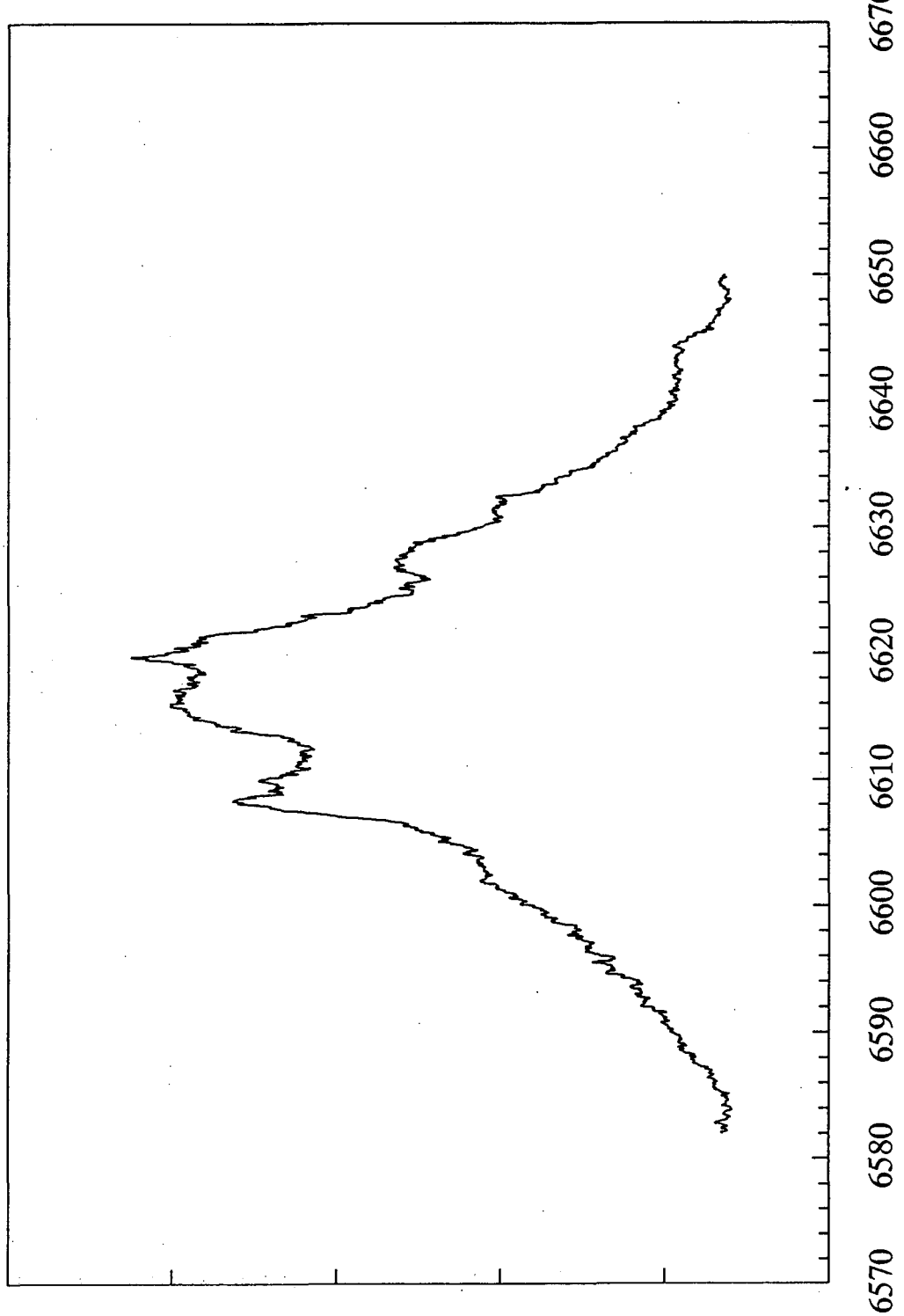
6570
6580
6590
6600
6610
6620
6630
6640
6650
6660
6670
wavelength(A)

Figure 5 E

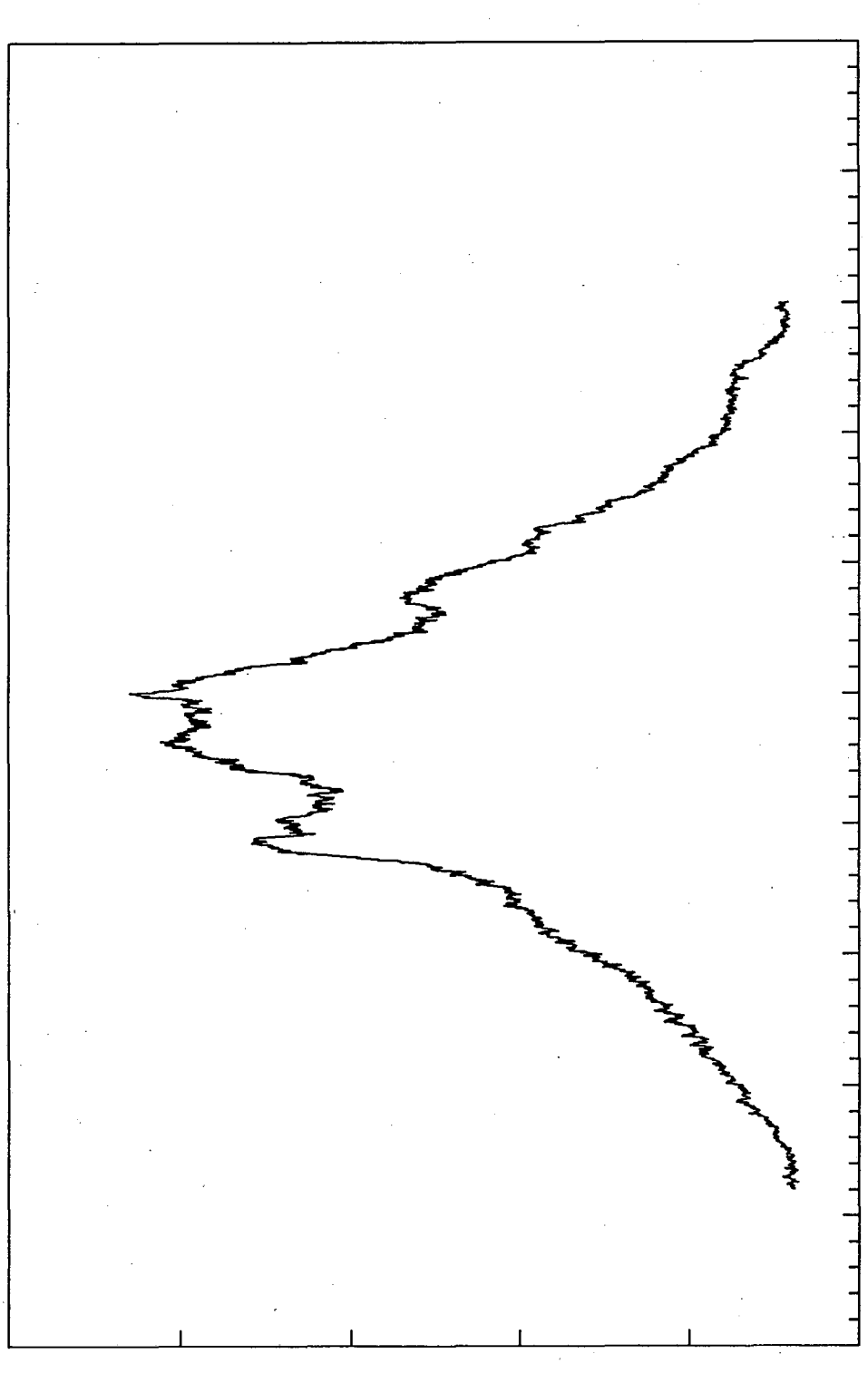
6570
6580
6590
6600
6610
6620
6630
6640
6650
6660
6670
wavelength(A)

Figure 5 F

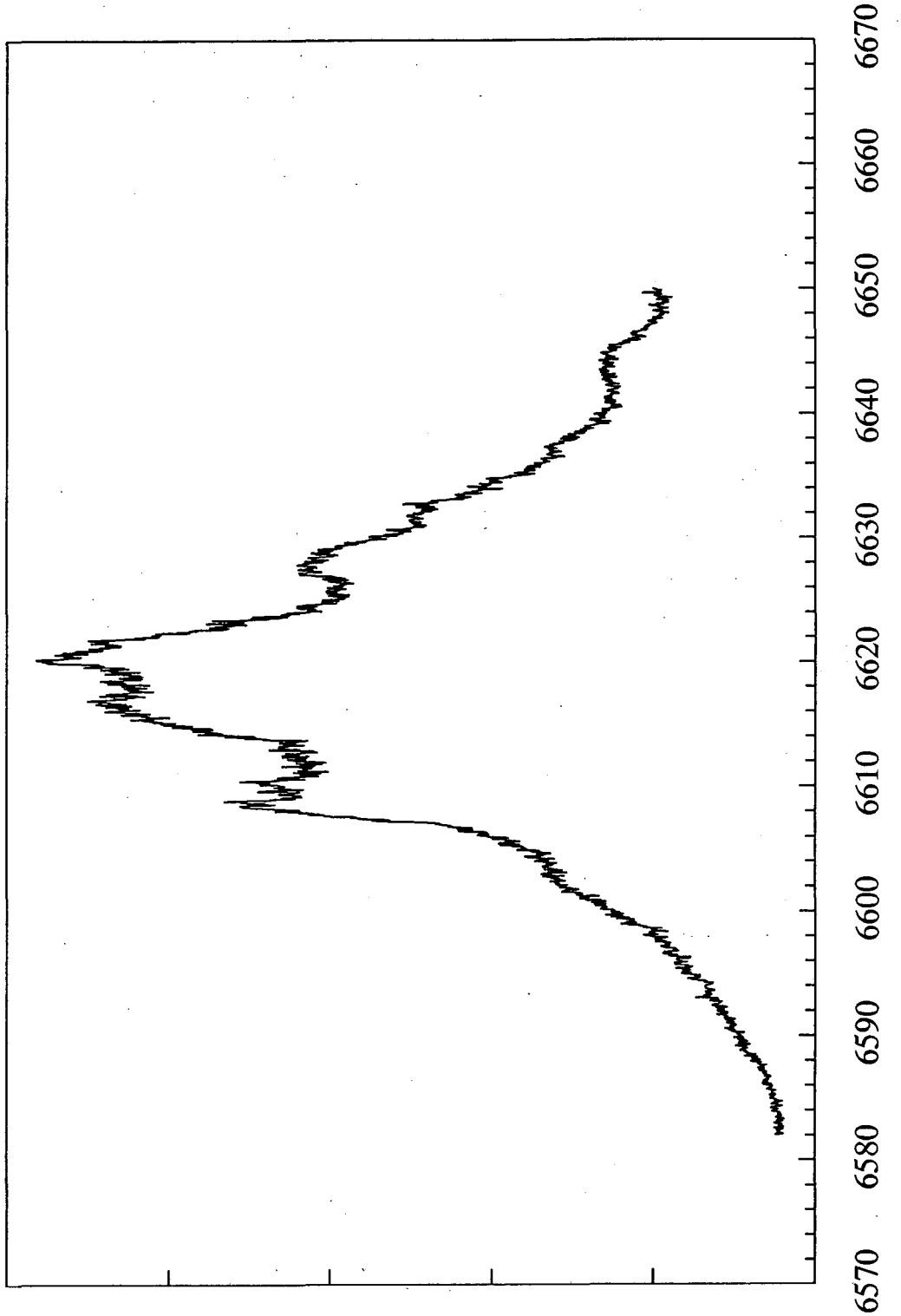
6570
6580
6590
6600
6610
6620
6630
6640
6650
6660
6670
wavelength(A)

Figure 5 G

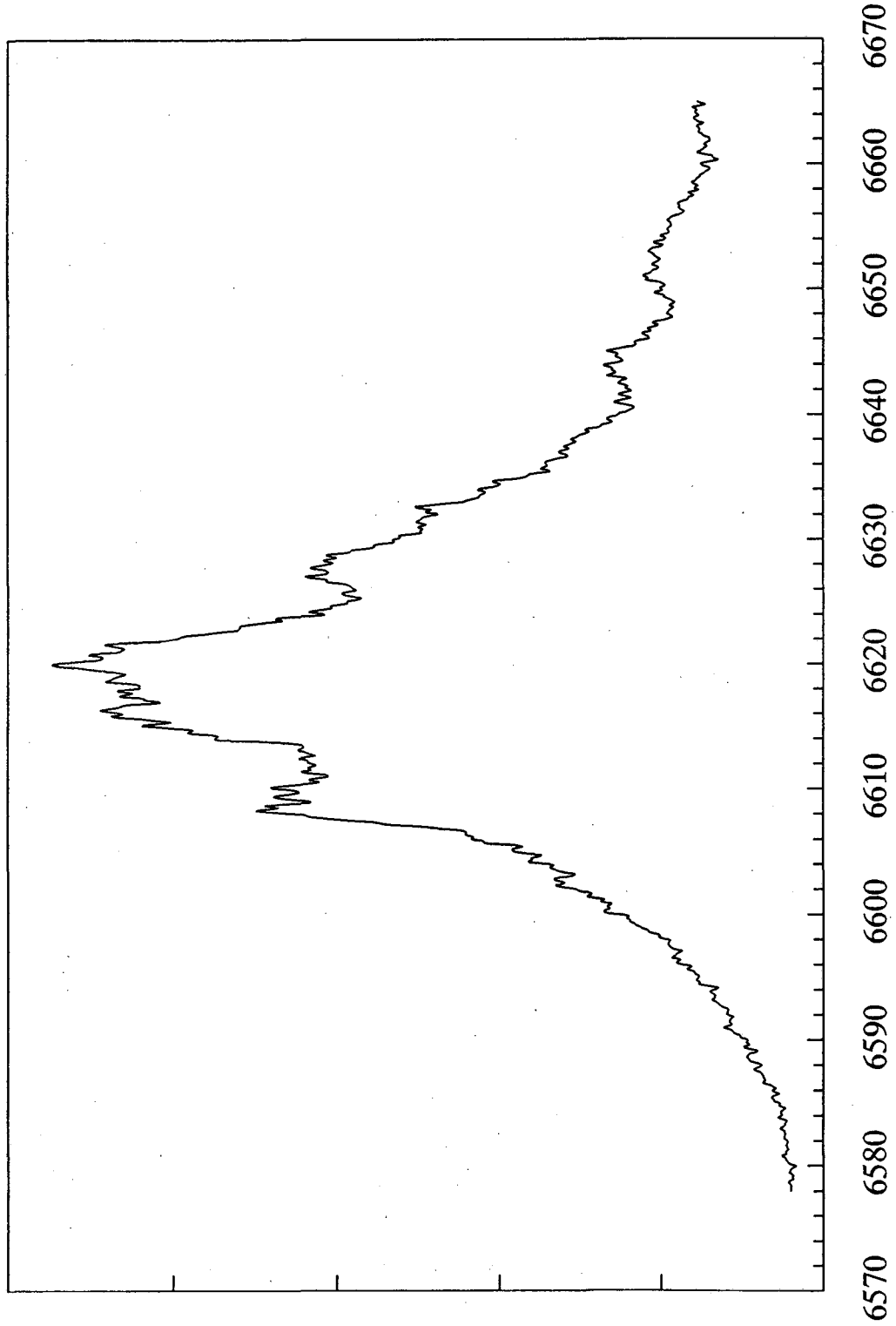
6570
6580
6590
6600
6610
6620
6630
6640
6650
6660
6670
wavelength(A)

Figure 5 H

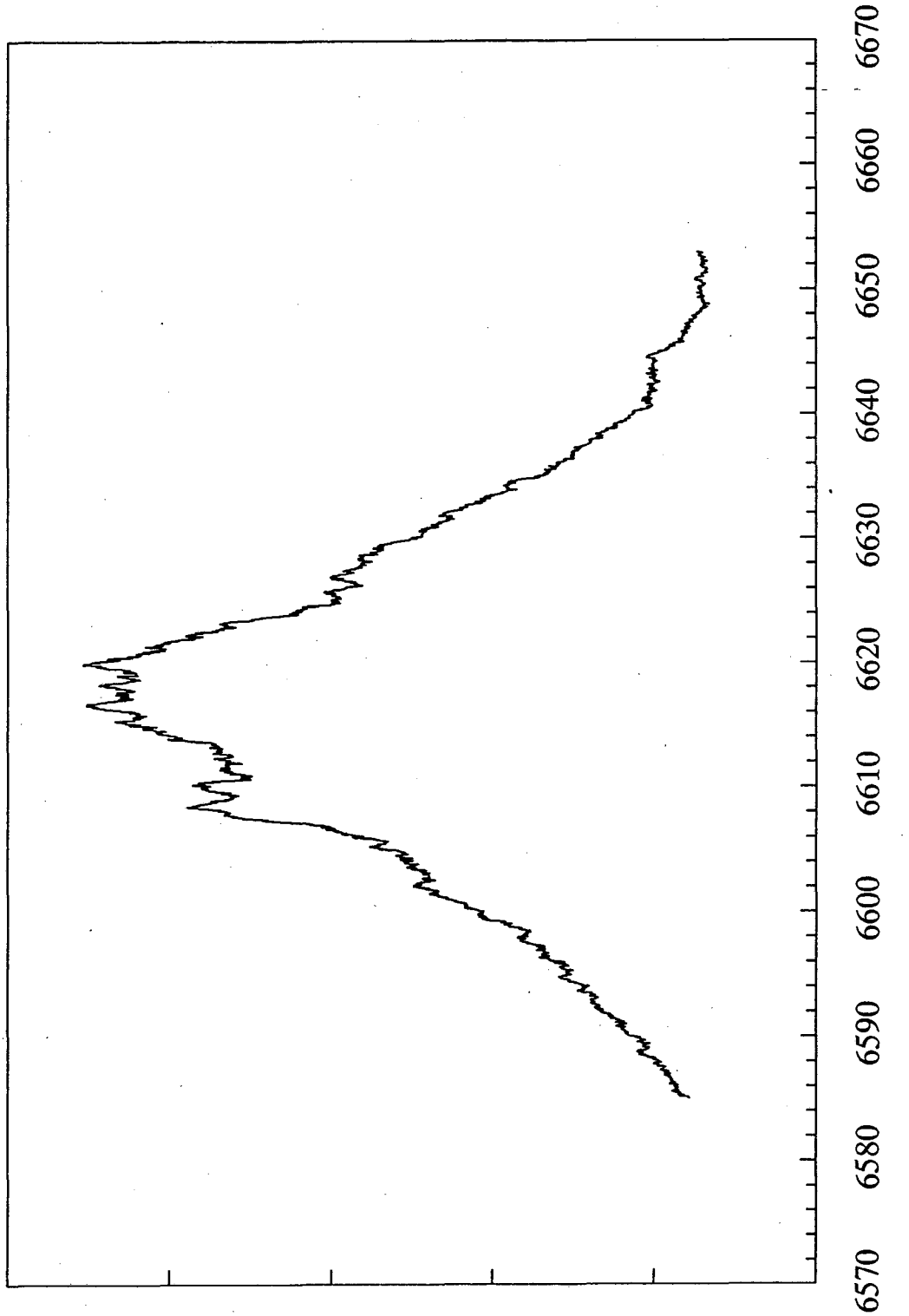
6570
6580
6590
6600
6610
6620
6630
6640
6650
6660
6670
wavelength(A)

Figure 5 I

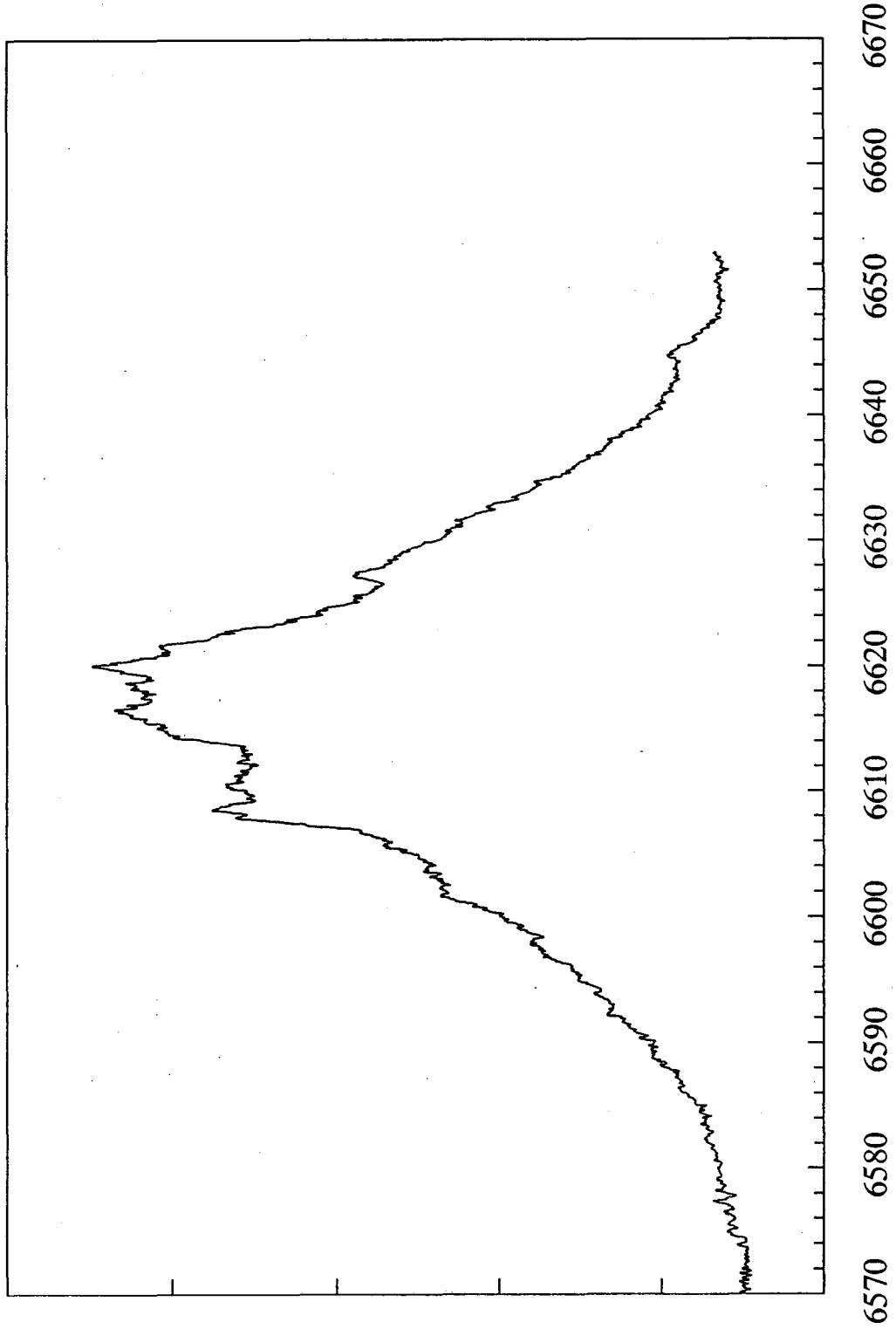
6570
6580
6590
6600
6610
6620
6630
6640
6650
6660
6670
wavelength(A)

Figure 5 J

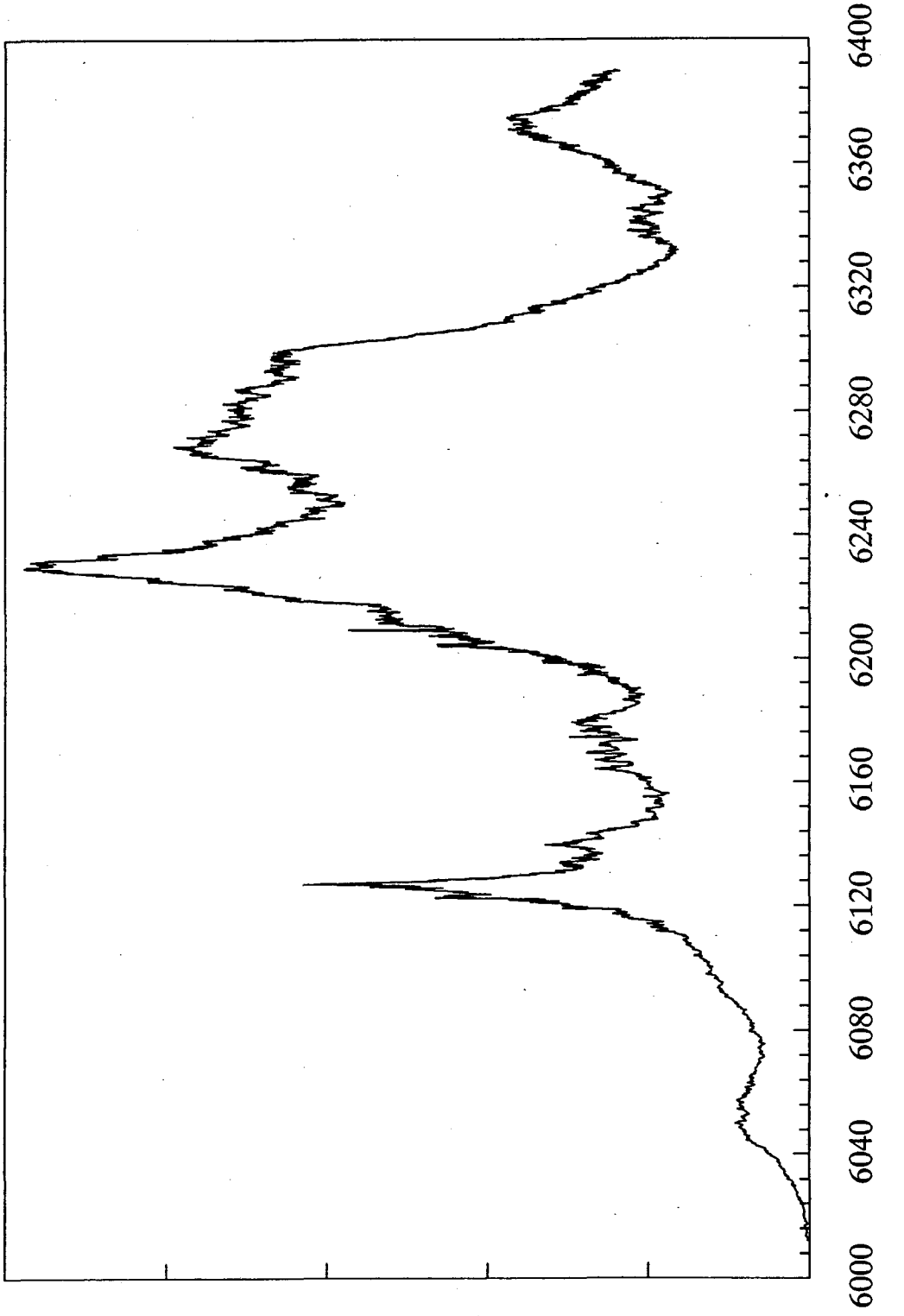
6000
6040
6080
6120
6160
6200
6240
6280
6320
6360
6400
wavelength(A)

Figure 5 K

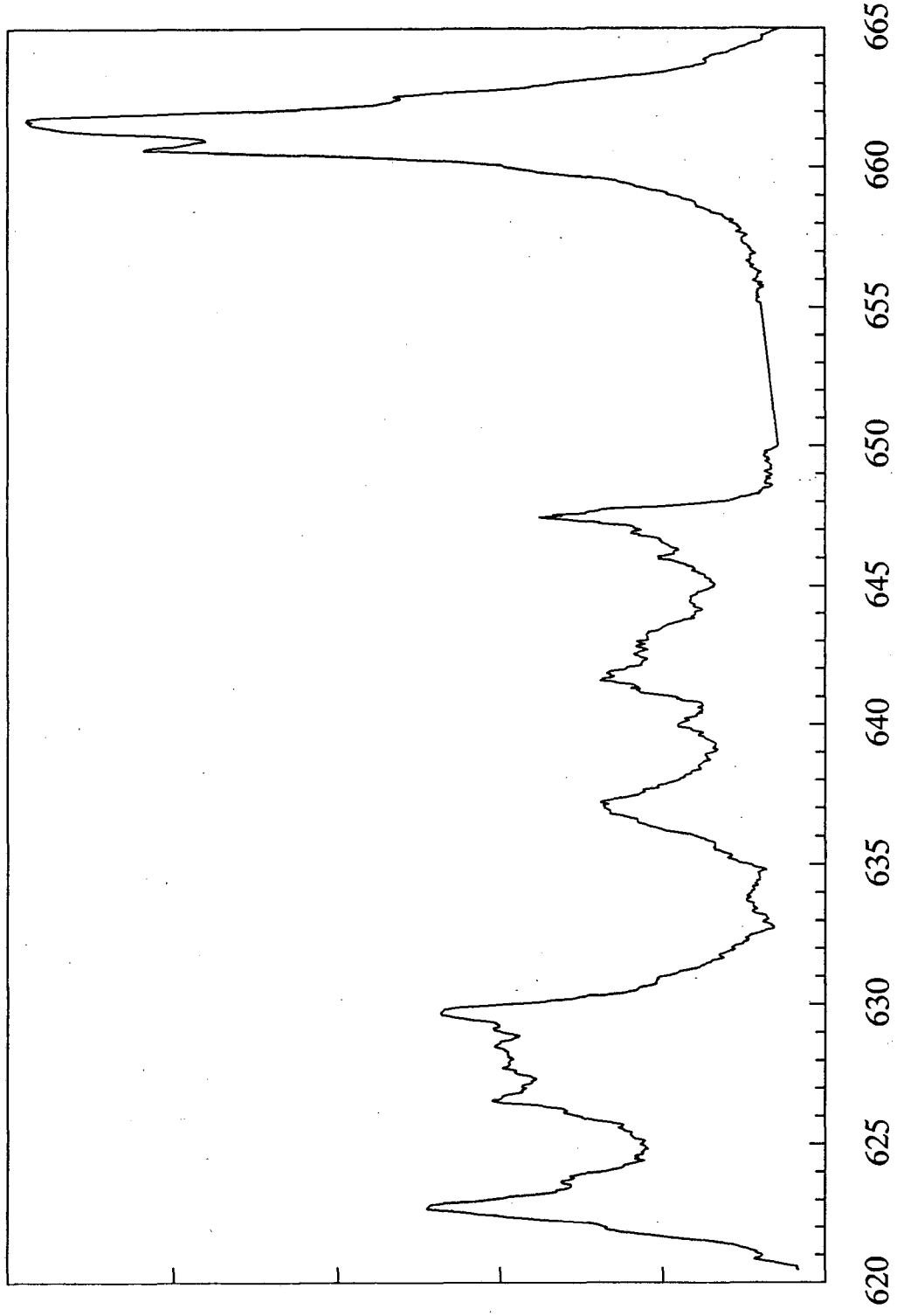


Figure 6 A

Figure 6 B

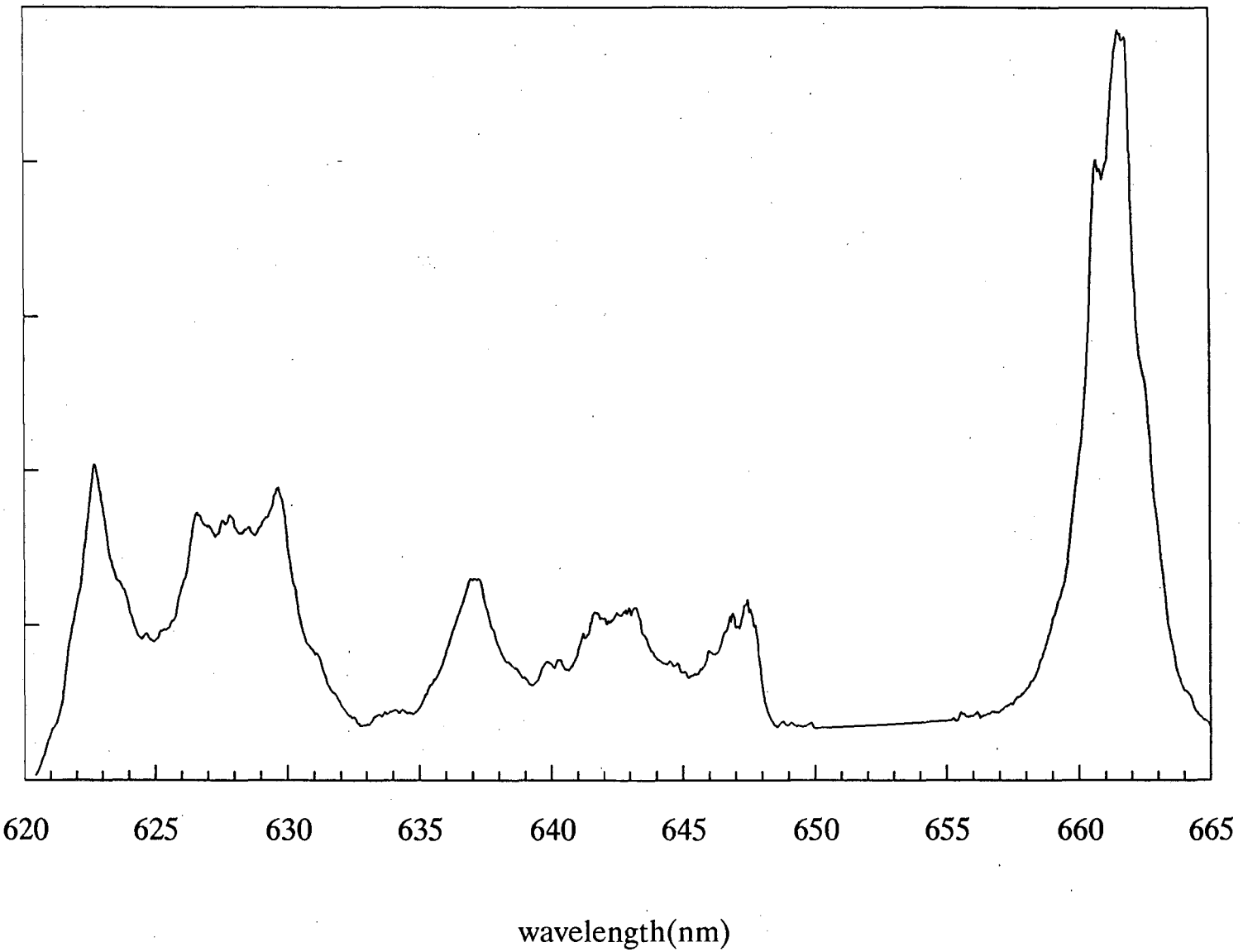

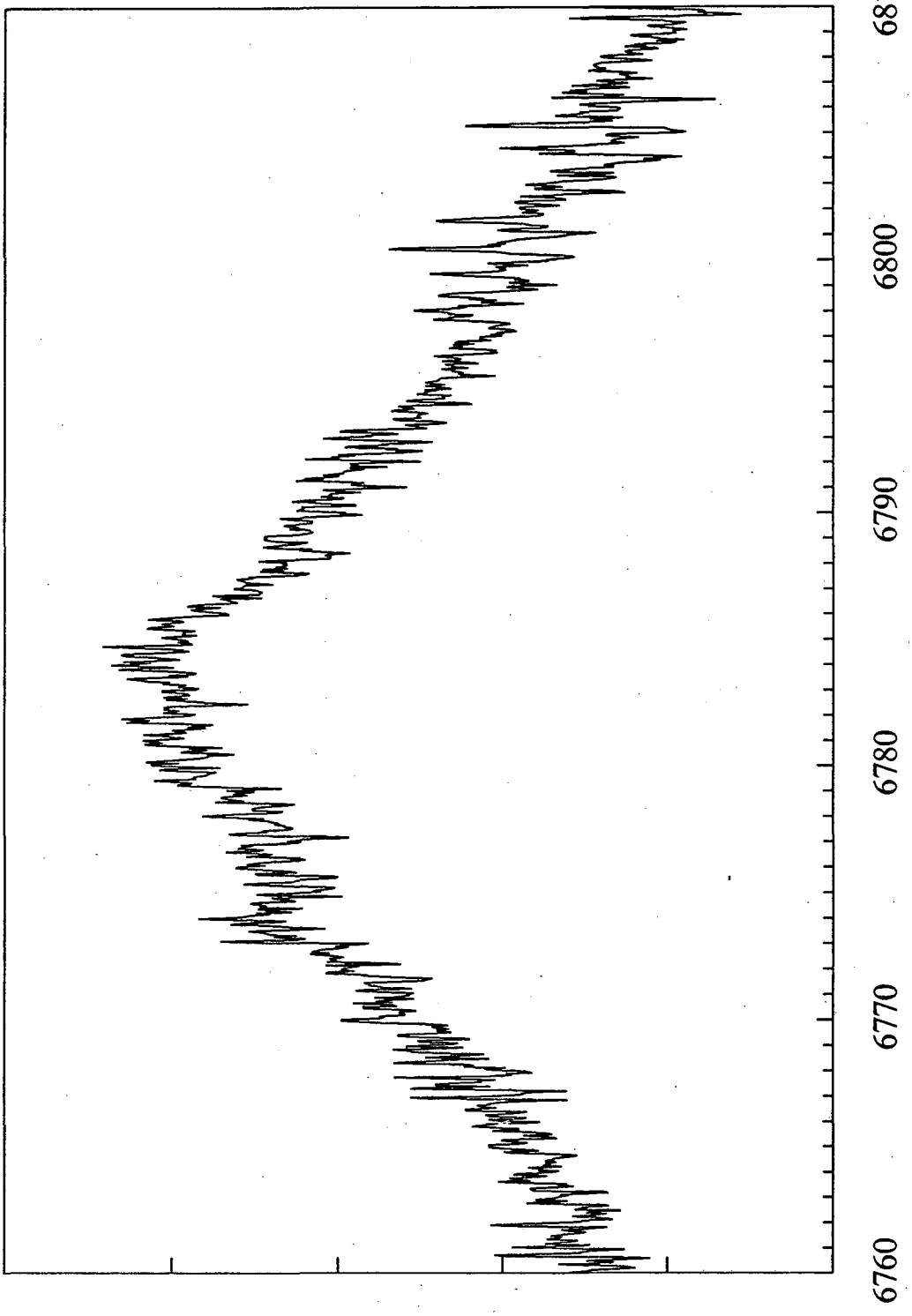


Figure 7

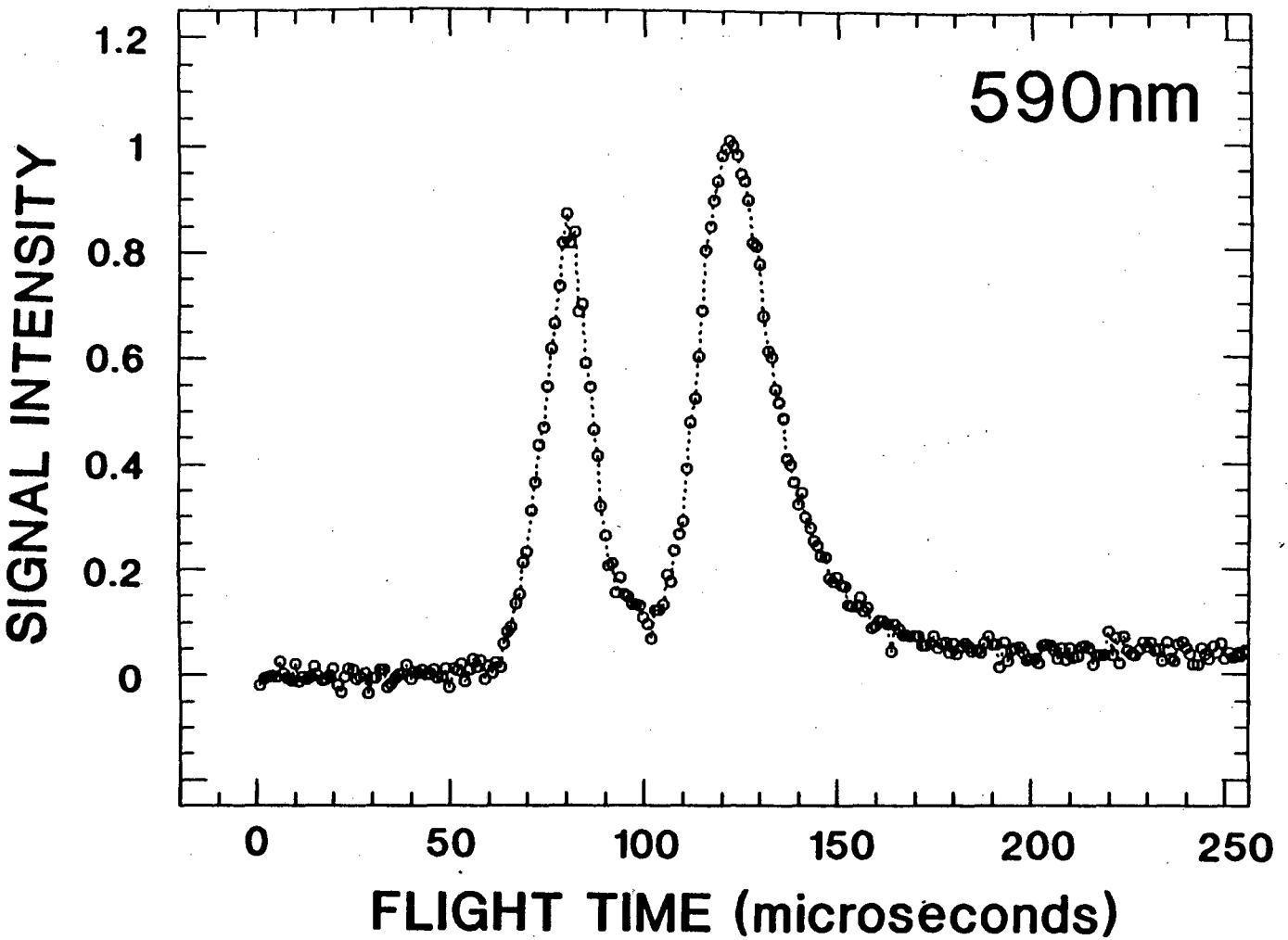
590nm
SIGNAL INTENSITY
1.2
1
0.8
0.6
0.4
0.2
0
0
50
100
150
200
250
FLIGHT TIME (microseconds)

Figure 8

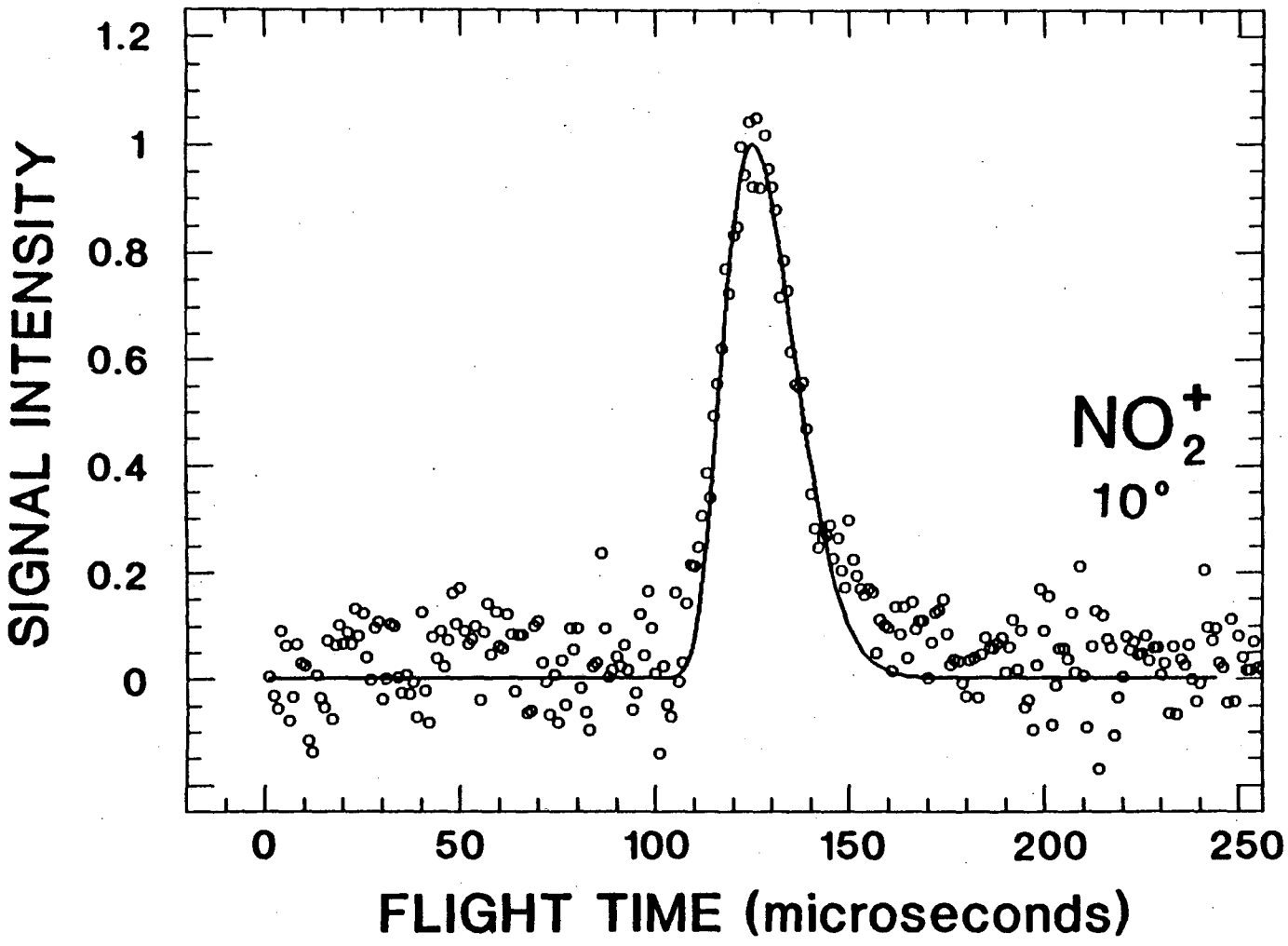
SIGNAL INTENSITY
1.2
1
0.8
0.6
0.4
0.2
0
0
50
100
150
200
250
FLIGHT TIME (microseconds)
$NO_2^+$
10°

Figure 9

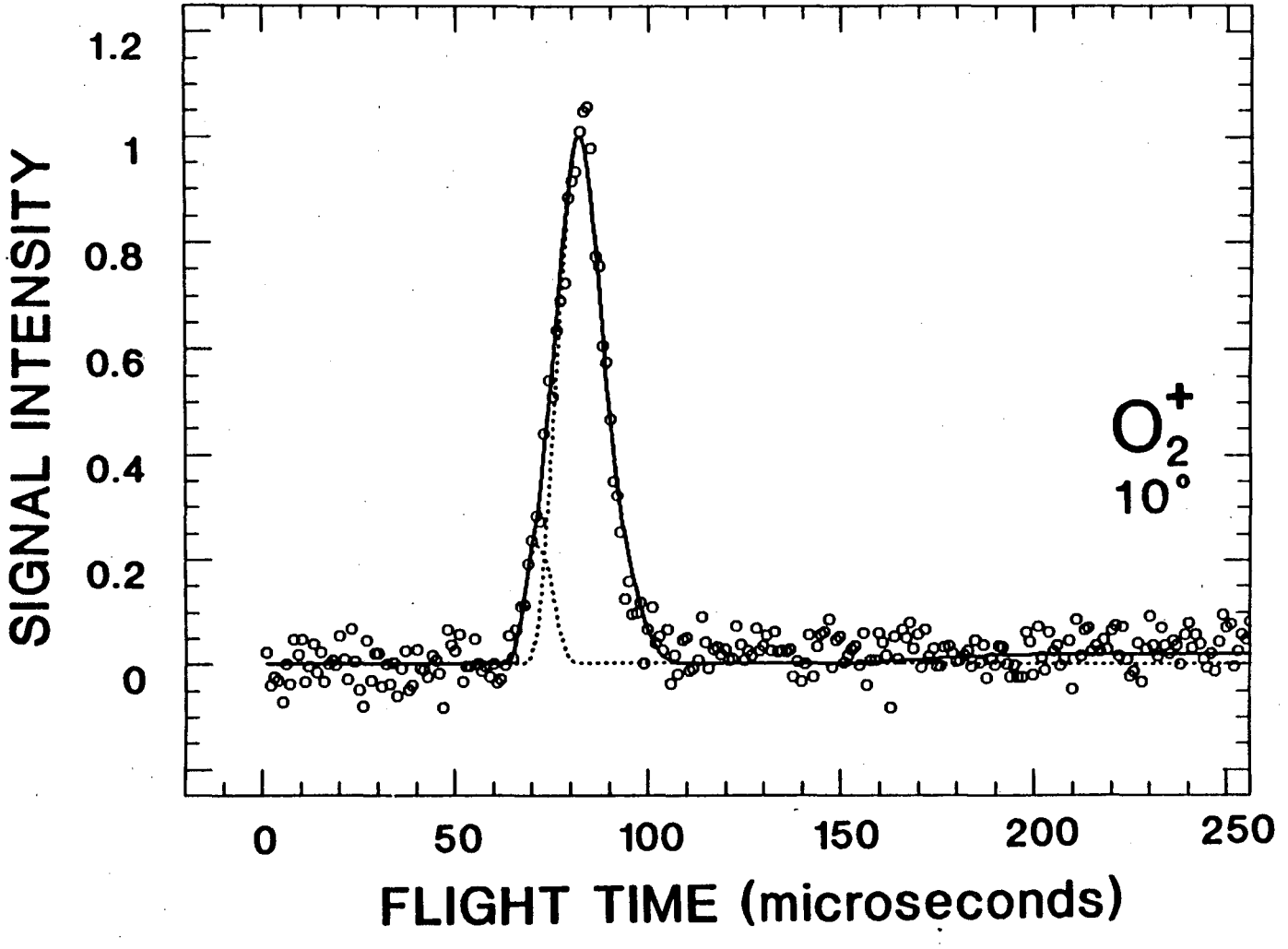
SIGNAL INTENSITY
1.2
1
0.8
0.6
0.4
0.2
0
0
50
100
150
200
250
FLIGHT TIME (microseconds)
$O_2^+$
10°

Figure 10

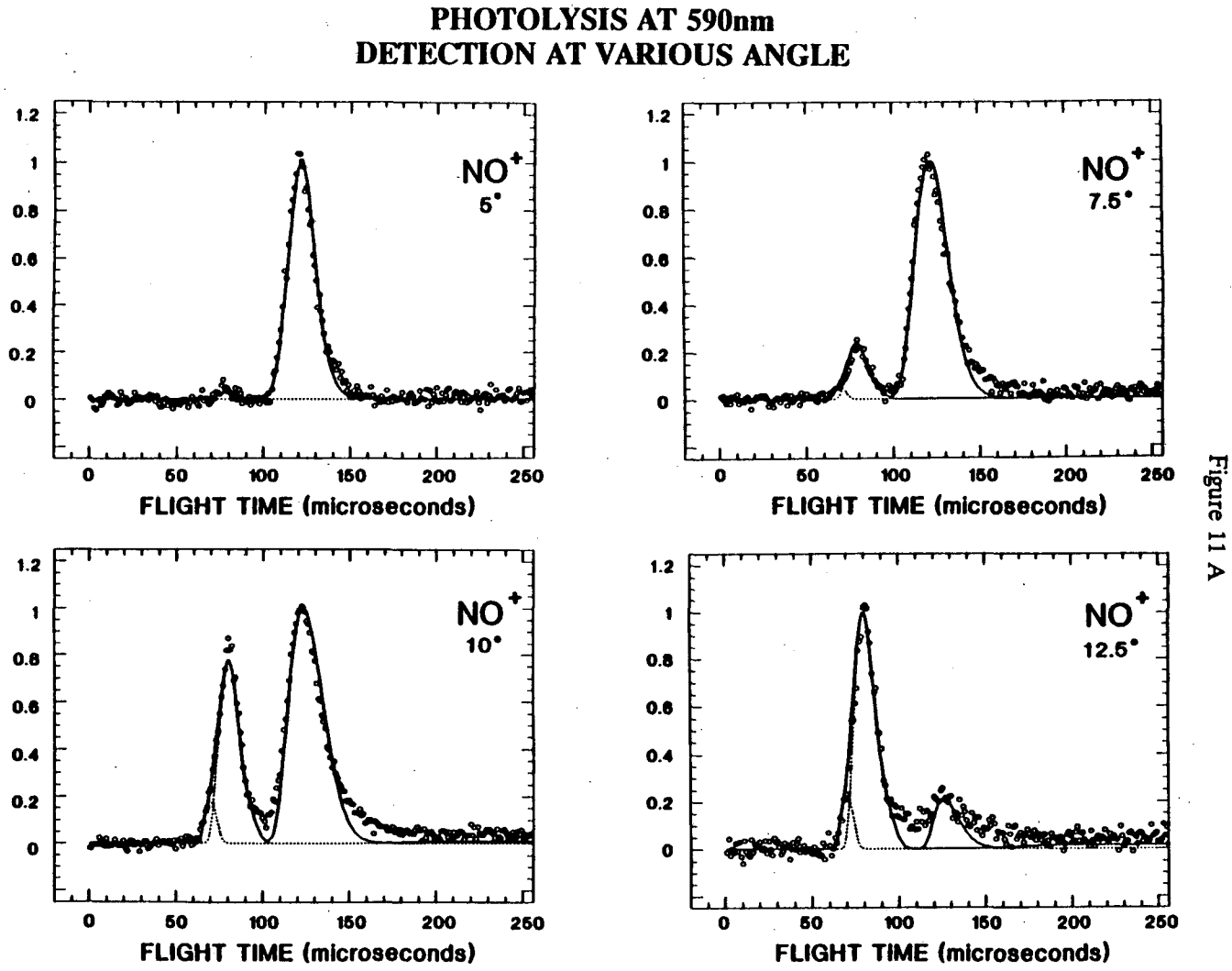
PHOTOLYSIS AT 590nm
DETECTION AT VARIOUS ANGLE
NO+
5°
NO+
7.5°
NO+
10°
NO+
12.5°
1.2
1
0.8
0.6
0.4
0.2
0
0
50
100
150
200
250
FLIGHT TIME (microseconds)

Figure 11 A

Figure 11 B

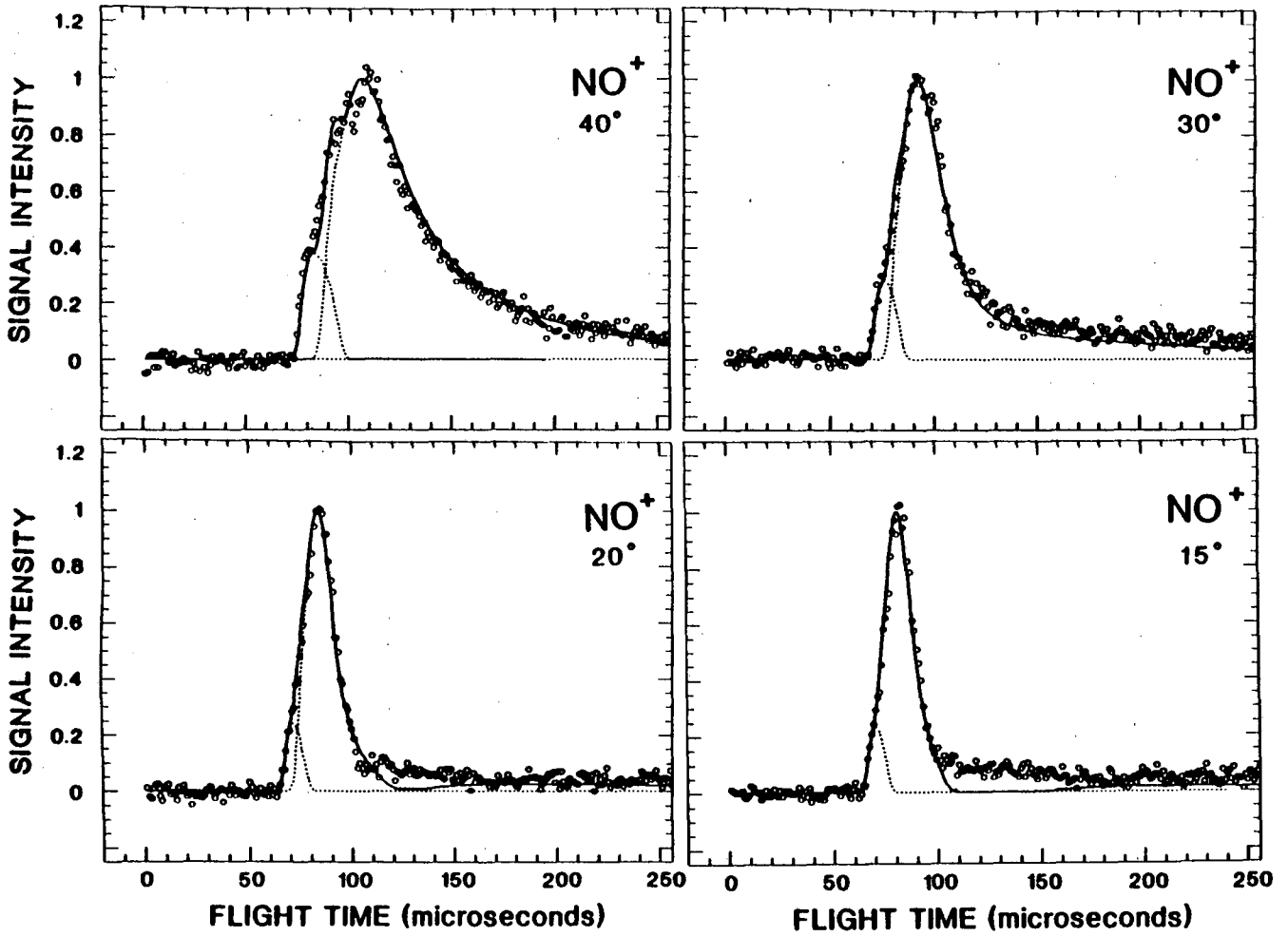
SIGNAL INTENSITY
1.2
1
0.8
0.6
0.4
0.2
0
NO+
40°
NO+
30°
NO+
20°
NO+
15°
0
50
100
150
200
250
FLIGHT TIME (microseconds)
FLIGHT TIME (microseconds)

Figure 12

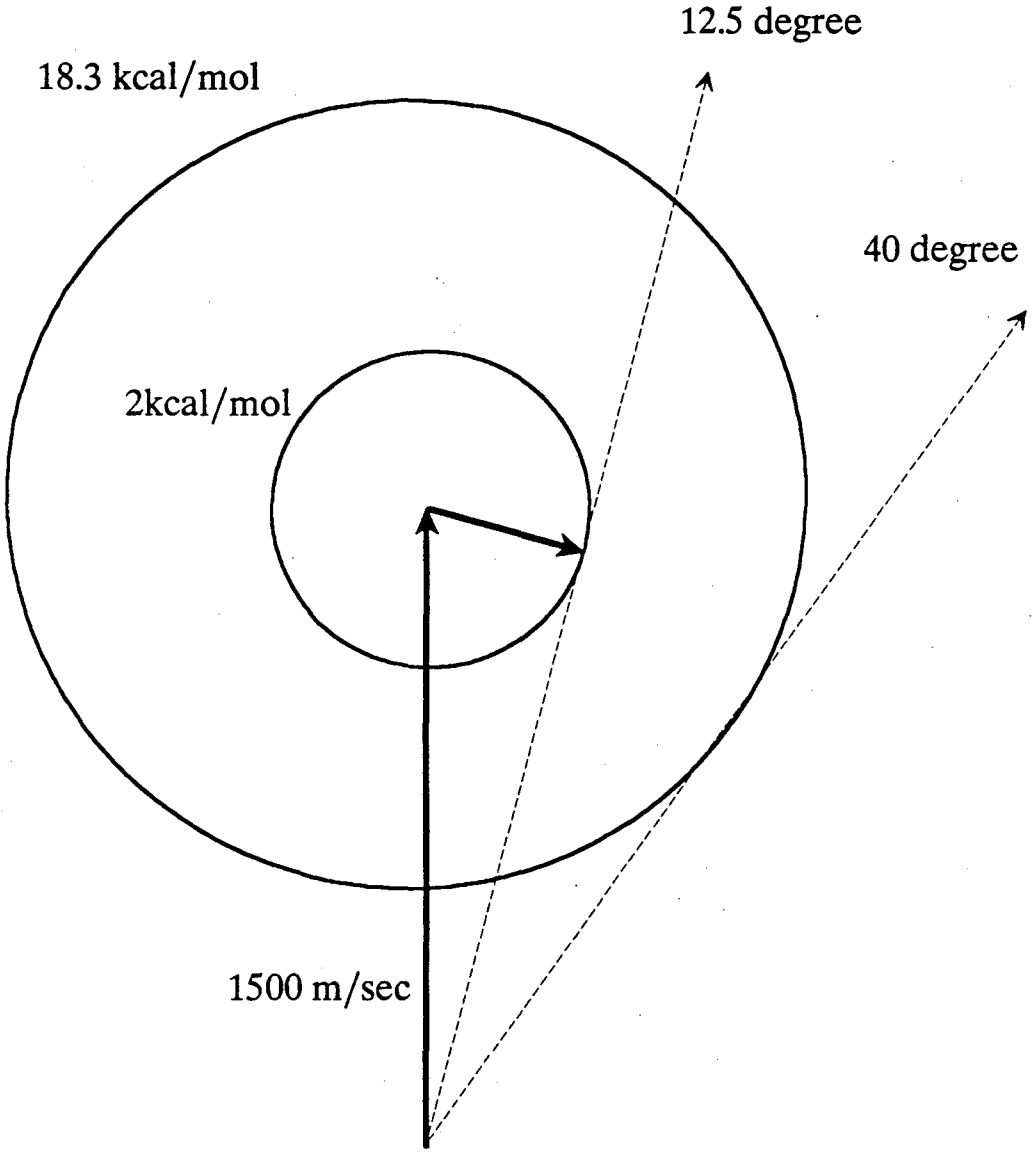

Figure 13

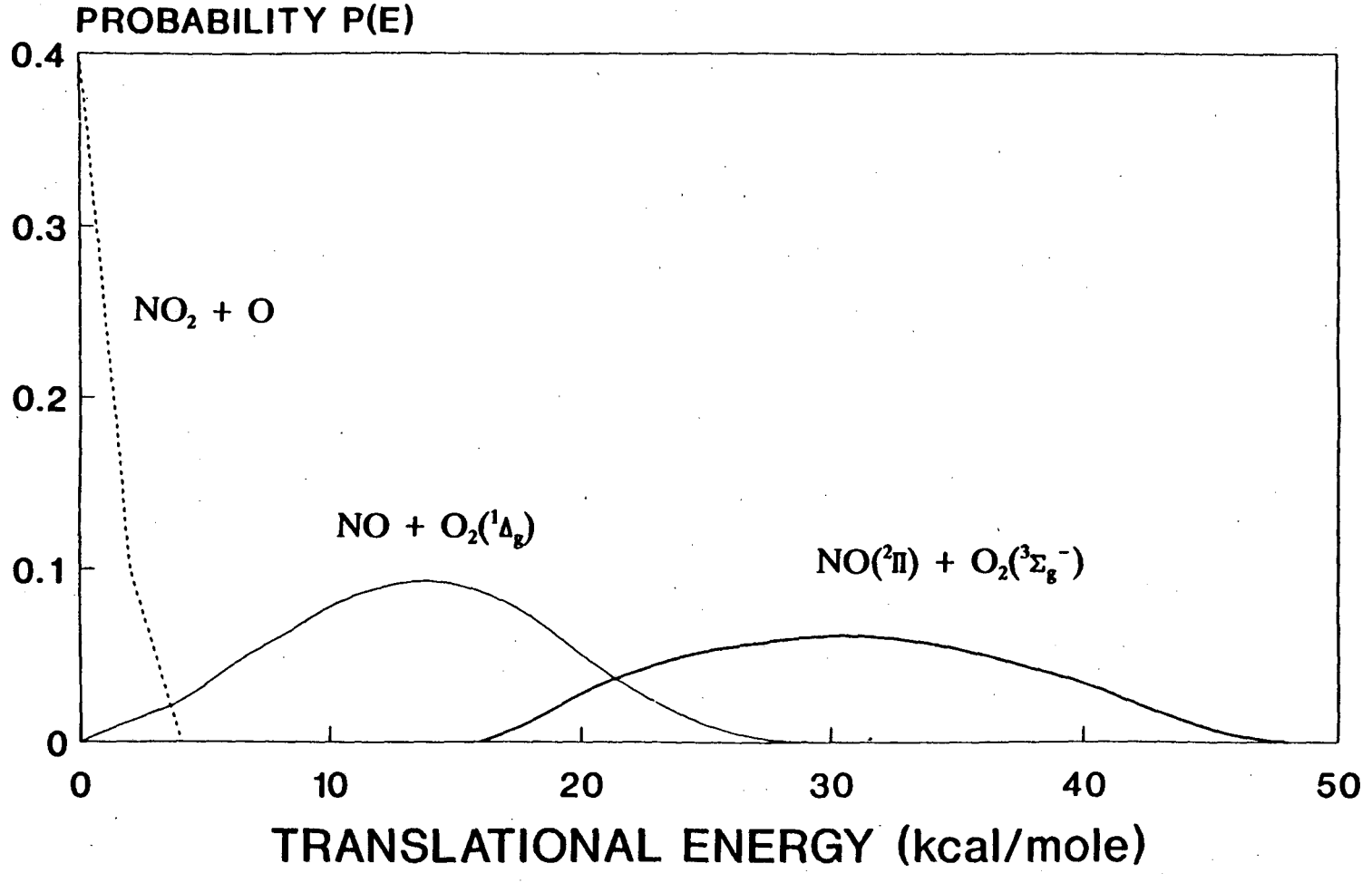
PROBABILITY P(E)
0.4
0.3
0.2
0.1
0
NO2 + O
NO + O2(1Δg)
NO(2Π) + O2(3Σg−)
0
10
20
30
40
50
TRANSLATIONAL ENERGY (kcal/mole)

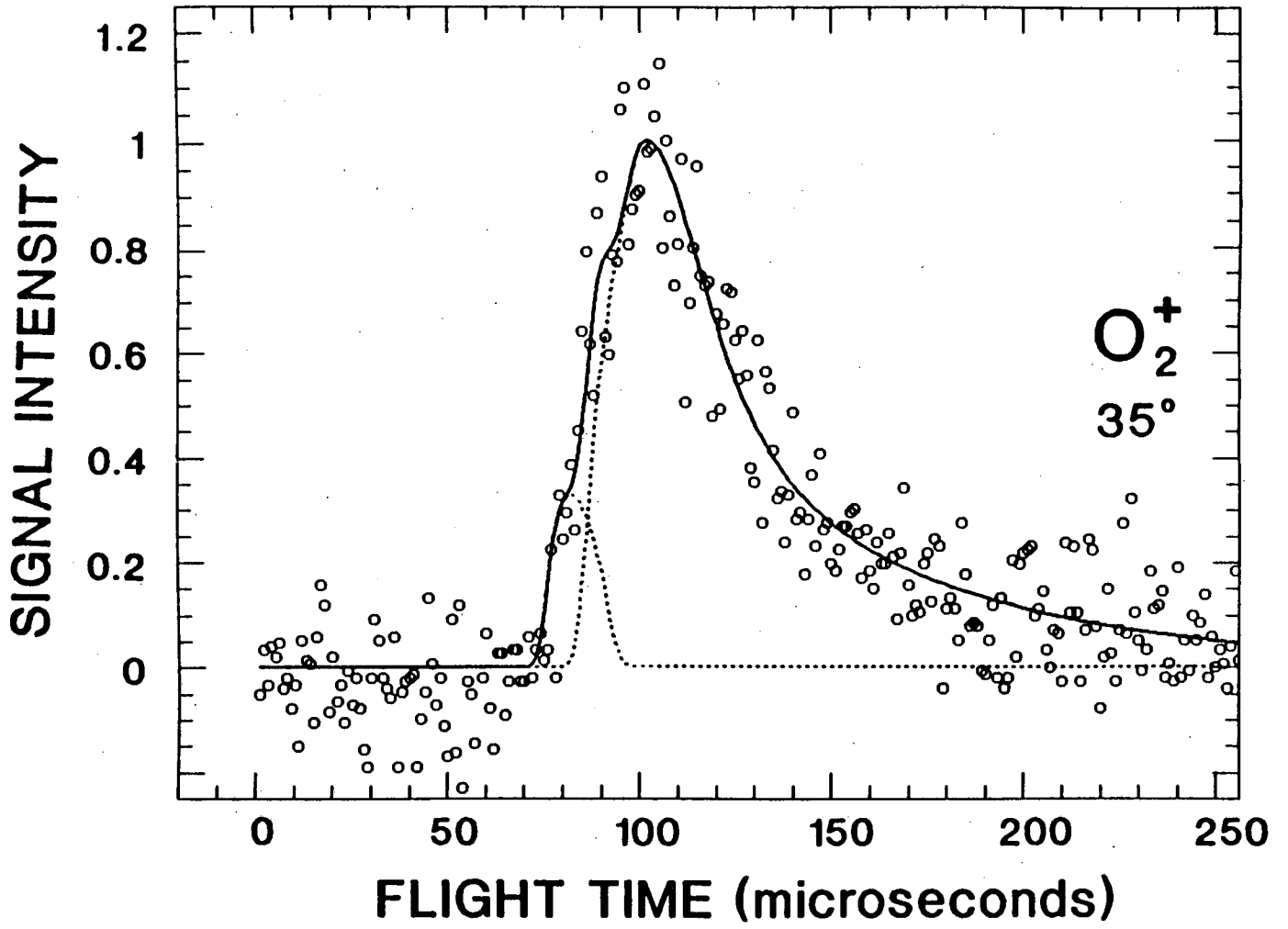
SIGNAL INTENSITY
1.2
1
0.8
0.6
0.4
0.2
0
0
50
100
150
200
250
FLIGHT TIME (microseconds)
$O_2^+$
35°

Figure 14

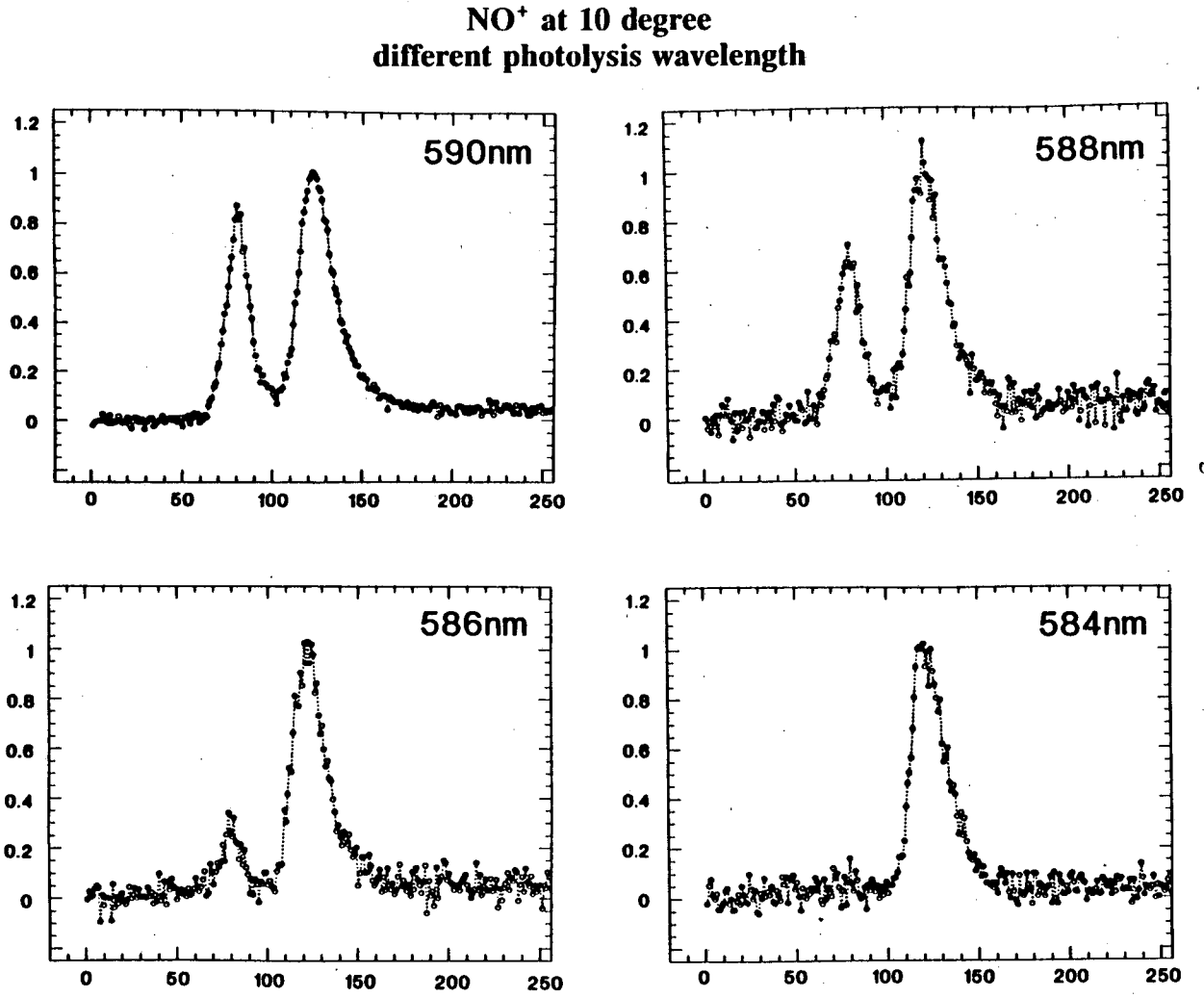
NO+ at 10 degree
different photolysis wavelength
590nm
588nm
586nm
584nm
1.2
1
0.8
0.6
0.4
0.2
0
0
50
100
150
200
250

Figure 15

**$NO^+$ at 10 degree**
**different photolysis wavelength**

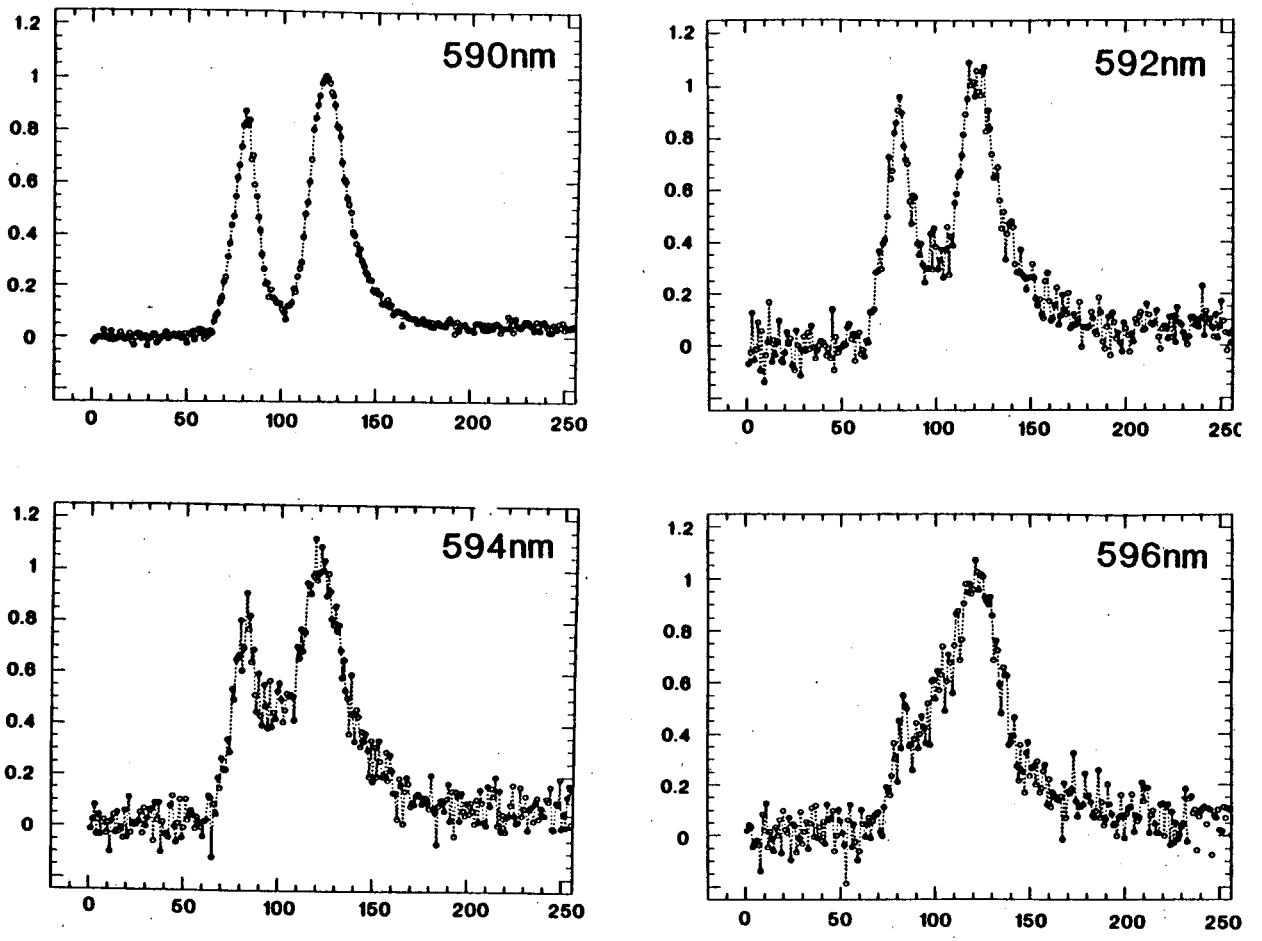


Figure 16

Figure 17 A

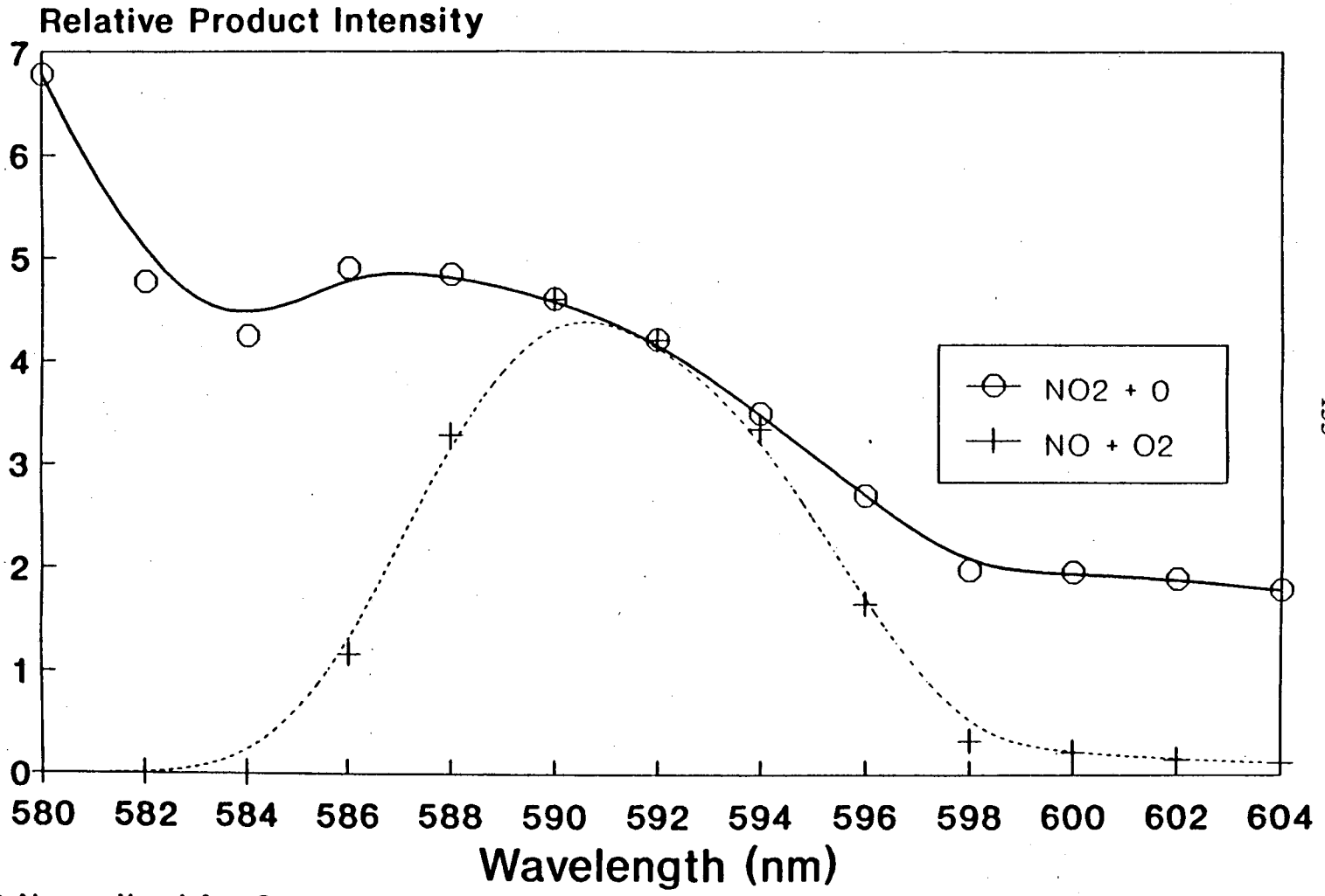


Not Normalized for Cross Sections

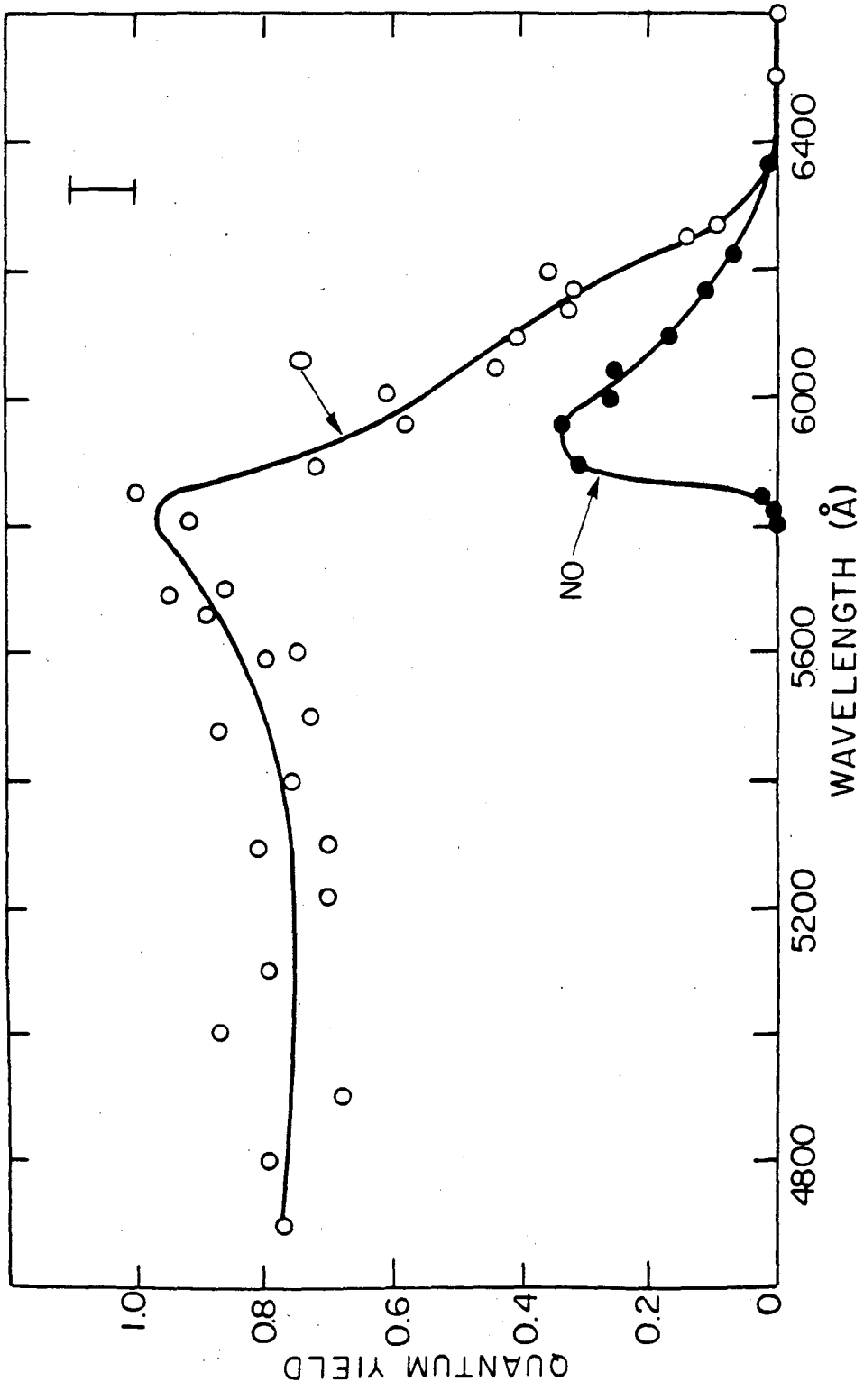
I
NO
QUANTUM YIELD
0
0.2
0.4
0.6
0.8
1.0
4800
5200
5600
6000
6400
WAVELENGTH (Å)

Figure 17 B

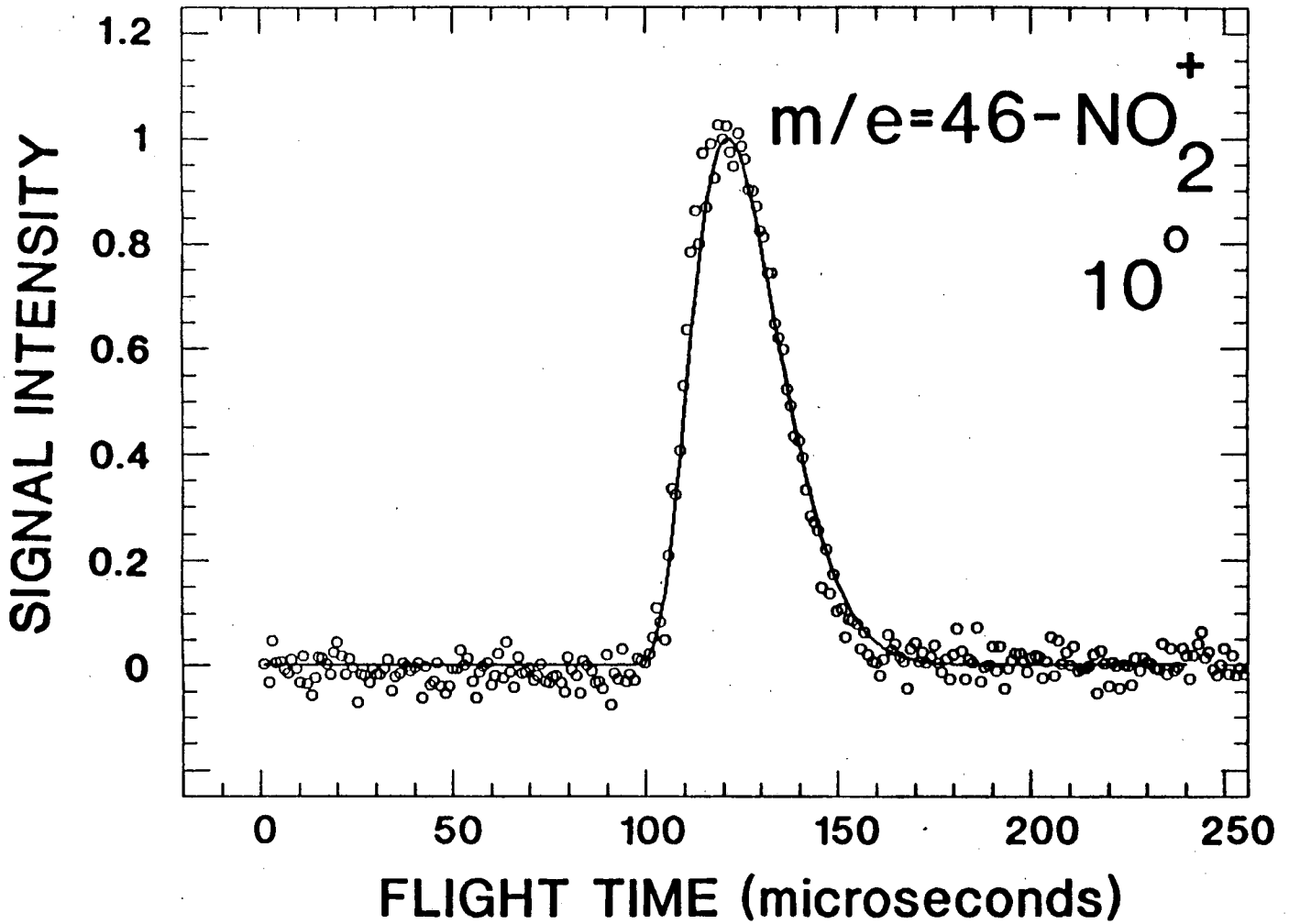
SIGNAL INTENSITY
1.2
1
0.8
0.6
0.4
0.2
0
m/e=46-NO2+
10°
0
50
100
150
200
250
FLIGHT TIME (microseconds)

Figure 18

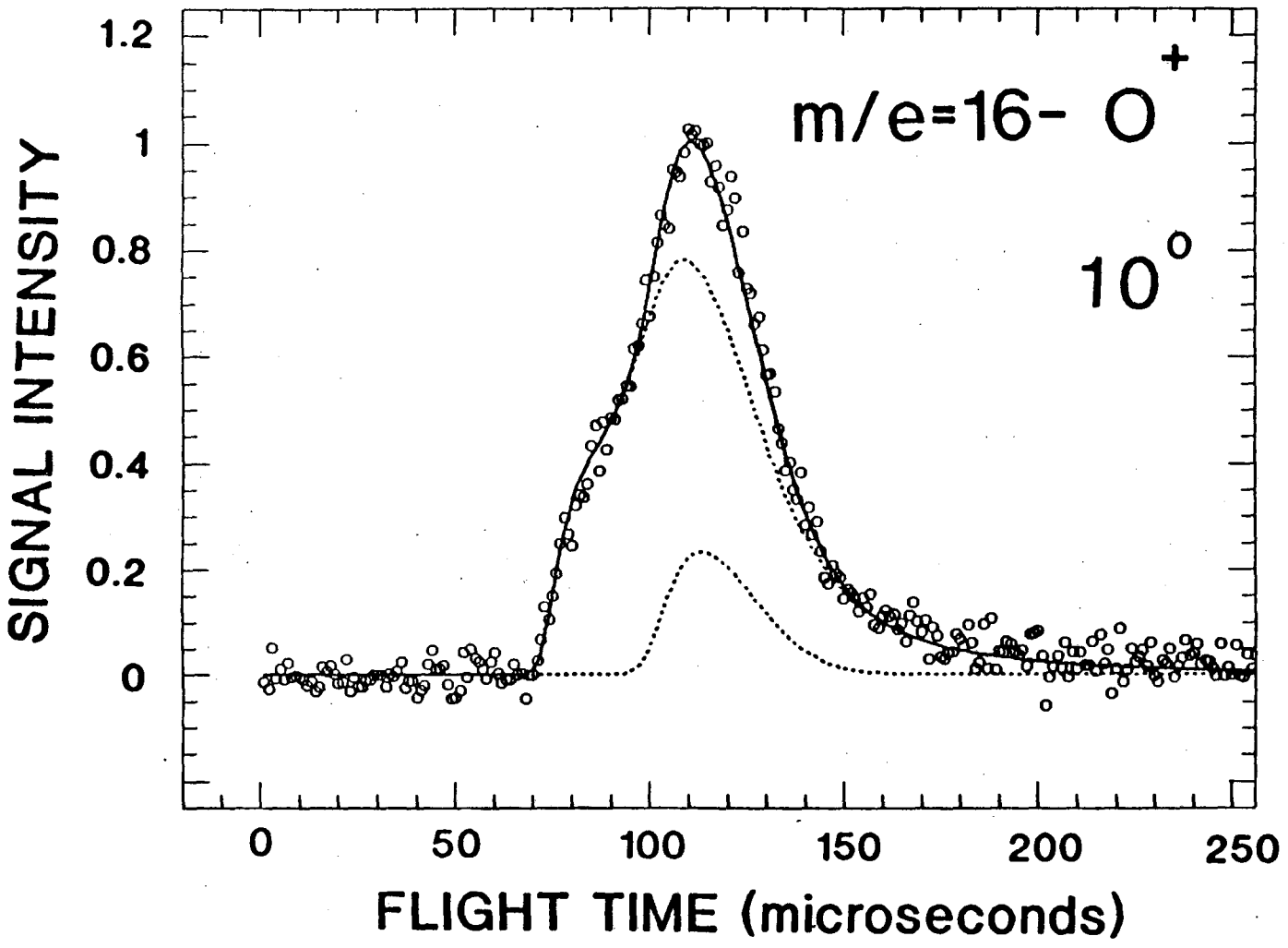
m/e=16- O+
10°
SIGNAL INTENSITY
1.2
1
0.8
0.6
0.4
0.2
0
0
50
100
150
200
250
FLIGHT TIME (microseconds)

Figure 19

Figure 20

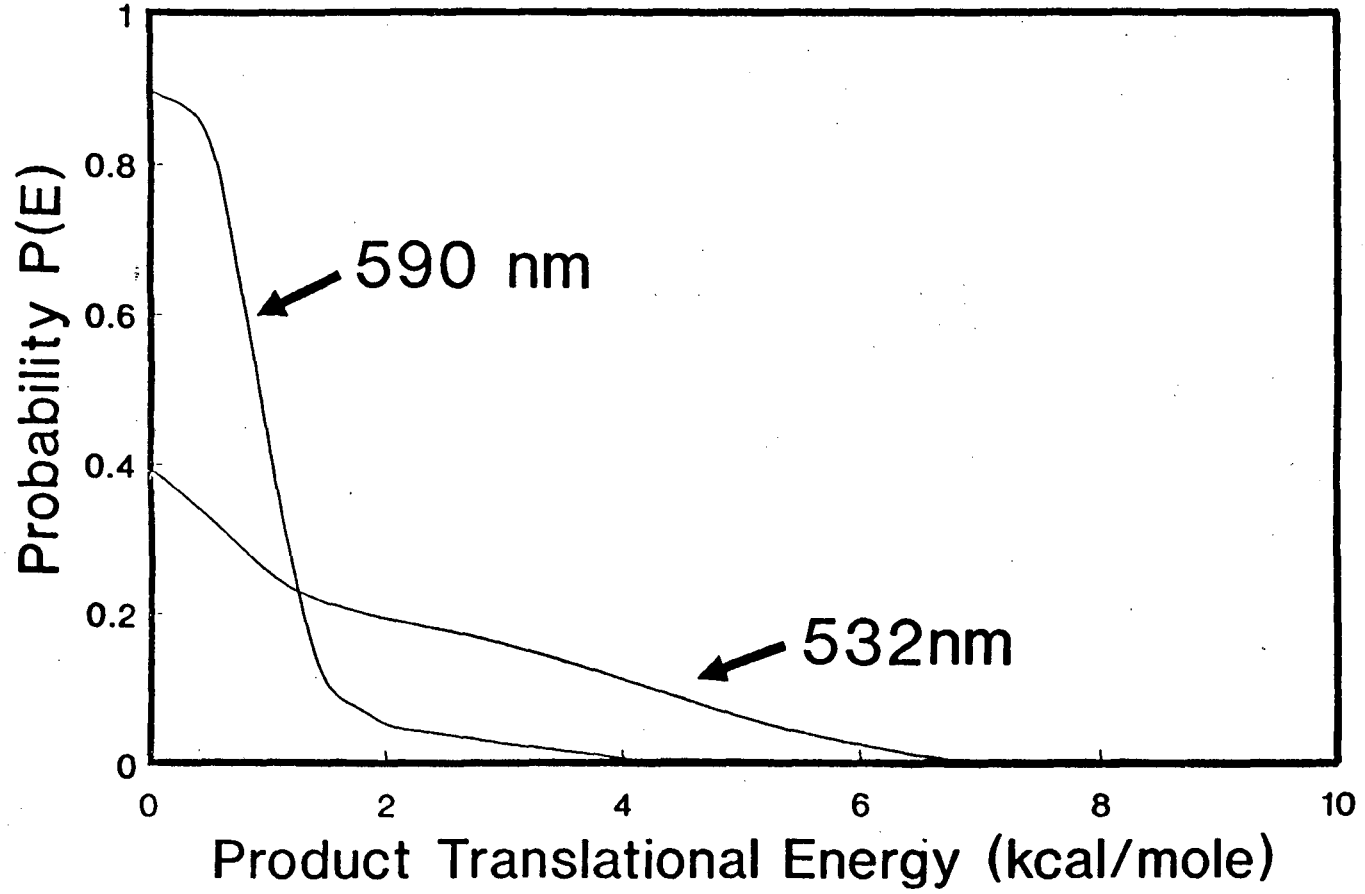
Probability P(E)
1
0.8
0.6
0.4
0.2
0
590 nm
532nm
0
2
4
6
8
10
Product Translational Energy (kcal/mole)

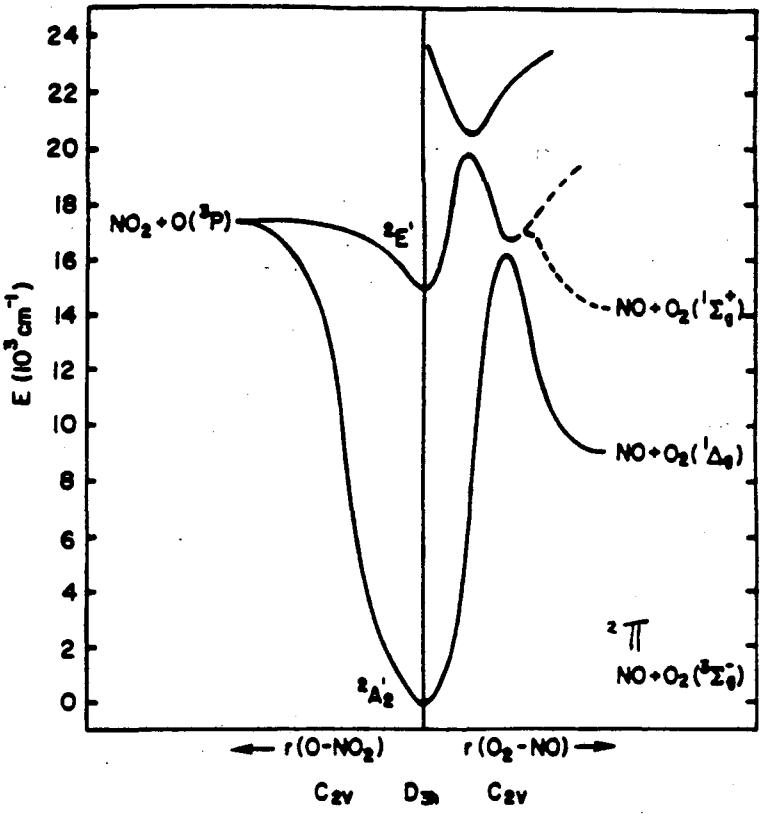
E ($10^3$ cm$^{-1}$)
24
22
20
18
16
14
12
10
8
6
4
2
0
$NO_2 + O(^3P)$
$^2E'$
$^2A_2'$
$NO + O_2(^1\Sigma_g^+)$
$NO + O_2(^1\Delta_g)$
$^2\Pi$
$NO + O_2(^3\Sigma_g^-)$
r(O-$NO_2$)
r($O_2$-NO)
$C_{2v}$
$D_{3h}$
$C_{2v}$

Figure 21

## Chapter 3. Vertical electronic spectrum of $NO_3$ : $^2A_2'$,$^2E''$($^2A_2$,$^2B_1$), and $^2E'$ states


### Abstract

*Ab initio* molecular quantum mechanics has been used to study the four lowest electronic states of the nitrate free radical at the $D_{3h}$ geometry deduced from the experiment (1985) by Ishiwata et al. Basis sets ranging from double zeta (9s5p/4s2p) to triple zeta plus double polarization quality were used. Both self-consistent-field (SCF) and configuration interaction (CI) wave functions were employed, with molecular orbitals determined for the various electronic states of $NO_3$ and for the ground state $NO_3^-$ anion. The CI wave functions included single (S), double (D), and (in some cases) triple (T) excitations.

The CISDT wave functions included as many as 511,474 configurations in $C_{2v}$ point group symmetry. The predicted energetic position of the $^2E'$ state agrees well with the known $T_0$ = 15,100 $cm^{-1}$. The $^2E''$ state, found to be the lowest excited electronic state of $NO_3$, is predicted to lie at a vertical excitation energy of ~ 3600 $cm^{-1}$. The relationship between this prediction and the 1986 experiments by Kawaguchi, Ishiwata, Tanaka, and Hirota suggesting an excited electronic state at 1490 $cm^{-1}$ is discussed.

## I. Introduction

### Ab Initio calculation

As a chemist, we are most interested in finding out the information about molecular system. Such information can be obtained by experimental measurements. However, by setting up the Hamiltonian of the system and finding out the eigenfunctions of the Hamiltonian we can acquire equivalent information. Ab initio method is an example of such methods. The main problem is that real molecular systems consist of many electrons and the Hamiltonian contains many-body-potential which makes the solution of the eigenvalue problem very complex. In most cases only approximate solution can be obtained.

The fundamental equation for the molecular system is the Schrödinger equation

$$\hat{H}(q,Q)\Psi(q,Q) = \epsilon\Psi(q,Q) \qquad (1)$$

where the wavefunctions for the molecular system is represented by $\Psi(q,Q)$, the eigenenergies by $\epsilon$ and the Hamiltonian can be expressed by

$$\hat{H}(q,Q) = T(q) + T(Q) + U(q,Q) + V(Q) \qquad (2)$$

where T(q) and T(Q) are the electronic and nuclear kinetic energies, respectively. V(Q) is the nuclear repulsion energy, and U(q,Q) includes the Coulomb energy between the electrons, and between the electrons and the nuclei. The set $\{q_i\}$ and

$\{Q_k\}$ are internal coordinates for electrons and nuclei, respectively. It is impossible to solve this equation exactly except for the hydrogen atom, because the variables $\{q_i\}$ and $\{Q_k\}$ cannot be separated in the Hamiltonian.

**Born-Oppenheimer approximation**

With the introduction of the Born-Oppenheimer approximation we can separate the nuclear and electronic motions by ignoring the off-diagonal matrix elements of the nuclear kinetic energy operator T(Q). In this approximation the molecular wavefunction may be written

$$\Psi_{ni}(q,Q) = \psi_n(q,Q)\chi_{ni}(Q) \qquad (3)$$

where the subindex *n* and *i* denote that the molecular wavefunction is associated with the electronic state *n* and nuclear state *i*. $\psi_n$ is the eigenfunction of the electronic Hamiltonian

$$\hat{H}_e(q,Q) = T(q) + U(q,Q) \qquad (4)$$

When the vibronic coupling is strong, however, the Born-Oppenheimer approximation fails and we need to solve the coupled differential equations.

**Hartree-Fock approximation**

Even within the Born-Oppenheimer approximation there are too many internal coordinates of electrons involved. Next step is to reduce the number of

electron coordinates. Now assume that the approximate solution of the electronic Hamiltonian has a form of the Slater determinant which consists of N electrons occupying N spin/orbitals.

$$\Psi(x_1, x_2, \ldots, x_N) = (N!)^{-1/2} \begin{vmatrix} \chi_i(x_1) & \chi_j(x_1) & \ldots & \chi_k(x_1) \\ \chi_i(x_2) & \chi_j(x_2) & \ldots & \chi_k(x_2) \\ . & . & \ldots & . \\ . & . & \ldots & . \\ \chi_i(x_N) & \chi_j(x_N) & \ldots & \chi_k(x_N) \end{vmatrix} \quad (5)$$

Then the internal coordinates of the electrons are separated.

According to variational principle, the best wavefunction of this functional form is that which gives the lowest possible energy. By minimizing the energy through changing the form of spin orbitals one can derive Hartree-Fock (H-F) equation, which determines the optimal spin orbitals. The essence of the H-F approximation is to replace the complicated many-electron problem by a one-electron problem in which electron-electron repulsion is treated in an average way.

However, since the averaged potential depends on the spin orbitals of the other electrons, the H-F equation is nonlinear and must be solved iteratively. The procedure for solving the H-F equation is called the self-consistent-field (SCF) method. From the H-F equation we can obtain the best (in a variational sense)

approximation to the ground state wave function, which has a single determinant form.

For the molecular system, even the H-F equation cannot be solved exactly. In order to obtain the approximate solution of the H-F equation, let's assume it has a form as shown below,

$$\psi_i(r) = \sum_{\mu=1}^{K} C_{\mu i}\phi_\mu(r) \qquad (6)$$

In this way we try to solve the H-F equation in the basis set of $\{\phi_\mu\}$. If the basis set $\{\phi_\mu\}$ is complete, the expansion will be exact and the exact solution of the H-F equation will be obtained. For practical computational reasons, however, we always restricts ourselves to a finite basis set.

It is very important to choose a good basis set that will provide a reasonably accurate expansions for the exact molecular orbitals $\{\Phi_i\}$. As the basis set gets more complete, more accurate solutions of the H-F equation will be obtained. The wavefunctions obtained by this method is called the H-F or SCF wavefunctions.

**Configuration Interaction**

From the H-F equation with a basis set of K spatial functions $\{\psi_\mu\}$ a set $\{\chi_i\}$ of 2K spin orbitals are obtained. The SCF solution which is the wavefunction of the ground state electronic state is represented as a form of a Slater determinant. However, it is only one of many determinants that could be formed from the 2K spin

orbitals. Now we assume the exact solution for the electronic Schrodinger equation has a form of

$$| \Phi \rangle = c_0 | \Psi_0 \rangle + \sum_{ra} c_a^r | \Psi_a^r \rangle + \sum_{a<b, r<s} c_{ab}^{rs} | \Psi_{ab}^{rs} \rangle + \cdots\cdots \qquad (7)$$

where $|\Psi_a^r>$ is a singly excited determinant in which an electron, which occupied $\chi_a$ spin orbital in the H-F ground state, has been promoted to a virtual spin orbital $\chi_r$,

$$|\Psi_a^r> = | \chi_1 \chi_2 \cdots \chi_r \chi_b \cdots \chi_n >$$

$|\Psi_{ab}^{rs}>$ is a doubly excited determinant in which electrons have been excited from $\chi_a$ and $\chi_b$ to $\chi_r$ and $\chi_s$,

$$|\Psi_{ab}^{rs}> = | \chi_1 \chi_2 \cdots \chi_r \chi_s \cdots \chi_n >$$

and so on.

In $\{ |\Psi_0>, |\Psi_a^r>, \cdots \}$ basis set the electronic Hamiltonian $\hat{H}_e$ is not diagonalized, and the most accurate solution of the electronic Schrodinger equation is achieved by diagonalizing the Hamiltonian in the basis set which includes all possible excited determinants. This method is called Full Configuration Interaction (Full CI). We often truncate the excited determinants at some excitation levels because of calculational difficulty. Frequently, a truncated CI which includes only the singly and doubly excited determinants is employed. Such a calculation is referred to as singly and doubly excited CI (CISD).

**Multi Configuration SCF calculation**

In the Multi-configuration SCF (MCSCF) model the total wavefunction is determined by optimizing variationally the configuration expansion coefficients in a many-configurational wavefunction, as well as the orbitals which are used to construct the configurations. The central idea of the MCSCF method is to reduce the number of configurations required, by simultaneously optimizing the orbitals. The wave function is presented of the form

$$\Psi = \Sigma_\mu C_\mu \Phi_\mu$$

where each configuration $\Phi_\mu$ is of the same form of wavefunctions obtained by SCF method. In the optimization the coefficients of the orbitals, $C_{ij}$, and the linear configuration interaction coefficients, $C_\mu$, are varied.

**The molecular property of $NO_3$**

The spectroscopy and photochemistry of the nitrate free radical ($NO_3$) have been of interest for many years.[1] In 1985 Ishiwata et al.[2] explored the infrared diode laser spectroscopy of the degenerate N-O stretching band $\nu_3$. By fitting the IR spectrum , they find out that $NO_3$ has a symmetrical $D_{3h}$ equilibrium geometry, of symmetry $^2A_2'$. Siegbahn's recent theoretical study[3] demonstrates that theory as well has had much difficulty characterizing the region of the ground state potential energy surface near the $D_{3h}$ stationary point.

The difficulty in establishing the ground state symmetry of $NO_3$ spills over to the understanding of the electronic spectrum. This first became apparent with the 1962 report by Ramsay[4] and has been confirmed by spectroscopic studies[5-9] in recent years. The absorption spectrum involves a series of intense bands in the region 400−680 nm, or 14700 to 25000 $cm^{-1}$. The absorption cross section of $NO_3$ is on the order of $10^{-17}$ $cm^2$. This spectrum is diffuse even under high resolution, making rotational analysis currently impractical.[2]

The ground state $NO_3$ radical electronic configuration is

$$.. 1a_2''^2 3e'^4 4e'^4 1e''^4 1a_2'^1 \qquad {}^2A_2'. \tag{8}$$

Walker and Horsley[10] predicted the existence of a low-lying $^2E''$ state at 3000 $cm^{-1}$,

$$.. 1a_2''^2 3e'^4 4e'^4 1e''^3 1a_2'^2 \qquad {}^2E'', \tag{9}$$

and a $^2E'$ state at 14,000 $cm^{-1}$:

$$.. 1a_2''^2 3e'^4 4e'^3 1e''^4 1a_2'^2 \qquad {}^2E', \tag{10}$$

Siegbahn's research[3] confirms that the $^2E''$ state is low lying, with two Jahn-Teller $C_{2v}$ components, $^2A_2$ and $^2B_1$. The $^2A_2$ component lies lower energetically, with the highest level of theory predicting $T_e \sim 6000$ $cm^{-1}$. The above prediction notwithstanding, Siegbahn's paper[3] is primarily concerned with the ground state of $NO_3$.

Here a systematic study of the vertical excitation energies of the $^2E''$ and $^2E'$ states of the nitrate free radical is presented. This study highlights a second aspect[11] of the symmetry-breaking problem[12] for $NO_3$, namely the degeneracy of the two components of the $^2E''$ state, represented by electron configuration (9).

The equilibrium geometry of the $^2E''$ state will in fact be of lower point group symmetry than $D_{3h}$, an example of the static Jahn-Teller effect.[13] In $C_{2v}$ symmetry, the two components of the degenerate state (9) are described by the electron configurations

$$...1b_1^2\ 7a_1^2\ 3b_2^2\ 8a_1^2\ 4b_2^2\ 1a_2^2\ 2b_1\ 5b_2^2 \qquad {}^2B_1, \qquad (10a)$$

and

$$...1b_1^2\ 7a_1^2\ 3b_2^2\ 8a_1^2\ 4b_2^2\ 1a_2\ 2b_1^2\ 5b_2^2 \qquad {}^2A_2, \qquad (10b)$$

For any single $D_{3h}$ nuclear geometry, the electronic states (10a) and (10b) must have identical energies. In fact, for most levels of theory, short of full configuration interaction (CI), there will be an artificial splitting between the $^2B_1$ and $^2A_2$ components. In this sense, the $^2B_1 - {}^2A_2$ splitting for $D_{3h}$ nuclear geometries is one measure of the quality of the wave functions being used. For example, it would be most unwise to place the reliability of a prediction of the important (but unknown) energy difference $\Delta E$ ($^2A_2' - {}^2E''$) at a value less than the predicted $^2B_1 - {}^2A_2$ $D_{3h}$ splitting, which must in fact be identically zero.

The recent experimental finding most closely related to the present research was presented in June 1986 by Kawaguchi, Ishiwata, Tanaka, and Hirota[14] at the Columbus Spectroscopy Symposium. They conclude that the IR spectrum of $NO_3$ in the 1490 $cm^{-1}$ region, previously assigned to the $\nu_3$ fundamental ($\perp$) band of the ground state, in fact corresponds to an *electronic* transition. Hirota and co-workers' analysis[14] indicates that the feature at 1490 $cm^{-1}$ is either a $^2A_2' - {}^2E''$ or $^2A_2' - {}^2E'$ electronic transition. The present theoretical study immediately precludes the possibility that the lowest state could be so low-lying energetically. We will discuss in detail the possibility that the $^2E''$ state could be involved in the spectroscopic transitions at 1490 $cm^{-1}$.

## II. Results

### A. Vertical excitation energy calculation

In this calculation basis sets ranging from double zeta (9s5p/4s2p) to triple zeta plus double polarization quality were used. Both self-consistent-field (SCF) and configuration interaction (CI) wave functions were employed, with molecular orbitals determined for the various electronic states of $NO_3$ and for the ground state $NO_3^-$ anion. The CI wave functions included single (S), double (D), and (in some cases) triple (T) excitations.

**double zeta (DZ) basis set**

Given the methodological emphasis of this study, a logical arrangement of the results is in terms of the different basis sets used. The smallest basis set, which allowed the most exhaustive CI treatments, was the standard DZ set of Huzinaga and Dunning. This basis may be designated N,O (9s5p/4s2p) and consists of 40 contracted Gaussian functions for the $NO_3$ molecule. Unless specifically indicated, all $NO_3$ results reported here were obtained at the $D_{3h}$ equilibrium geometry deduced by Ishwata et al., namely r(N−O) = 1.240 Å.

The first set of DZ basis wave functions used self-consistent-field (SCF) molecular orbitals (MOs) determined separately in $C_{2v}$ symmetry for each of the four electronic states considered. These four states are the $^2A_2'$ state (1), which becomes $^2B_2$ in $C_{2v}$, the $^2B_1$ and $^2A_2$ components of the $^2E''$ state (2), and $^2A_1$ component of the $^2E'$ state (3). There is also a $^2B_2$ component of (3), but in $C_{2v}$ point group this component is of the same symmetry as the $NO_3$ ground state, compounding the existing theoretical difficulties. Therefore, only the $^2A_1$ component of the spatially degenerate $^2E'$ state(3) was considered in this research.

In the course of theoretical studies of the $NO_3$ ground state, one peculiar and persistent feature appeared. Namely, there are two energetically distinct ground state SCF wave functions for $NO_3$. Both solutions were obtained within the confines of $C_{2v}$ point group symmetry. Both solutions are given throughout Tables I, III, V-VIII, and X. Although the discussion here is almost entirely based on the lower energy SCF solution, the other solution (~0.035 hartrees (=7680 $cm^{-1}$) higher in

energy) is also mentioned. The presence of these two solutions points to the desirability of some sort of an MCSCF starting point. In the next chapter MCSCF calculation results will be shown. However, it should be noted that a satisfactory CASSCF treatment will be very large scale calculation which will consume gigantic amount of computer time and memory for a system such as $NO_3$ with 23 valence electrons.

Table I summarizes the DZ basis results obtained with SCF MOs separately optimized for each of the four $C_{2v}$ electronic states. Note first in Table I that the single configuration SCF approximations do a very poor job of reproducing the known $^2B_1 - ^2A_2$ degeneracy. Specifically the two degenerate components are predicted to lie 5700 $cm^{-1}$ apart. In addition the $^2E'$ state is predicted to lie much higher (by ~7000 $cm^{-1}$) than the experimental $T_0$ = 15100 $cm^{-1}$ at the SCF level of theory.

The next higher level of theory considered was configuration interaction including all single and double excitations (CISD). In the present research the four core SCF MOs (1s-like on nitrogen and oxygen) are held doubly occupied in all configurations and the four 1s-like virtual MOs (i.e., the four highest-lying virtual orbitals) are deleted from the CI procedure. With these restrictions, in $C_{2v}$ symmetry the CISD wave functions include 8519 ($^2B_2$), 8349 ($^2B_1$), 8336 ($^2A_2$), and 8532 ($^2A_1$) configurations, respectively.

The DZ CISD results are an improvement over the DZ SCF predictions in that the former predict the $^2E'$ state to lie much closer to the experimental $T_0$ =

15100 $cm^{-1}$. However, while the spurious $^2B_1 - ^2A_2$ separation is significantly decreased by CISD (from 5700 to 1700 $cm^{-1}$), the discrepancy between these two degenerate components remains significant.

Our final results from SCF MOs for each separate state of $NO_3$ were obtained by appending Davidson's correction for unlinked quadruple excitation to the CISD energies. This simple approach has proved quite useful in many chemical applications. Table I shows that with the DZ basis set the Davidson corrected CISD method (designated CISD + Q hereafter) does indeed give the smallest predicted energy difference (500 $cm^{-1}$) for the splitting between the degenerate components of the unobserved $^2E''$ state. In that particular sense, it might appear that the Davidson correction is giving an improved description of the energetics compared to CISD.

The 5700 $cm^{-1}$ energy difference between the $^2B_1$ and $^2A_2$ components of the $^2E''$ state at the DZ SCF level of theory shows that the orbitals differ in a major way from $D_{3h}$ symmetry. Therefore it was thought worthwhile to carry out some theoretical studies beginning with MOs of proper $D_{3h}$ characteristics. Ground state SCF MOs for the $NO_3^-$ anion were considered a reasonable choice in this respect. As Table II shows, these $NO_3^-$ MOs necessarily provide a single configuration description in which the $^2B_1 - ^2A_2$ energy splitting is identically zero (to within computer roundoff, at least).

Although the single-configuration energies of the $^2B_1$ and $^2A_2$ components are correctly identical, the $^2A_2' - ^2E''$ energy difference in Table II is only 600 $cm^{-1}$,

considerably less than found at higher levels of theory with the same DZ basis set. Therefore, CISD wave functions were obtained with this same $NO_3^-$ set of SCF MOs, and these results are also included in Table II. These CISD results demonstrate that the use of a properly symmetrized set of $D_{3h}$ orbitals is not sufficient to avoid symmetry breaking for the $NO_3$ free radical. At the CISD level with DZ $NO_3^-$ orbitals, the $^2B_1 - {}^2A_2$ splitting is 118 $cm^{-1}$, small but not vanishing. When the Davidson correction is appended to these CISD energies, the $^2B_1 - {}^2A_2$ splitting increases to 295 $cm^{-1}$.

Using the SCF MOs for the ground state $NO_3^-$ anion, it was decided to press further and include all *triple* excitations in an analogous variational treatment, i.e., CISDT. This procedure results in CI wave functions of size 511 430 ($^2B_2$), 507 586 ($^2B_1$), 507 542 ($^2A_2$), and 511 474 ($^2A_1$) configurations. The total and relative CISDT energies are included in Table II. Note that the CISDT energies from $NO_3^-$ orbitals (Table II) are uniformly lower (by roughly 0.02 hartree) than the CISD energies obtained using SCF orbitals appropriate to each separate electronic state of the $NO_3$ free radical. This means that the most complete variational results reported here with a DZ basis are the CISDT results in Table II. In this light, it is disappointing that the spurious $^2B_1 - {}^2A_2$ energy splitting is rather large, namely 900 $cm^{-1}$. It may be inferred that quadruple excitations are relatively important in reducing this energy separation between degenerate components.

**Double zeta plus polarization (DZ+P) basis set**

Without polarization functions, i.e., *d* functions on the N and O atoms for the $NO_3$ molecule, it is not possible in general to achieve results of chemical reliability. Therefore a set of six *d*-like Gaussian functions was appended to the DZ basis set for each atom. Polarization function orbital exponents were $\alpha_d(N) = 0.80$ and $\alpha_d(O) = 0.85$. The resulting DZ+P basis set may be designated N,O (9s5p1d/4s2p1d), and includes a total of 64 contracted Gaussian basis functions. Results obtained using SCF MOs for the four different $C_{2v}$ electronic states of $NO_3$ are summarized in Table III.

Again with the DZ+P basis set, the SCF method predicts the $^2E'$ state to lie much higher energetically than the experimental $T_0 = 15100\ cm^{-1}$. Equally seriously, the degenerate $^2B_1 - ^2A_2$ pair is predicted to be split by 5300 $cm^{-1}$ at the DZ+P SCF level of theory.

With the DZ+P basis set the CISD wave functions include 38041 ($^2B_2$), 37735 ($^2B_1$), 37714 ($^2A_2$), and 38062 ($^2A_1$) configurations, respectively. The DZ+P CISD value of the $^2B_1 - ^2A_2$ splitting is 1700 $cm^{-1}$, the same as that predicted with the smaller DZ basis set. The main effect of adding polarization functions is to increase the unknown $^2A_2' - ^2E''$ energy difference, by 1700 $cm^{-1}$ at the CISD level. The Davidson correction reduces the spurious $^2B_1 - ^2A_2$ splitting from 1700 to 700 $cm^{-1}$ with the DZ+P basis set. The $^2A_2' - ^2E'$ energy difference is predicted to be 13300 $cm^{-1}$, in fair agreement with the experimental $T_0$ value.

Ground state $NO_3^-$ SCF MOs have also been used in conjunction with the DZ+P basis set, and these results are summarized in Table IV. Since the $NO_3^-$ orbitals display pure $D_{3h}$ symmetry, the single configuration energies of the $^2B_1$ and $^2A_2$ states are necessarily identical. The DZ+P relative energies for the $^2E''$ state remain nearly degenerate, differing by only 100 $cm^{-1}$ at the CISD and Davidson corrected levels of theory.

The largest difference between the predictions based on $NO_3^-$ orbitals and those from orbitals optimized for the individual electronic states of $NO_3$ lies with the unknown $^2A_2' - ^2E''$ energy difference. With the DZ+P basis set,, the former approach (CISD+Q) yields an average [(8000 + 8100) / 2] $^2A_2' - ^2E''$ separation of 8000 $cm^{-1}$, while that for the latter approach is 4400 $cm^{-1}$. However, with the $NO_3$ orbital set and the DZ basis set, the effect of triple excitations is to reduce the CISD $\Delta E$ ( $^2A_2' - ^2E''$ ) by 100 $cm^{-1}$. Such a correction to the DZ+P $NO_3^-$ orbital results would yield an estimated $\Delta E$ ($^2A_2' - ^2E''$) ~ 7000 $cm^{-1}$.

**Larger basis sets**

There is no guarantee that DZ+P basis sets always provide definitive theoretical predictions, even were a full CI to be carried out. Therefore, several larger basis sets have been used in this study to reduce the likelihood of any surprise due to basis set incompleteness. First the DZ+P basis was extended to triple zeta polarization (TZ+P). The TZ basis set is the N,O (9s5p/5s3p) set of Huzinaga and Dunning. The CISD wave functions constructed from this TZ+P basis set included

in $C_{2v}$ symmetry 70093 ($^2B_2$), 69651 ($^2B_1$), 69622 ($^2A_2$), and 70122 ($^2A_1$) configurations, respectively. Table V summarizes the theoretical results obtained with the TZ+P basis set.

The next basis set, labeled TZ+diffuse+P, added diffuse *s* and *p* basis functions to the TZ+P basis set. The Gaussian orbital exponents of these diffuse functions were $\alpha_s(N) = 0.065$, $\alpha_p(N) = 0.051$ and $\alpha_s(O) = 0.086$, $\alpha_p(N) = 0.064$. The final designation for the TZ+diffuse+P basis set is thus N,O (10s6p1d/6s4p1d). The numbers of configurations included in the CISD wave functions were 111869 ($^2B_2$), 111291 ($^2B_1$), 111254 ($^2A_2$), and 111906 ($^2A_1$). Table VI summarizes the predictions made with the TZ+diffuse+P basis set.

The TZ+2P basis set included two sets of polarization functions on the N and O atoms. Gaussian orbital exponents for these polarization functions were $\alpha_d(N,O) = 1.5, 0.35$. The CISD wave functions constructed from the TZ+2P basis set included

135 075 ($^2B_2$), 134 497 ($^2B_1$), 134 460 ($^2A_2$), and 135 112 ($^2A_1$) configurations, respectively. As in all the other correlated wave functions considered in this study, the four lowest occupied MOs and the four highest unoccupied (virtual) MOs were deleted from the CI procedure. Table VII summarizes the *ab initio* results obtained with the TZ+2P basis set.

The final basis with which CI studies were carried out was DZ+diffuse+2P, an abbreviation which should be clear from the earlier described basis sets. The CI wave functions constructed from the DZ+diffuse+2P basis include the same numbers

of configurations as the TZ+2P cases cited in the previous paragraph. Table VIII summarizes the theoretical predictions made with the DZ+diffuse+2P basis set.

All of the theoretical methods show the existence of two different $C_{2v}$ SCF solutions for the $^2B_2$ ground state of $NO_3$. In every case, the two $^2B_2$ solutions are separated by 7500−7600 $cm^{-1}$. However, CISD wave functions using the two independent sets of molecular orbitals give much closer ground state total energies, the differences being only 400−700 $cm^{-1}$. In every case the orbitals giving the lower SCF energy also yield the lower CISD energy. Therefore, the higher energy $^2B_2$ SCF solutions are not discussed hereafter.

The $NO_3$ vertical excitation energies are remarkably insensitive to basis set once the DZ+P set is reached. This is seen most clearly in Table IX, which summarizes the CISD and Davidson corrected CISD results for the $\tilde{X}\,^2A_2' - \tilde{A}\,^2E'$ vertical energy difference. The range of excitation energies for the $^2B_1$ component is 4000−4200 $cm^{-1}$, the spread being only 200 $cm^{-1}$. Similarly the $^2A_2$ component CISD excitation energies are 5900−6000 $cm^{-1}$, the spread being even smaller in this case.

The most reliable value of the $\tilde{X}\,^2A_2' - \tilde{A}\,^2E'$ vertical energy difference is probably that given by the average of the $^2B_1$ and $^2A_2$ component energies obtained via the Davidson correction. These excitation energies, as seen in Table IX, again fall in a narrow range, 4300−4500 $cm^{-1}$. The analogous theoretical treatment of the $^2A_2' - {}^2E'$ energy difference yields predictions in the range 13 300 (DZ+P) − 13 700 (DZ+diffuse+2P). The latter predictions are 1800−1400 $cm^{-1}$ below the observed

$T_0$ = 15100 $cm^{-1}$. Clearly it would be unwise to assume an error of less than 200 $cm^{-1}$ for other $NO_3$ vertical excitation energies.

Some final SCF energies with an even larger TZ+diffuse+2P basis are seen in Table X. However, these results for both component of the $\tilde{X}^2A_2' - \tilde{A}^2E'$ transitions are the same (to within 100 $cm^{-1}$) as the analogous TZ+2P results. Thus the conclusion is that there is little basis set sensitivity in these $NO_3$ vertical excitation energies and that the standard DZ+P basis set is adequate for meaningful theoretical predictions.

**A natural orbital based multireference CISD approach**

A multireference CISD treatment was done. With the DZ+P basis set, we began by performing CISD natural orbital iteration on the $^2B_2$, $^2B_1$, and $^2A_2$ components. When the natural orbital iterations reached a minimum in the total energy, those natural orbitals were chosen for the ensuing multireference CISD procedure. For the $^2B_2$ ground state the four-reference CISD wave function included 446 705 configurations ($C_{2v}$ symmetry) and the total energy was −279.470 45 hartrees. Similarly for the $^2B_1$ component, the four-reference CISD wave function included 312 513 configurations, with E = −279.452 22 hartrees. Finally, for the $^2A_2$ component of the $^2E''$ state, the four-reference CISD included 428 427 configurations and yielded a total energy of −279.455 48 hartrees.

The above multireference CISD wave functions place the vertical $^2B_1$ and $^2A_2$ components of the $^2E''$ state of $NO_3$ at 4000 and 3300 $cm^{-1}$, respectively, above the

$^2B_2$ ground state. The average of the two $^2E''$ excitation energies is 3600 $cm^{-1}$, which was taken as our final prediction of the $^2A_2' - ^2E'$ vertical energy separation for $NO_3$.

**B. Geometry Optimization for the four lowest electronic states**

Geometry optimization for the four lowest electronic states using HF wave functions is done using the same calculational method as used in previous section.

The results of the calculations are shown in Table XI. DZ is the standard basis set of Huzinaga and Dunning (9s5p/4s2p)[15] and includes 40 contracted Gaussian functions. DZP is the basis set with DZ + polarization functions, which consists of 64 contracted Gaussian functions. Polarization function orbital exponents for nitrogen and oxygen atoms were $\alpha_d(N) = 0.8$, and $\alpha_d(O) = 0.85$.

As mentioned in previous section, another SCF wavefunction for ground state with the same symmetry was obtained. The main difference between the two states is the shape of the highest occupied $b_2$ orbital ($5b_2$). The other SCF solution can be obtained by changing the order of the two highest $b_2$ orbitals ($4b_2$ and $5b_2$) of the one SCF solution and use that configuration as a starting guess for the SCF iteration. Most of other theoretical studies report that the $^2B_2$ state is the ground state.

The geometry was optimized using analytic SCF gradient technique. For $^2B_2$ state both of the two wave functions are optimized in geometry.

**III. Concluding remarks for Vertical energy calculation**

At the highest level of theory considered here, the vertical $\tilde{X}^2A_2' - \tilde{A}^2E''$ energy separation is predicted to be 3600 $cm^{-1}$. We have shown that the $\tilde{A}^2E''$ state of $NO_3$ is the only possible candidate for the hypothetical electronic transition identified by Kawaguchi, Ishiwata, Tanaka, and Hirota[14] at 1490 $cm^{-1}$. If Hirota's identification of the 1490 $cm^{-1}$ $NO_3$ feature as an electronic transition involving the ground $^2A_2'$ state is correct, it would be a *lower limit* to the vertical energy separation predicted here. Friedl and Sander[20] have reported absolute line strength measurements of the $NO_3$ band centered at 1492 $cm^{-1}$. Friedl and Sander do not appear to be aware of Hirota's reassignment[14] of the 1492 $cm^{-1}$ feature from the $\nu_3$ asymmetric stretch to an electronic transition. However, Friedl and Sander[20] give a possible explanation for the anomalous spectral features in the $\nu_3$ band and continue to attribute the 1492 $cm^{-1}$ band to $\nu_3$.

Very recently, 2 years after this calculation was done, Weaver et al.[21] found from the photoelectron spectrum of $NO_3^-$ that the $^2E''$ state of $NO_3$ lies 0.868 ± 0.046 eV (7000 $cm^{-1}$) above the ground state, which is 3400 $cm^{-1}$ higher than the calculated energy here. One possible source of error could be the inaccuracy of the ground state geometry since this study calculated the vertical excitation energy at the experimentally reported $D_{3h}$ geometry by Ishiwata et al.[3]

**Acknowledgement**

I would like to acknowledge the enormous help from Prof. Schaefer, who directed this study and provided the vast amount of his knowledge in quantum chemistry to solve the difficult problem of $NO_3$. This calculation is done using the program written by Profs. Pitzer and Schaefer. Prof. Schaefer's computer time was used. Allen Clabo, then a graduate student in Prof. Schaefer group, collaborated in the study. I appreciate his help in solving many difficult problems in the calculation. Part of this chapter includes the published article (B. Kim, H. S. Johnston, D. A. Clabo, Jr., and H. F. Schaefer III, J. Chem. Phys. **88**, 3204 (1988)) which was written by Prof. Schaefer based on the report prepared by the author. This work was supported by the Director, Office of Energy Research, Office of Basic energy Sciences, Chemical Sciences Division of the U.S. Department of Energy under Contract No. DE-AC03-76SF00098. This DOE support includes the research done in Prof. Schaefer group.

**References**

1. G. Herzberg, Electronic Spectra and Electronic Structure of Polyatomic Molecules (Van Nostrand Reinhold, New York, 1966), pp. 525, 615.

2. T. Ishiwata, I. Tanaka, K. Kawaguchi, and E. Hirota, J. Chem. Phys. 82, 2196 (1985).

3. P. E. M. Siegbahn, J. Comput. Chem. **6**, 182 (1985).

4. D. A. Ramsay, Proc. Colloq. Spectrosc. Int. **10**, 583 (1962).

5. R. A. Graham and H. S. Johnston, J. Phys. Chem. **82**, 254 (1978).

6. D. N. Mitchell, R. P. Wayne, P. J. Allen, R. P. Harrison, and R. J. Twin, J. Chem. Soc. Faraday Trans. 2 **76**, 785 (1980).

7. W. J. Marinelli, D. M. Swanson, and H. S. Johnston, J. Chem. Phys. **76**, 2864 (1982).

8. (a) H. H. Nelson, L. Pasternack, and J. R. McDonald, J. Phys. Chem., **87**, 1286 (1983).

   (b) H. H. Nelson, L. Pasternack, and J. R. McDonald, J. Chem. Phys. **79**, 4279 (1983).

9. T. Ishiwata, I. Fugiwara, Y. Naruge, K. Obi, and I. Tanaka, J. Phys. Chem. **87**, 1349 (1983).

10. T. E. H. Walker and J. A. Horsely, Mol. Phys. **21**, 939 (1971).

11. The first aspect, studied in detail by Siegbahn, (Ref. 3) revolves around the fact that many levels of theory predict the $NO_3$ grounds state to have a $C_{2v}$ geometry, while the recent Hirota experiments (Ref. 2) favors a $D_{3h}$ structure.

12. See, for example; the bibliography given by R. Murphy, H. F. Schaefer, R. H. Nobes, L. Radom, and R. M. Pitzer, Int. Rev. Phys. Chem. **5**, 229 (1986).

13. P. R. Bunker, Molecular Symmetry and Spectroscopy ( Academic, New York, 1979), p. 298.

14. K. Kawaguchi, T. Ishiwata, I. Tanaka, and E. Hirota, Abstract #TE4, 41st Symposium on Molecular Spectroscopy, Ohio State University, Columbus, Ohio, June 16-20, 1986; Annual Review, Institute for Molecular Science (Okazaki, Japan, 1986) pp. 29-30.

15. S. Huzinaga, J. Chem. Phys. **42**, 1293 (1965); T. H. Dunning, ibid. **53**, 2823 (1970).

16. E. R. Davidson, The World of quantum Chemistry, edited by R. Daudel and B. Pullman (Reidel, Dordrecht, 1974), pp. 17-30.

17. H. F. Schaefer, Quantum Chemistry. The Development of Ab Initio Methods in Molecular Electronic Structure Theory (Clarendon, Oxford, 1984).

18. H. F. Schaefer, The Electronic Structure of Atoms and Molecules: A survey of Rigorous quantum Mechanical Results (Addison-Wesley, Reading, Mass, 1972).

19. C. F. Bender and E. R. Davidson, J. Phys. Chem. **70**, 2675 (1966).

20. R. R. Friedl and S. P. Sander, J. Phys. Chem. **91**, 2721 (1987).

21. A. Weaver, D. W. Arnold, S. E. Bradforth, and D. M. Neumark, submitted to J. Chem. Phys.

Table I. Vertical excitation energies of the $NO_3$ molecule based on SCF MOs optimized separately for each of four electronic states in $C_{2v}$ symmetry. A $D_{3h}$ nuclear framework is assumed, with r(N−O) = 1.240 Å. All wave functions were constructed from a double zeta (DZ) basis set. Results in parentheses refer to the higher energies of the two ground state SCF solutions.

| | | $^2B_2(^2A_2')$ | $^2B_1(^2E'')$ | $^2A_2(^2E'')$ | $^2A_1(^2E')$ |
|---|---|---|---|---|---|
| SCF | hartrees | −278.67999<br>(−278.65822) | −278.68430 | −278.65835 | −278.59675 |
| | $cm^{-1}$ | 0 | 3000<br>(−5700) | 8700<br>(−30) | 22200<br>(13500) |
| CISD | hartrees | −279.09863<br>(−279.09591) | −279.08765 | −279.07990 | −279.03594 |
| | $cm^{-1}$ | 0 | 2400<br>(1800) | 4100<br>(3500) | 13800<br>(13200) |
| CISD + Q | hartrees | −279.15071<br>(−279.15662) | −279.14002 | −279.13780 | −279.09691 |
| | $cm^{-1}$ | 0 | 2300<br>(3600) | 2800<br>(4100) | 11800<br>(13100) |
| Experiment | | 0 | .... | .... | $T_0$ = 15100 $cm^{-1}$ |

Table II. Total energies obtained via the use of ground state $NO_3^-$ SCF molecular orbitals to describe the low-lying electronic states of the $NO_3$ free radical. A $D_{3h}$ nuclear framework is assumed, with r(N−O) = 1.240 Å. Molecular orbitals were constructed from a double zeta (DZ) basis set.

| | | $^2B_2(^2A_2')$ | $^2B_1(^2E'')$ | $^2A_2(^2E'')$ | $^2A_1(^2E')$ |
|---|---|---|---|---|---|
| SCF | hartrees | −278.60834 | −278.60564 | −278.60564 | −278.55125 |
| | $cm^{-1}$ | 0 | 600 | 600 | 12500 |
| CISD | hartrees | −279.08912 | −279.06563 | −279.06509 | −279.02272 |
| | $cm^{-1}$ | 0 | 5200 | 5300 | 14600 |
| CISD + Q | hartrees | −279.15917 | −279.13667 | −279.13532 | −279.09200 |
| | $cm^{-1}$ | 0 | 4900 | 5200 | 14700 |
| CISDT | hartrees | −279.11974 | −279.10257 | −279.09850 | −279.05611 |
| | $cm^{-1}$ | 0 | 3800 | 4700 | 14000 |
| Experiment | | 0 | .... | .... | $T_0$ = 15100 $cm^{-1}$ |

Table III. DZ+P basis set results for $NO_3$ using SCF MOs optimized separately for each of four electronic states in $C_{2v}$ symmetry. A $D_{3h}$ nuclear framework is assumed, with r(N−O) = 1.240 Å. Results in parentheses refer to the higher energies of the two ground state SCF solutions.

| | | $^2B_2(^2A_2')$ | $^2B_1(^2E'')$ | $^2A_2(^2E'')$ | $^2A_1(^2E')$ |
|---|---|---|---|---|---|
| SCF | hartrees | −278.85827 (−278.82398) | −278.83819 | −278.81411 | −278.75365 |
| | $cm^{-1}$ | 0 | 4400 (−3100) | 9700 (−2200) | 23000 (15400) |
| CISD | hartrees | −279.44407 (−279.44297) | −279.42541 | −279.41723 | −279.37366 |
| | $cm^{-1}$ | 0 | 4100 (3900) | 5900 (5600) | 15500 (15200) |
| CISD + Q | hartrees | −279.52468 (−279.53247) | −279.50610 | −279.50294 | −279.46386 |
| | $cm^{-1}$ | 0 | 4100 (5800) | 4800 (6500) | 13300 (15100) |
| Experiment | | 0 | .... | .... | $T_0$ = 15100 $cm^{-1}$ |

Table IV. DZ+P basis set predictions using molecular orbitals from $NO_3^-$ SCF ground state wave function. A $D_{3h}$ nuclear framework is assumed, with r(N−O) = 1.240 Å.

| | | $^2B_2(^2A_2')$ | $^2B_1(^2E'')$ | $^2A_2(^2E'')$ | $^2A_1(^2E')$ |
|---|---|---|---|---|---|
| SCF | hartrees | −278.77731 | −278.76038 | −278.76038 | −278.70698 |
| | $cm^{-1}$ | 0 | 3700 | 3700 | 15400 |
| CISD | hartrees | −279.43384 | −279.39859 | −279.39825 | −279.35739 |
| | $cm^{-1}$ | 0 | 7700 | 7800 | 16800 |
| CISD + Q | hartrees | −279.53389 | −279.49767 | −279.49680 | −279.45717 |
| | $cm^{-1}$ | 0 | 8000 | 8100 | 16800 |
| Experiment | | 0 | .... | .... | $T_0$ = 15100 $cm^{-1}$ |

Table V. TZ+P basis set results for $NO_3$ using SCF MOs optimized separately for each of four electronic states in $C_{2v}$ symmetry. A $D_{3h}$ nuclear framework is assumed, with r(N−O) = 1.240 Å. Results in parentheses refer to the higher energies of the two ground state SCF solutions.

| | | $^2B_2(^2A_2')$ | $^2B_1(^2E'')$ | $^2A_2(^2E'')$ | $^2A_1(^2E')$ |
|---|---|---|---|---|---|
| SCF | hartrees | −278.86452 (−278.83024) | −278.84451 | −278.82048 | −278.76014 |
| | $cm^{-1}$ | 0 | 4400 (−3100) | 9700 (−2100) | 22900 (15400) |
| CISD | hartrees | −279.50187 (−279.49946) | −279.48365 | −279.47489 | −279.43096 |
| | $cm^{-1}$ | 0 | 4000 (3500) | 5900 (5400) | 15600 (15000) |
| CISD + Q | hartrees | −279.58773 (−279.59437) | −279.56983 | −279.56611 | −279.52668 |
| | $cm^{-1}$ | 0 | 3900 (5400) | 4700 (6200) | 13400 (14900) |
| Experiment | | 0 | .... | .... | $T_0$ = 15100 $cm^{-1}$ |

Table VI. TZ+diffuse+P basis set results for $NO_3$ using SCF MOs optimized separately for each of four electronic states in $C_{2v}$ symmetry. A $D_{3h}$ nuclear framework is assumed, with r(N−O) = 1.240 Å. Results in parentheses refer to the higher energies of the two ground state SCF solutions.

| | | $^2B_2(^2A_2')$ | $^2B_1(^2E'')$ | $^2A_2(^2E'')$ | $^2A_1(^2E')$ |
|---|---|---|---|---|---|
| SCF | hartrees | −278.86865 (−278.83407) | −278.82438 | −278.82438 | −278.76375 |
| | $cm^{-1}$ | 0 | 4400 (−3200) | 9700 (2100) | 23000 (15400) |
| CISD | hartrees | −279.50826 (−279.50571) | −279.48982 | −279.48104 | −279.43684 |
| | $cm^{-1}$ | 0 | 4000 (3500) | 6000 (5400) | 15700 (15100) |
| CISD + Q | hartrees | −279.59490 (−279.60148) | −279.57674 | −279.57301 | −279.53339 |
| | $cm^{-1}$ | 0 | 4000 (5400) | 4800 (6200) | 13500 (14900) |
| Experiment | | 0 | .... | .... | $T_0$ = 15100 $cm^{-1}$ |

Table VII. TZ+2P basis set results for $NO_3$ using SCF MOs optimized separately for each of four electronic states in $C_{2v}$ symmetry. A $D_{3h}$ nuclear framework is assumed, with r(N−O) = 1.240 Å. Results in parentheses refer to the higher energies of the two ground state SCF solutions.

| | | $^2B_2(^2A_2')$ | $^2B_1(^2E'')$ | $^2A_2(^2E'')$ | $^2A_1(^2E')$ |
|---|---|---|---|---|---|
| SCF | hartrees | −278.87552 (−278.84091) | −278.85540 | −278.83140 | −278.77035 |
| | $cm^{-1}$ | 0 | 4400 (−3200) | 9700 (2100) | 23100 (15500) |
| CISD | hartrees | −279.55989 (−279.55696) | −279.54141 | −279.53241 | −279.48775 |
| | $cm^{-1}$ | 0 | 4100 (3400) | 6000 (5400) | 15800 (15200) |
| CISD + Q | hartrees | −279.55264 (−279.65905) | −279.63443 | −279.63049 | −279.59060 |
| | $cm^{-1}$ | 0 | 4000 (5400) | 4900 (6300) | 13600 (15000) |
| Experiment | | 0 | .... | .... | $T_0$ = 15100 $cm^{-1}$ |

Table VIII. DZ+diffuse+2P basis set results for $NO_3$ using SCF MOs optimized separately for each of four electronic states in $C_{2v}$ symmetry. A $D_{3h}$ nuclear framework is assumed, with r(N−O) = 1.240 Å. Results in parentheses refer to the higher energies of the two ground state SCF solutions.

| | | $^2B_2(^2A_2')$ | $^2B_1(^2E'')$ | $^2A_2(^2E'')$ | $^2A_1(^2E')$ |
|---|---|---|---|---|---|
| SCF | hartrees | −278.87448 (−278.83991) | −278.85408 | −278.83002 | −278.76844 |
| | $cm^{-1}$ | 0 | 4500 (−3100) | 9800 (2200) | 23300 (15700) |
| CISD | hartrees | −279.51782 (−279.51601) | −279.49876 | −279.49027 | −279.44542 |
| | $cm^{-1}$ | 0 | 4200 (3800) | 6000 (5600) | 15900 (15500) |
| CISD + Q | hartrees | −279.60668 (−279.61415) | −279.58767 | −279.58423 | −279.54425 |
| | $cm^{-1}$ | 0 | 4200 (5800) | 4900 (6600) | 13700 (15300) |
| Experiment | | 0 | .... | .... | $T_0$ = 15100 $cm^{-1}$ |

Table IX. Theoretical predictions for the vertical excitation energy $\tilde{X}\ ^2A_2' - \tilde{A}\ ^2E'$ of $NO_3$ in $cm^{-1}$.

| Level of theory | | $^2B_1$ component | $^2A_2$ component | Average |
|---|---|---|---|---|
| CISD | DZ | 2400 | 4100 | 3300 |
| | DZ+P | 4100 | 5900 | 5000 |
| | TZ+P | 4000 | 5900 | 5000 |
| | TZ+diffuse+P | 4000 | 6000 | 5000 |
| | TZ+2P | 4100 | 6000 | 5000 |
| | DZ+diffuse+2P | 4200 | 6000 | 5100 |
| CISD+Q | DZ | 2300 | 2800 | 2600 |
| | DZ+P | 4100 | 4800 | 4400 |
| | TZ+P | 3900 | 4700 | 4300 |
| | TZ+diffuse+P | 4000 | 4800 | 4400 |
| | TZ+2P | 4000 | 4900 | 4400 |
| | DZ+diffuse+2P | 4200 | 4900 | 4500 |

Table X. TZ+diffuse+2P basis set results for $NO_3$ using SCF MOs optimized separately for each of four electronic states in $C_{2v}$ symmetry. A $D_{3h}$ nuclear framework is assumed, with r(N−O) = 1.240 Å. Results in parentheses refer to the higher energies of the two ground state SCF solutions.

| | | $^2B_2(^2A_2')$ | $^2B_1(^2E'')$ | $^2A_2(^2E'')$ | $^2A_1(^2E')$ |
|---|---|---|---|---|---|
| SCF | hartrees | −278.87976<br>(−278.84509) | −278.85952 | −278.83549 | −278.77389 |
| | $cm^{-1}$ | 0 | 4400<br>(−3200) | 9700<br>(2100) | 23200<br>(15600) |
| Experiment | | 0 | .... | .... | $T_0$ = 15100 $cm^{-1}$ |

Table XI. Geometry optimization results of $NO_3$. The symmetry was restricted to $C_{2v}$. $R_2=R_3$, and $\angle O_2NO_3$ is the angle the two equivalent NO bonds are making. $\Delta E$ is the energy separation from the $^2B_2$ ground state.

| state | basis set | $R_1$ (Å) | $R_2,R_3$ (Å) | $\angle O_2NO_3$ (degree) | energy (hartree) | $\Delta E$ ($cm^{-1}$) |
|---|---|---|---|---|---|---|
| $^2A_1$ | DZP | 1.217 | 1.245 | 123 | −278.755787 | 27678 |
| $^2A_2$ | DZP | 1.190 | 1.248 | 112 | −278.821935 | 13162 |
| $^2B_1$ | DZP | 1.379 | 1.180 | 130 | −278.864166 | 3901 |
| $^2B_2$ | DZ | 1.196 | 1.293 | 104.8 | −278.675765 | |
| | | 1.402 | 1.219 | 132 | −278.721253 | |
| | DZP | 1.167 | 1.239 | 104.6 | −278.845759 | |
| | | 1.338 | 1.180 | 131.5 | −278.881950 | 0 |

## Chapter 4. Ab initio study of the vibrational spectra of $NO_3$

**Abstract**

The vibrational spectra and geometry of the $NO_3$ molecule is studied using *ab initio* SCF and CASSCF methods. For all levels of theory and basis set the highest symmetry found is $C_{2v}$. Vibrational levels agree well with recent experimental results.

### I. Introduction

As an intermediate in atmospheric conversions involving oxides of nitrogen and ozone in both the stratosphere and the troposphere, the nitrate free radical, $NO_3$, is one of the important molecules in atmospheric chemistry. However, the electronic and molecular structure of nitrate radical has not been well characterized. The difficulty associated with experimental studies of its structure lies mainly in the diffuseness of the visible spectrum, either in absorption or fluorescence spectrum due to extensive vibronic (Douglas) coupling.

In 1983, Nelson et al.[1] and Ishiwata et al.[2] independently obtained a laser induced fluorescence spectrum of $NO_3$, showing about 10 vibrational bands. The

former group favored an assignment of $C_{2v}$ point group symmetry and the latter $D_{3h}$. Neither group could assign all the bands in the spectrum.

In 1985, Ishiwata et al.[3] deduced that $NO_3$ has $D_{3h}$ symmetry from an analysis of the vibrational band of the IR spectrum around 1490 $cm^{-1}$. Although several anomalies accompanied their analysis, it was generally accepted that the equilibrium geometry of $NO_3$ has $D_{3h}$ symmetry. Later in 1986 Ishiwata et al. found evidence[4] that the band at 1490 $cm^{-1}$ was an electronic transition of either $^2A_2' - ^2E''$ or $^2A_2' - ^2E'$.

From the analysis of the high resolution Fourier transform (FT) IR spectrum, which they fitted to $D_{3h}$ symmetry, Friedl and Sander[5] obtained similar result to that of Ishiwata et al. Also they suggested a possible existence of a very low lying excited state around 100 $cm^{-1}$ above the ground state.

Few theoretical studies have been done in which the geometry has been optimized for $NO_3$.[6-11] Except for the work of Lund and Thuomas, who reported $D_{3h}$ geometry with $R_{NO}$ = 1.240 Å, no other studies reported an absolute minimum at a geometry of $D_{3h}$ symmetry.

Recently, we resolved more than 20 vibrational bands in the study of the laser induced fluorescence spectrum of $NO_3$, and were able to obtain a good fitting of the vibrational bands assuming $C_{2v}$ symmetry. Surprisingly, however, no vibrational frequency analysis on $NO_3$ had been reported which we could compare with the experimental analysis at the time of the experiment. One motivation for this study was to obtain theoretical guidance in interpreting the laser induced fluorescence data.

The present study examines the equilibrium geometry and vibrational frequencies using *ab initio* self-consistent-field (SCF) and complete-active-space SCF (CASSCF) analytic derivatives with no assumption of symmetry.

## II. Vibrational Frequency Analysis

In Table I the results of the vibrational frequency analysis on the level of Hartree-Fock method using the program HONDO version 7.0[12] are shown. STO-3G, 4-31G, DZ, DZP, TZP basis sets were used, where DZ and DZP basis set is the same Huzinaga and Dunning basis set as mentioned above. TZP basis set is the Huzinaga and Dunning N,O(9s5p/5s3p) plus polarization functions.

Geometries were optimized using analytic gradients without any restriction on the symmetry of the nuclear structure, until the largest component of the gradient became smaller than $10^{-6}$ in atomic unit (hartree/bohr). Vibrational frequencies were calculated using 2 point difference between the analytic first derivatives. The results are shown in Table I. All of the results were obtained using RHF (restricted Hartree-Fock) wavefunction. UHF (unrestricted Hartree-Fock) result puts $^2A_2$ state to the lowest energy state, which does not seem to be proper. Most of the calculations predict $^2B_2$ state to be the lowest state.

In Table II the results of CASSCF calculations are summarized. CASSCF wave functions were obtained using the routine included in HONDO program. The

orbitals which participated in the CASSCF scheme are given in the first two rows of Table II. Geometry optimization was done using the analytical CASSCF gradient method. In some cases the geometry optimization resulted in structures of different symmetry other than $C_{2v}$. When only $\pi$-orbitals were included as active orbitals, geometry optimization yielded an out-of-plane structure. When more than 3 $\sigma$-orbitals were included in the active orbitals, it yielded a distorted $C_{2v}$ structure. $C_{2v}$ geometry was not obtained as the true minimum when the DZP basis set was employed, but either a distorted $C_{2v}$ structure or an out-of-plane structure was obtained as the minimum. This kind of symmetry breaking in a CASSCF calculation is also reported for $HCO_2$ radical.[14]

Overall, similar geometries and vibrational frequencies were obtained by adopting bigger basis set or by using CASSCF wavefunction. In Table III the vibrational frequency assignment of $NO_3$ is compared with that of $FNO_2$ and $NO_2Cl$. Surprisingly, even the vibrational frequencies obtained by STO-3G basis set for $NO_3$ match well with our tentative experimental frequencies.

The four vibrational frequencies for the totally symmetric modes and the asymmetric stretching mode reproduced well the experimentally observed fundamentals. However, there is an ambiguity in assigning the remaining two modes. In our laser induced fluorescence experiment a vibrational peak is found at 775 $cm^{-1}$ above the ground state when $NO_3$ is excited by 623 nm and 605 nm laser light. When the numerical values are compared, the band at 775 $cm^{-1}$ is closer to the value 884 $cm^{-1}$ calculated as asymmetric bend mode. However, from the

experimental viewpoint it is not clear to which vibrational mode the 368 $cm^{-1}$ band corresponds. That point was discussed in the Chapter 1 where the experimental results are reported.

Calculated IR transition intensities are listed in Table III along with the vibrational frequencies. The IR intensity for the asymmetric stretch mode, which is observed at 2010 $cm^{-1}$ in LIF (laser induced fluorescence), is the largest. Friedl and Sander observed the bands at 1500 $cm^{-1}$ and 753 $cm^{-1}$ using Fourier Transform IR spectrometer.[5] One of the reason that they deduced the structure of $NO_3$ as $D_{3h}$ is they could not see any band around 1053 $cm^{-1}$ which is forbidden in IR transition if the structure is $D_{3h}$. The calculated IR intensities indicate that the intensity of this transition is weak. A fruitful approach might be a study of the $b_2$ asymmetric stretch mode, the strongest calculated absorber, which has not been reported elsewhere.

**Acknowledgement**

I appreciate the enormous support from Prof. W. A. Lester and his coworker. This work is done under the direction of Prof. W. Lester, using the program HONDO 7.0 in his group. B. L. Hammond, then a graduate student of Prof. Lester, collaborated in this study and helped a lot in solving many problems in CASSCF study. A paper was published based on this report (B. Kim, B. L. Hammond, W. A. Lester, and H. S. Johnston, Chem. Phys. Lett., **168**, 131 (1990)). This work was supported by the Director, Office of Energy Research, Office of Basic energy Sciences, Chemical Sciences Division of the U.S. Department of Energy under Contract No. DE-AC03-76SF00098.

Table I. SCF optimization and the vibrational frequency analysis. $R_2 = R_3$, and $\angle O_2NO_3$ is the angle the two equivalent NO bonds ($R_2$, $R_3$) are making.

| basis set | STO-3G | 4-31G | DZ[a] | DZP | TZP |
|---|---|---|---|---|---|
| $R_1$(Å) | 1.4442 | 1.4057 | 1.4024 | 1.3394 | 1.3421 |
| $R_2$(Å) | 1.2706 | 1.1999 | 1.2197 | 1.1808 | 1.1757 |
| $\angle O_2NO_3$ (degree) | 129.6 | 131.1 | 130.7 | 131.5 | 131.8 |
| energy (hartree) | −275.0704 | −278.3630 | −278.7212 | −278.8807 | −278.8892 |
| | 11.8[b] | 29.5 | | 5.4 | 14.8 |
| | 0.6 | 1.0 | | 5.1 | 7.3 |
| | 0.2 | 0.1 | | 0.2 | 1.1 |
| | 15.4 | 13.5 | | 14.2 | 12.8 |
| | 16.1 | 17.4 | | 17.2 | 34.3 |
| | 37.5 | 60.4 | | 53.9 | 83.2 |
| $\nu_1$ ($cm^{-1}$) | 1089.5 (1.4)[c] | 932.7 (11.9) | | 1128.7 | 1111.9 (7.5) |
| $\nu_2$ | 1472.1 (13.7) | 1388.0 (21.8) | | 1594.3 | 1561.5 (26.6) |
| $\nu_3$ | 575.7 (6.8) | 665.4 (0.2) | | 741.5 | 738.4 (0.87) |
| $\nu_4$ | 594.3 (3.2) | 778.7 (3.6) | | 875.3 | 883.9 (3.1) |
| $\nu_5$ | 1698.6 (100) | 1627.1 (100) | | 1888.1 | 1864.4 (100) |
| $\nu_6$ | 464.9 (0.2) | 548.9 (0.9) | | 592.6 | 595.2 (0.9) |

[a]With DZ basis set the energy calculation did not converge when the geometry was changed out of plane ($N_x$ = +0.01 Bohr).

[b]Numbers in $cm^{-1}$ obtained for other degrees of freedom (translation and rotation).

[c]Numbers in parenthesis are the calculated infrared transition intensities, which are normalized to $\nu_5$ (100).

Table II. Multi-configuration SCF result for the geometry optimization and the frequency analysis

| basis set | 4-31G | 4-31G | DZV[a] | DZV | DZ | DZP[b] | DZP[c] |
|---|---|---|---|---|---|---|---|
| no. of π-orbital[d] | 2 | 3 | 3 | 3 | 3 | 2 | 3 |
| no. of σ-orbital[e] | 2 | 3 | 4 | 3 | 3 | 3 | 3 |
| no. of configurations[f] | 20 | 210 | 490 | 210 | 105 | 75 | 210 |
| $R_1$(Å) | 1.4198 | 1.5427 | 1.4096 | 1.4057 | 1.4024 | 1.3421 | 1.3544 |
| $R_2$(Å) | 1.2140 | 1.2094 | 1.2817<br>1.2315 | 1.1999 | 1.2197 | 1.1928<br>1.2104 | 1.1965 |
| $\angle O_2NO_3$ (degree) | 130.5 | 132.4 | 131.2 | 131.1 | 130.7 | 113.92<br>114.9 | 131.4 |
| energy(hartree) | −278.4101 | −278.4596 | −278.8339 | −278.8119 | −278.7212 | −278.9548 | −278.9528 |
| $\nu_1(cm^{-1})$ | 1089.5 | 812.6 | 936.4 | | | 1094(6)[g] | |
| $\nu_2$ | 1472.1 | 1316.9 | 1207.9 | | | 1503(34) | |
| $\nu_3$ | 575.7 | 494.7 | 612.8 | | | 704(2) | |
| $\nu_4$ | 594.3 | 581.6 | 643.6 | | | 802(3) | |
| $\nu_5$ | 1698.6 | 1810.1 | 1548.7 | | | 1810(100) | |
| $\nu_6$ | 464.9 | 428.6 | 515.5 | | | 577(1) | |

[a]$C_s$ structure.

[b]$C_s$ structure.

[c]This is not an absolute minimum. Out-of-plane geometry gives lower energy.

[d]Number of the $\pi$ orbitals in active space orbitals.

[e]Number of the $\sigma$ orbitals in active space orbitals.

[f]Number of the configurations in MCSCF calculation.

[g]Infrared transition intensities normalized for $\nu_5$ (100).

**References**

1. H. H. Nelson, L. Pasternack, and J. R. McDonald, J. Chem. Phys. **87**, 1286 (1983).

2. T. Ishiwata, I. Fugiwara, Y. Naruge, K. Obi, and I. Tanaka, J. Phys. Chem. **87**, 1349 (1983).

3. T. Ishiwata, I. Tanaka, K. Kawaguchi, and E. Hirota, J. Chem. Phys. **82**, 2196 (1985).

4. K. Kawaguchi, T. Ishiwata, T. Tanaka, and E. Hirota, Abstract #TE4, 41st Symposium on Molecular Spectroscopy, Ohio State University, Columbus, Ohio, June 16–20, 1986.

5. R. R. Friedl and S. P. Sander, J. Phys. Chem. **91**, 2721 (1987).

6. T. E. H. Walker and J. A. Horsely, Mol. Phys. **21**, 939 (1971).

7. J. F. Olsen and L. Burnelle, J. Am. Chem. Soc. **92**, 3659 (1970).

8. A. Lund and K. Thuomas, Chem. Phys. Lett. **44**, 569 (1976).

9. N. C. Baird and K. F. Taylor, Chem. Phys. Lett. **80**, 83 (1981).

10. P. E. M. Siegbahn, J. Comput. Chem. **6**, 182 (1985).

11. R. C. Boehm and L. L. Lohr, J. Phys. Chem. **93**, 3430 (1989).

12. M. Dupuis, J. D. Watts, H. O. Villar, and G. J. B. Hurst, IBM corporation, Scientific and Engineering Computations, Dept. 48 B/MS 428, Neighborhood Road, Kingston, N.Y. 12401.

13. D. Feller, E. S. Huyser, W. T. Borden, and E. R. Davidson, J. Am. Chem. Soc. **105**, 1459 (1983).

LAWRENCE BERKELEY LABORATORY
UNIVERSITY OF CALIFORNIA
INFORMATION RESOURCES DEPARTMENT
BERKELEY, CALIFORNIA 94720